THE UNIVERSITY
of ADELAIDE

FACULTY OF SCIENCES
SCHOOL OF PHYSICAL SCIENCES

Direct CP Violation in B Meson Decays

Liam Christopher Hockley

Supervisors:
Professor Anthony THOMAS
Associate Professor Ross YOUNG

February 2020

Contents

List of Figures

List of Tables

Abstract

The matter-antimatter asymmetry observed in nature is one of the largest open questions in particle physics and CP violation is a key requirement for such an asymmetry to exist. Although measurements of CP violation are typically too small to account for this asymmetry, in 2017 the Belle Collaboration reported a significant CP violation of $\mathcal{A}_{CP} = -0.90 \pm 0.17 \pm 0.03$ in the $0.8 \leq m_{KK} \leq 1.1$ GeV/c^2 region of the K^+K^- invariant mass in $B^\pm \to K^+K^-\pi^\pm$ decays.

Direct CP violation in B meson decays arises through the interference of tree and penguin amplitudes and can only occur if there are both strong and weak phase differences between the diagrams. We present several models for tree and penguin diagrams which proceed through a two stage decay process. These involve the $f_0(980)$ and $\phi(1020)$ resonances, both with masses around 1 GeV/c^2, and we also test models involving non-resonant tree decay. Using these models, we calculate the CP asymmetry $\mathcal{A}_{CP}$ in an attempt to justify the Belle results. We use an effective Hamiltonian based on the four-fermion interaction and the Operator Product Expansion to calculate the tree and penguin amplitudes, with Naive Factorisation applied to the hadronic matrix elements. We take several form factor descriptions of the factorised matrix elements, namely monopole and dipole dominance models.

We find evidence that there may be a significant asymmetry present in the case of $f_0(980)$ tree interference with $\phi(1020)$ penguin intermediate states, although other models involving non-resonant tree decays perform better when taking into account the finite resolution of detectors. We present the following estimates of the CP asymmetry; $\mathcal{A}_{CP} = -0.0007$ to -0.0554 for the case of a tree diagram involving the $f_0(980)$ and a penguin involving the $\phi(1020)$; $\mathcal{A}_{CP} = -0.0819$ to -0.346 for the case of a non-resonant tree diagram and a penguin involving the $f_0(980)$; $\mathcal{A}_{CP} = -0.0196$ to -0.101 for the case of a tree amplitude receiving both non-resonant and $f_0(980)$ contributions, and a penguin involving the $f_0(980)$.

Future work could look to use QCD factorisation or Lattice QCD to compute the hadronic matrix elements. If narrower constraints are placed on the properties of the $f_0(980)$ and the CKM matrix parameters, a more definitive conclusion may be reached on the influence of the $f_0(980)$ on the Belle result.

Statement of Originality

I certify that this work contains no material which has been accepted for the award of any other degree or diploma in my name, in any university or other tertiary institution and, to the best of my knowledge and belief, contains no material previously published or written by another person, except where due reference has been made in the text. In addition, I certify that no part of this work will, in the future, be used in a submission in my name, for any other degree or diploma in any university or other tertiary institution without the prior approval of the University of Adelaide and where applicable, any partner institution responsible for the joint-award of this degree.

I give permission for the digital version of my thesis to be made available on the web, via the University's digital research repository, the Library Search and also through web search engines, unless permission has been granted by the University to restrict access for a period of time.

I acknowledge the support I have received for my research through the provision of an Australian Government Research Training Program Scholarship.

23/01/2020

Acknowledgements

As I reflect on the past two years I realise that though this thesis is a culmination of my own academic learning, it really exists as a testament to all the people who've supported me.

First, I'd like to thank my supervisors Anthony Thomas and Ross Young. You've had endless patience for my questions and have been great sources of inspiration and ideas for this work. You've simultaneously guided me in my learning and allowed me to explore ideas on my own. Thank you both for all the work you've put in alongside me, and I hope that this thesis is something you can be proud of contributing to.

My fellow research students also deserve some gratitude. In particular I'd like to thank Albert, Joe and Tomas for the illuminating conversations we shared in front of a whiteboard or section of code. Special mention to Anthony for his quick wit which made every day in the office one to look forward to.

Finally, I want to thank my family. Thank you for your understanding and respect for my time and space, for listening to problems I've had and being there for my successes as well. And last but not least, thank you for your tireless love and support, for which I am ever grateful.

Preface

CP violation is an exciting area of research in particle physics and the aim of this work was to provide an explanation of the CP asymmetry results reported from a recent Belle experiment. In chapter 1 we start with a brief introduction to the Standard Model, including the key building blocks (the fermions and bosons) and describe the interactions available to these particles (strong, weak and electromagnetic). Chapter 2 introduces the important idea of discrete symmetries, in particular the symmetries which arise due to parity and charge conjugation. We also discuss the violation of these symmetries in weak interactions and the measurements of CP violation made by Belle which motivated this work.

Chapters 3, 4 and 5 act as a discourse on our initial calculation of the CP asymmetry. In chapter 3 we describe the four-fermion interaction formulation of the weak interaction and apply the Operator Product Expansion to construct the effective Hamiltonian used in later chapters. Importantly, we define the tree and penguin processes which interfere in B meson decays to give rise to CP violation. In chapter 4 we outline the general method for calculating CP asymmetries and propose a model involving the $f_0(980)$ and $\phi(1020)$ resonances. We begin the calculation of the CP asymmetry and as part of this one inevitably needs to calculate hadronic matrix elements of B mesons transitioning through $V - A$ currents to two particle states. This is non-trivial and chapter 5 is entirely devoted to this. We use the Naive Factorisation approximation to decompose each matrix element into two simpler matrix elements which we then parametrise using form factors. Preliminary results are also presented here.

In chapter 6 we discuss an extension of our method to account for the phase space dependence of the tree and penguin amplitudes. We also propose two new models involving non-resonant tree decays and compute the asymmetry for these. The results and discussion therein lie in chapter 7. We summarise the work in chapter 8 and present some final remarks on our results with comments on future directions for this project.

Throughout this work we use normal text, such as p, to denote a scalar or 4-vector while bold script, such as $\boldsymbol{p}$, denotes 3-vectors. We use the Minkowski space-time metric $g^{\mu\nu} = \text{diag}(+1, -1, -1, -1)$. Latin indices are understood to run from 1 to 3 unless otherwise stated, and Greek indices run from 0 to 3.

Chapter 1

Introduction

One of the longest scientific endeavours in human history has been the search for the theory of the most fundamental building blocks of matter. The realm of these particles is governed by the probabilistic interpretation of matter ascribed to quantum mechanics, and the principles of special relativity. The unification of these two regimes into relativistic quantum mechanics and quantum field theory underpins our current understanding of the subatomic world. One of the early results of this work was the Klein-Gordon (KG) equation, which describes the motion of spin-0 particles (bosons). Interestingly, this equation allows solutions which correspond to particles with negative energies and give rise to negative probability densities in the KG equation. For these reasons, the KG equation was quickly abandoned. Not long later, Dirac proposed the Dirac equation for spin-1/2 particles (fermions). Although the Dirac equation solves the issue of a negative probability density, it still allows negative energy solutions. The question for physicists at the time was how should these solutions be interpreted physically?

Dirac's original explanation for these negative energy solutions was given in terms of the electron. In his interpretation there is a sea of electrons, all with negative charge. Negative energy solutions then correspond to a "hole" or the absence of an electron. This hole is interpreted as a particle of positive charge, known as the positron. The electron and positron were thus the first case of a particle-antiparticle pair, and the positron was discovered in 1932 shortly after Dirac's proposed explanation [1].

Unfortunately, although the Dirac sea interpretation was perfectly valid for particles obeying the Dirac equation (fermions), it could not account for the negative energy solutions of the KG equation (corresponding to bosons) since these aren't restricted by the Pauli Exclusion Principle. Furthermore, the idea of exciting an electron from the Dirac sea and essentially creating an antiparticle seemed to violate conservation of particle number. This was the catalyst for a new description of matter in the form of quantum field theory and a new interpretation of the particle-antiparticle dynamic. The physical interpretation which superseded that of Dirac can be attributed to Feynman and saw positive energy antiparticle solutions identified with negative 4-momentum particle solutions. This applies equally well for both fermions and bosons and is fully compatible with the quantum field theo-

retic description of matter, which allows for particle and antiparticle creation and annihilation [1].

Although on the face of it there is no reason we should observe more matter than antimatter, we in fact do, and it has been well known for decades that there is a non-zero matter-antimatter asymmetry in the universe. The possible causes for this asymmetry include the violation of CP invariance, a symmetry which sees particles and antiparticles switched, with their momentum directions inverted. We will go into more detail about this symmetry in the next chapter, but first we briefly introduce the framework underpinning our currently most successful understanding of particle physics, the Standard Model.

1.1 The Standard Model

The Standard Model (SM) is a gauge field theory combining the work of countless particle physicists. From the building blocks of quantum field theory, the SM consists of two classes of fields, fermionic and bosonic, and it is the excitation of these which leads to the observation of the particles known as fermions and bosons.

The term "fermion" includes both particles and antiparticles with the key types being quarks and anti-quarks (q and $\bar{q}$), leptons and anti-leptons (l and $\bar{l}$), and neutrinos and anti-neutrinos (ν_l and $\bar{\nu}_l$). Each of these classes of fermion comes in various flavours, shown in Figure 1.1.

One of the most bizarre phenomena in particle physics is that to do with quark confinement, which amounts to the fact that one can never observe a single quark. Rather, quarks are only ever observed in $q_1\bar{q}_2$ pairs known as *mesons*, $q_1q_2q_3$ structures known as *baryons*, or possibly in more exotic structures such as $q_1q_2q_3q_4\bar{q}_5$ called pentaquarks. Collectively, these composite particles are known as *hadrons*, with examples such as the proton and neutron (baryons) and the pions and kaons (mesons). In this work we will only encounter mesons, and the list of relevant mesons with associated properties is given in Appendix C.

The interactions which take place in the SM are facilitated by the gauge bosons shown in Figure 1.1. Each corresponds to one of three forces in nature which arise from gauge symmetries [1]. These are the electromagnetic force (mediated by the photon γ), the weak nuclear force (mediated by the W bosons $W^{\pm}$ and Z boson Z^0) and the strong nuclear force (mediated by the gluon g). When the electromagnetic force is married with quantum mechanics we obtain a theory known as quantum electrodynamics (QED), with the strong force likewise being governed by quantum chromodynamics (QCD). The weak nuclear force and QED arise from the unified electroweak force [2–4]. The fourth force of nature, gravity, is as of yet non-conducive with the SM. Nevertheless, the SM currently provides the most successful model of particle physics. In this chapter we'll briefly introduce the electroweak force and QCD and outline how these allow the particles which exist in the SM (see Figure 1.1) to interact. A more detailed look at the weak interactions between quarks will be given in chapter 3.

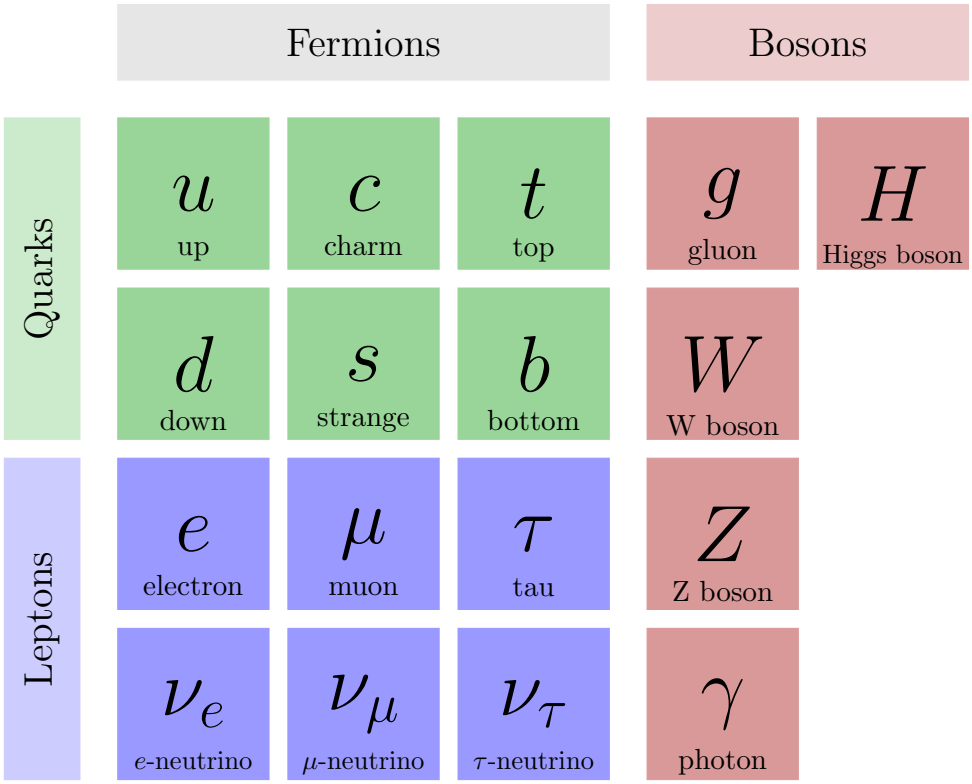

Figure 1.1: Table of the various elementary particles in the Standard Model arranged into fermions and bosons.

1.1.1 The Electroweak Force

The electroweak interaction is defined by the symmetry group $\mathrm{SU}(2)_L \times \mathrm{U}(1)_Y$ where the subscript L denotes left-handed chirality and Y denotes weak hypercharge [1]. The Lagrangian for the gauge fields arising through $\mathrm{SU}(2)_L \times \mathrm{U}(1)_Y$ symmetry breaking is given by [1] as

$$\mathcal{L} = (D_\mu \phi)^\dagger (D^\mu \phi) + \mu^2 \phi^\dagger \phi - \frac{\lambda}{4}(\phi^\dagger \phi)^2 - \frac{1}{4}\boldsymbol{F}_{\mu\nu} \cdot \boldsymbol{F}^{\mu\nu} - \frac{1}{4} G_{\mu\nu} G^{\mu\nu}\,, \tag{1.1}$$

where the covariant derivative is written

$$D^\mu \phi = \left(\partial^\mu + i\frac{g}{2}\boldsymbol{\tau} \cdot \boldsymbol{W}^\mu + i\frac{g'}{2} B^\mu\right)\phi\,, \tag{1.2}$$

and the terms proportional to μ^2 and λ are for the Higgs potential. The field strength tensor for the SU(2) symmetry is

$$\boldsymbol{F}^{\mu\nu} = \partial^\mu \boldsymbol{W}^\nu - \partial^\nu \boldsymbol{W}^\mu - g \boldsymbol{W}^\mu \times \boldsymbol{W}^\nu\,, \tag{1.3}$$

while that for U(1) is

$$G^{\mu\nu} = \partial^\mu B^\nu - \partial^\nu B^\mu\,. \tag{1.4}$$

The fields $\boldsymbol{W}^\mu = (W_1^\mu, W_2^\mu, W_3^\mu)$ and B^μ form the gauge bosons for the electromagnetic and weak interactions through the following linear combinations. The physical W bosons have fields given by

$$W_\pm^\mu \equiv \frac{1}{\sqrt{2}}(W_1^\mu \mp iW_2^\mu)\,, \tag{1.5}$$

while for the Z boson and photon we take the orthogonal linear combinations

$$Z^\mu \equiv \cos\theta_W W_3^\mu - \sin\theta_W B^\mu\,, \tag{1.6}$$
$$A^\mu \equiv \sin\theta_W W_3^\mu + \cos\theta_W B^\mu\,. \tag{1.7}$$

The mixing angle θ_W is known as the Weinberg angle, and takes the value such that the electromagnetic charge e, the mass of the W bosons m_W and Fermi's constant G_F are related by

$$\frac{G_F}{\sqrt{2}} = \frac{e^2}{8m_W^2\sin^2(\theta_W)} = 8.25\times10^{-6}\ \text{GeV}^{-2}\,. \tag{1.8}$$

Fermi's constant is an important indication of the strength of the weak interactions, as we'll come to see in chapter 3. The interactions mediated by the electroweak bosons are depicted in Figures 1.2 and 1.3.

To round out our discussion of the electroweak interactions, we note that the Higgs boson is the most recent of the gauge bosons to have been discovered, and is responsible for the W and Z bosons gaining mass as well as the renormalizability of the electroweak interactions [1].

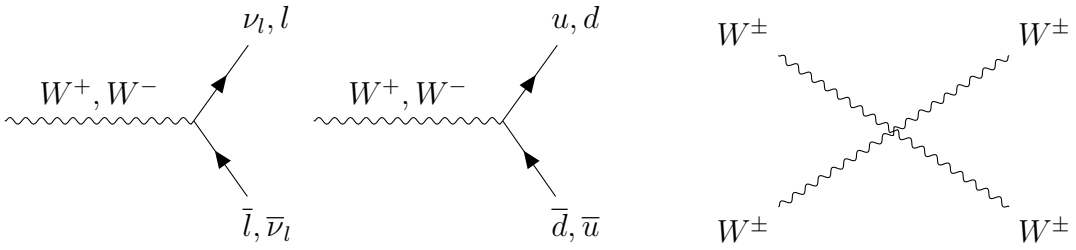

Figure 1.2: Feynman diagrams showing the interaction vertices involving fermions and the weak bosons $W^\pm$. l denotes an electron, muon or tau lepton, with ν_l the corresponding neutrino. u and d denote up- and down-type quarks respectively ($u = u\,, c\,, t$ and $d = d\,, s\,, b$).

1.1.2 Quantum Chromodynamics

Quantum Chromodynamics (QCD) is a gauge field theory under the SU(3) colour symmetry [1]. We thus attribute a degree of freedom known as colour to the quarks and this allows the force carrier for QCD, the gluons, to interact with the quarks.

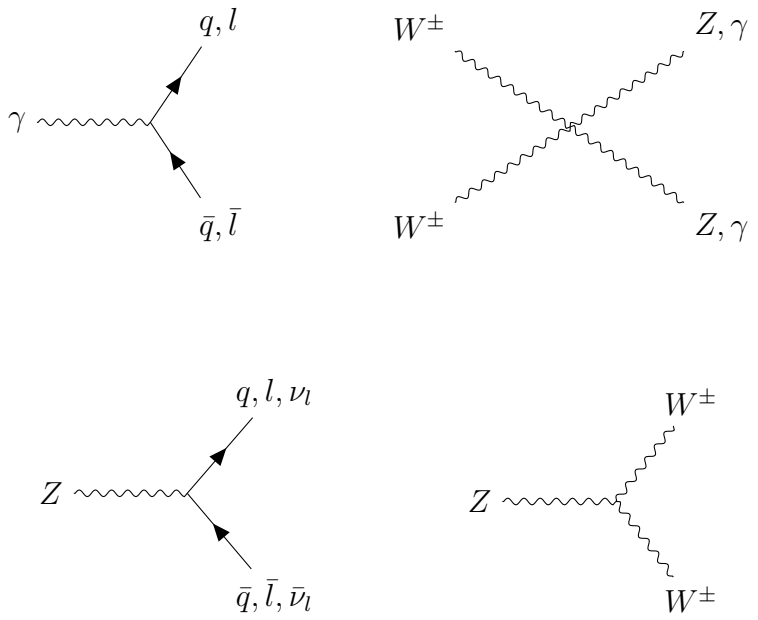

Figure 1.3: Feynman diagrams showing the interaction vertices involving the electroweak bosons Z^0 and γ. All the interactions shown are flavour conserving, so in this case q denotes a single flavour of quark (likewise, the label l denotes a single flavour of lepton/neutrino).

Additionally, since the gluons themselves carry colour, they self interact. We can see this from the full QCD Lagrangian

$$\mathcal{L}_{QCD} = -\frac{1}{4}(\partial_\mu A^a_\nu - \partial_\nu A^a_\mu + g f^{abc} A^b_\mu A^c_\nu)(\partial^\mu A^{a\nu} - \partial^\nu A^{a\mu} + g f^{ade} A^{d\mu} A^{e\nu}) - \frac{1}{2\xi}(\partial_\mu A^{a\mu})^2 - \bar{\eta}^a \partial_\mu (\partial^\mu \delta^{ac} - g f^{abc} A^{b\mu}) \eta^c + \bar{\psi}[i\gamma_\mu(\partial^\mu - igA^{a\mu}T^a) - m]\psi \,. \quad (1.9)$$

Here, A^a_μ are the gluon fields with colour index a, g is the gluon gauge coupling and f^{abc} are the structure constants for the $\mathrm{SU}(3)_{\mathrm{colour}}$ lie algebra. The first line comes from the gauging of $\mathrm{SU}(3)_{\mathrm{colour}}$ and contains terms where the gluons self interact [5]. The term involving ξ is a gauge fixing term with, for example, $\xi = 1$ in Feynman gauge. The term involving η^a describes the Faddeev-Popov interaction where the gluons interact with the ghost field η^a [5]. The last term is of most interest to us as it contains the interaction of the gluon field with that of a quark ψ. Here T^a refers to the generators of $\mathrm{SU}(3)_{\mathrm{colour}}$. The various interactions mediated by the gluons are depicted in Figure 1.4.

One of the defining qualities of QCD is to do with its coupling strength. This is typically characterised by α_S, which is related to the gluon coupling in the QCD Lagrangian by $\alpha_s = g^2/4\pi$. To be more precise, the coupling strength is written as $\alpha_S(Q^2)$ where Q^2 is the relevant momentum scale. In good agreement with the theoretical prediction, the coupling strength is characteristically large at low momenta and takes small values in high momenta regions. This then means we can encounter QCD in two regimes; at high momenta (equivalently high energies) one

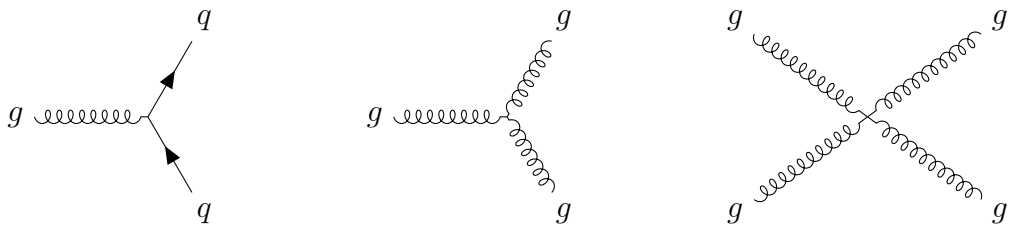

Figure 1.4: Feynman diagrams showing the interaction vertices involving gluons. The left diagram shows a gluon-quark-antiquark interaction, while the central and right diagrams depict gluon self interactions.

can solve QCD perturbatively. Conversely, at low energies, one must rely on non-perturbative methods such as Lattice QCD and factorisation in order to compute QCD amplitudes and other measurable quantities [6]. The running of the coupling is depicted in Figure 1.5. This behaviour of the strong nuclear force will be of particular interest for us when we discuss the Operator Product Expansion in chapter 3.

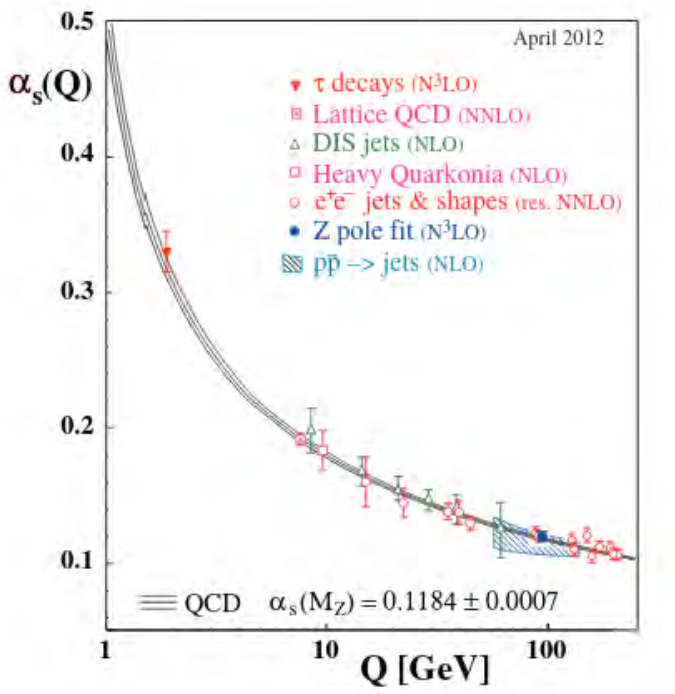

Figure 1.5: Plot of the running of α_S as a function of Q the momentum transfer. The solid curves show the theoretical prediction from perturbation theory, with the various data points taken from different experimental measurements. Figure taken from [6].

1.2 Chirality

To finish this chapter, we will briefly introduce the idea of "handedness" and chirality. If we consider a particle which has a spin vector in some direction and a

momentum vector in some (possibly different) direction, we can assign the particle a helicity. The helicity operator is defined as

$$h(\boldsymbol{p}) = \begin{pmatrix} \dfrac{\boldsymbol{\sigma}\cdot\boldsymbol{p}}{|\boldsymbol{p}|} & 0 \\ 0 & \dfrac{\boldsymbol{\sigma}\cdot\boldsymbol{p}}{|\boldsymbol{p}|} \end{pmatrix}, \tag{1.10}$$

where $\boldsymbol{\sigma}$ are the Pauli spin matrices

$$\sigma_1 = \begin{pmatrix} 0 & 1 \\ 1 & 0 \end{pmatrix}, \qquad \sigma_1 = \begin{pmatrix} 0 & -i \\ i & 0 \end{pmatrix}, \qquad \sigma_1 = \begin{pmatrix} 1 & 0 \\ 0 & -1 \end{pmatrix}. \tag{1.11}$$

The eigenstates of the helicity operator have the physical interpretation of eigenstates of the spin operator resolved along the direction of the particle momentum $\boldsymbol{p}$ [1].

We can then connect this idea of helicity with the eigenstates of the Dirac equation. In the representation where $\gamma_5 = \begin{pmatrix} 1 & 0 \\ 0 & -1 \end{pmatrix}$ and the Dirac spinors are written $u = \begin{pmatrix} \phi \\ \chi \end{pmatrix}$, the two-component spinors ϕ and χ satisfy

$$(\boldsymbol{\sigma}\cdot\boldsymbol{p})\phi = E\phi - m\chi \qquad \text{and} \qquad (\boldsymbol{\sigma}\cdot\boldsymbol{p})\chi = -E\chi + m\phi\,. \tag{1.12}$$

In the limit of massless particles (an often useful approximation for the masses of the u and d quarks) $E \to |\boldsymbol{p}|$ and the two component spinors of the Dirac equation become helicity eigenstates with $h(\boldsymbol{p})\phi = +\phi$ and $h(\boldsymbol{p})\chi = -\chi$. Typically, one then defines the left and right **projection operators**

$$P_R = \frac{1+\gamma_5}{2}, \qquad P_L = \frac{1-\gamma_5}{2}. \tag{1.13}$$

These are so named since clearly

$$P_R \begin{pmatrix} \phi \\ \chi \end{pmatrix} = \begin{pmatrix} \phi \\ 0 \end{pmatrix}, \qquad P_L \begin{pmatrix} \phi \\ \chi \end{pmatrix} = \begin{pmatrix} 0 \\ \chi \end{pmatrix}, \tag{1.14}$$

and so the operators project out those components with positive or negative helicity. The names left- and right-handed originate from the right-hand rule for angular momentum and refer to the idea that a right-handed state has its spin and 3-momentum completely aligned while a left-handed state has its spin and 3-momentum entirely anti-aligned. In the theory of weak interactions, we'll see that the W bosons only connect quark spinors which are left-handed. We write these spinors as q_L, with q the flavour of the quark; conversely the right-handed spinors are written q_R.

Chapter 2

CP Violation

With the brief introduction to the SM in the previous chapter, we move on to describing the idea of symmetry in the SM. Specifically, we discuss the charge conjugation and parity symmetries individually before discussing the combined CP symmetry. We do this from a formal standpoint with historical examples given of key experimental results. In particular, we use typical examples of the first evidence of CP violation in the kaon system. We then proceed with a summary of the decays of B mesons and go on to describe the typical B-factory. The chapter closes with a summary of a key result obtained at the Belle detector facility from recent years.

2.1 Symmetries

Symmetries play an integral role in physics, informing one about conserved quantities and guiding the construction of new theories of the universe. We say that a system or theory exhibits a particular symmetry when it remains invariant under the corresponding transformation. Typically we consider two main classes of symmetry; continuous and discrete. Continuous symmetries are observed under the repeated application of infinitesimal transformations such as translations and rotations. These examples lead to the famous conservation laws for linear and angular momentum. The second class of symmetries are the discrete symmetries. Typical examples of the discrete transformations giving rise to these symmetries are parity, charge conjugation and time reversal. We elaborate on these below. Additionally, here we introduce the notation that P, C and T refer to the parity, charge conjugation and time reversal transformations while P, C and T denote the associated symmetries.

2.1.1 Parity

The parity transformation P is defined as

$$P: \qquad (t, \boldsymbol{x}) \to (t, -\boldsymbol{x}) \,, \tag{2.1}$$

where we recognise that this really just means "reverse all the signs of the components of a state's position vector". This is not the only way we can interpret P.

When it acts on a coordinate system rather than a state, it changes a right handed frame to a left handed frame and vice versa [7] and this has implications for allowed processes. For our case we mainly consider P acting on states rather than coordinate frames.

Clearly, if we act twice with P on a state, we should observe no change ($P^2 = \mathbb{I}$) and so, for the action of P on some real scalar field ϕ, we have

$$P: \qquad \phi(t, \boldsymbol{x}) \to \pm\phi(t, -\boldsymbol{x})\,. \tag{2.2}$$

Generalising to complex scalar fields, we have

$$P: \qquad \phi(t, \boldsymbol{x}) \to \eta\phi(t, -\boldsymbol{x})\,, \tag{2.3}$$

where η is a complex phase referred to as the *intrinsic parity* of a particle. A priori there is no reason the intrinsic parity of a particle should take a particular value. However, we can refine our definition of parity to give particular particles values of $+1$ for their parity; the result of this is that others receive a -1.

Consider the following global symmetry for QED,

$$\tilde{P}: \qquad \phi \to e^{i\alpha Q}\phi \tag{2.4}$$

for any $\alpha \in \mathbb{R}$ and for Q the charge of the field ϕ. Then suppose P^2 is a subgroup of this global symmetry. Since

$$\tilde{P}^2: \qquad \phi(t, \boldsymbol{x}) \to e^{i\alpha Q}e^{i\alpha' Q}\phi(t, \boldsymbol{x}) = e^{i\beta Q}\phi(t, \boldsymbol{x})$$

for some $\beta \in \mathbb{R}$, we observe $\eta^2 = e^{i\beta Q}$ and so $\eta = \pm e^{i\frac{\beta}{2}Q}$. Now we are free to redefine the parity operator to be $P' = Pe^{-i\frac{\beta}{2}Q}$ such that

$$P': \qquad \phi(t, \boldsymbol{x}) \to Pe^{-i\frac{\beta}{2}Q}\phi(t, \boldsymbol{x}) = \pm e^{-i\frac{\beta}{2}Q}e^{i\frac{\beta}{2}Q}\phi(t, -\boldsymbol{x}) = \pm\phi(t, -\boldsymbol{x})\,. \tag{2.5}$$

Hence all elementary particles have an intrinsic parity of ± 1 under this new definition of parity. We can go a step further by recognising two more global symmetries within the Standard Model; lepton number L and baryon number B. In much the same way as for the global symmetry due to electric charge, we have that, if P^2 is also a subgroup of these other global symmetries, then

$$P^2 = e^{i(\alpha B + \beta L + \gamma Q)} \tag{2.6}$$

for some α, β and $\gamma \in \mathbb{R}$. Redefining our parity operator once more to be $P' = Pe^{-\frac{i}{2}(\alpha B + \beta L + \gamma Q)}$, we observe that now all SM particles, including hadrons, have parity ± 1.

It is a simple matter of convention now as to which particles have odd ($\eta = -1$) or even ($\eta = +1$) parity. If we happened to assign odd parity to the proton for instance, we could introduce another phase to set the intrinsic parity of the proton

to be positive. Taking $P'' = (-1)^B P'$ then under this new definition of parity, the proton has $\eta = +1$ (where we recognise that the proton has baryon number $B = 1$). Similarly, one typically requires that the neutron and electron have even parity as well, and these are set by choosing phases corresponding to L and Q. All other baryons then have their intrinsic parities determined by this convention.

To assign intrinsic parities to the mesons, we can use the fact that Dirac bilinears transform according to the associated label (vector, pseudovector/axial vector, scalar, pseudoscalar and tensor) [8]. The forms of the bilinears are

$\bar{\psi}_1(x)\psi_2(x)$	Scalar S
$\bar{\psi}_1(x)\gamma_\mu\psi_2(x)$	Vector V
$\bar{\psi}_1(x)\sigma_{\mu\nu}\psi_2(x)$	Antisymmetric Tensor T
$\bar{\psi}_1(x)i\gamma_\mu\gamma_5\psi_2(x)$	Axial Vector A
$\bar{\psi}_1(x)\gamma_5\psi_2(x)$	Pseudoscalar P.

For completeness, the Dirac matrices $\gamma^\mu = (\gamma^0, \boldsymbol{\gamma})$ are given by

$$\gamma^0 = \beta\,, \qquad \boldsymbol{\gamma} = \beta\boldsymbol{\alpha}\,, \tag{2.7}$$

where the matrices β and α_i are given by

$$\beta = \begin{pmatrix} 1 & 0 \\ 0 & -1 \end{pmatrix}\,, \qquad \alpha_i = \begin{pmatrix} 0 & \sigma_i \\ \sigma_i & 0 \end{pmatrix}\,. \tag{2.8}$$

We've written the matrices in 2×2 block form where 1 represents the 2×2 identity matrix and the σ_i are the Pauli spin matrices. Thus, for example, the parity transformation acts on scalars and pseudoscalars as

$$P\,|S(t,\boldsymbol{x})\rangle = +\,|S(t,-\boldsymbol{x})\rangle\,, \qquad P\,|P(t,\boldsymbol{x})\rangle = -\,|P(t,-\boldsymbol{x})\rangle\,, \tag{2.9}$$

and for vectors and axial vectors as

$$P\,|V(t,\boldsymbol{x})\rangle = -\,|V(t,-\boldsymbol{x})\rangle\,, \qquad P\,|A(t,\boldsymbol{x})\rangle = +\,|A(t,-\boldsymbol{x})\rangle\,. \tag{2.10}$$

Then, the associated bilinear label for a meson tells us its action under parity.

Practically, one uses a convention to assign parities to some observable particles and then measures parities of other particles relative to this convention. Typically, the convention is

$$\eta_p = \eta_n = \eta_e \equiv +1\,, \qquad \eta_{K^-} = \eta_{D^-} = \eta_{B^-} \equiv -1\,, \tag{2.11}$$

where p and n denote the proton and neutron (baryons), e is the electron (lepton) and K^-, D^- and B^- are $\bar{u}s$, $\bar{u}c$ and $\bar{u}b$ mesons [9]. In order to relate parities between different particles, one uses conservation of parity; this requires electromagnetic and

strong processes only since, as we'll come to see, weak interactions do not conserve parity. Before we look at this though, we'll briefly note a second type of symmetry.

2.1.2 Charge Conjugation

The other type of discrete transformation we are interested in is charge conjugation C and this, like parity, was thought to produce an exact symmetry in all physical systems. C is the operator which "interchanges particles with their antiparticles without changing their positions or spins". To describe this transformation formally, we consider the Dirac equation, the equation of motion for all spin-1/2 particles.

Suppose we have some particle with electric charge e and spinor ψ_e. It obeys the Dirac equation

$$(i\not{D} - m)\psi_e = 0 \tag{2.12}$$

where D_μ is the covariant derivative for QED, defined to be $D_\mu \equiv \partial_\mu + ieA_\mu$ where A_μ is the electromagnetic 4-vector potential, and m is the mass of the particle. Expanding out the covariant derivative, we obtain

$$(\gamma^\mu(i\partial_\mu - eA_\mu) - m)\psi_e = 0\,. \tag{2.13}$$

Now, consider an antiparticle with charge $-e$ and antiparticle spinor ψ_{-e}; it obeys its own Dirac equation

$$(\gamma^\mu(i\partial_\mu + eA_\mu) - m)\psi_{-e} = 0\,. \tag{2.14}$$

From here, we'd like to investigate whether or not we can introduce a transformation of the particle spinor ψ_e such that we obtain a new spinor which obeys equation (2.14). If we can, then this transformation has exactly the property of the C operator, that is, it interchanges particles and antiparticles! We start by considering the gauge transformation

$$\psi \to \exp(ie\phi)\psi\,. \tag{2.15}$$

Taking the complex conjugate we obtain

$$\psi^* \to \exp(-ie\phi)\psi^* = \exp(i(-e)\phi)\psi^*\,. \tag{2.16}$$

This implies that the complex conjugate of a particle spinor transforms as the antiparticle spinor (opposite sign for the electric charge). This motivates us to consider the complex conjugate of equation (2.13)

$$(-\gamma^{\mu *}(i\partial_\mu + eA_\mu) - m)\psi_e^* = 0\,. \tag{2.17}$$

Then, we multiply on the left by some invertible matrix C and also multiply by the identity $C^{-1}C = \mathbb{I}$ to obtain

$$\begin{aligned} &C(-\gamma^{\mu *}(i\partial_\mu + eA_\mu) - m)C^{-1}C\psi_e^* = 0\,, \\ &(-C\gamma^{\mu *}C^{-1}(i\partial_\mu + eA_\mu) - m)C\psi_e^* = 0\,. \end{aligned} \tag{2.18}$$

At this point, if we can show that there exists some matrix C with $-C\gamma^{\mu *}C^{-1} = \gamma^\mu$ then $C\psi_e^*$ looks very much like it could be ψ_{-e}. We state without proof that a possible candidate for the charge conjugation operator is

$$C = -i\gamma_2 \tag{2.19}$$

where γ_2 is one of the Dirac matrices given in equation (2.7). We can then write the corresponding spinor transformation

$$C: \qquad \psi_e \to -i\gamma_2\psi_e^* \equiv \psi_{-e} \tag{2.20}$$

and take the complex conjugate to get the transformation of ψ^* under C

$$C: \qquad \psi_e^* \to (-i\gamma_2\psi_e^*)^* = +i\gamma_2^*\psi_e = -i\gamma_2\psi_e\,. \tag{2.21}$$

Returning to equation (2.20) we can write the transformation for the antiparticle spinor as

$$C: \qquad \psi_{-e} = -i\gamma_2\psi_e^* \to -i\gamma_2 C\psi_e^* = -i\gamma_2(-i\gamma_2\psi_e) = +\psi_e\,. \tag{2.22}$$

Hence we see that C is capable of interchanging particle and antiparticle spinors, and it also has the important property that $C^2 = \mathbb{I}$.

In much the same way as for parity, one defines some intrinsic charge parities for a selection of observable particles and then all others are determined relative to these. Importantly, only particles which are their own antiparticles have intrinsic charge-parities [9], for example the π^0 and the $\phi(1020)$. These particles consist of $q\bar{q}$ pairs exclusively and so C acts to just interchange the particles within each pair, so the result is just the original particle. With an odd number of quarks, the baryons cannot be eigenstates of C and so do not have intrinsic C-parities; only those mesons which are their own antiparticles do.

2.2 C and P Violation

Over the previous two sections we've looked at how one typically defines the parity and charge conjugation transformations. We will now look at the historical developments which led to our current understanding of CP violation, namely the work pioneered by Lee, Yang and Wu, which led to the overthrow of the idea that parity and charge conjugation were conserved quantities.

2.2.1 Parity Violation in the Decays of ^{60}Co Nuclei

Until the mid 1950s, parity conservation was taken for granted in every area of particle physics, an assumption supported by an abundance of examples of parity conservation in both electromagnetic and strong interactions. Even though there was nothing to show it was a symmetry of the weak interaction, it wasn't until 1956, when Lee and Yang first realised this, that P violation was seriously considered [10]. Motivated by the "$\theta - \tau$ puzzle" (more on this later) and after realising that weak interactions could be a source of P violation, Lee and Yang proposed the now famous ^{60}Co experiment which would later be conducted by Wu and her collaborators [11]. The experiment involved taking a sample of ^{60}Co nuclei and aligning their spins. This in and of itself presented many challenges, such as needing to lower the temperature of the sample to 0.01K, so perhaps it isn't so surprising that such an experiment had not been performed prior to this! The sample then decayed via the weak process

$$^{60}\text{Co} \rightarrow ^{60}\text{Ni} + e^- + \bar{\nu}_e \tag{2.23}$$

and the emission of the electrons was measured using an array of detectors. The parity transformed system was then considered, as shown in Figure 2.1.

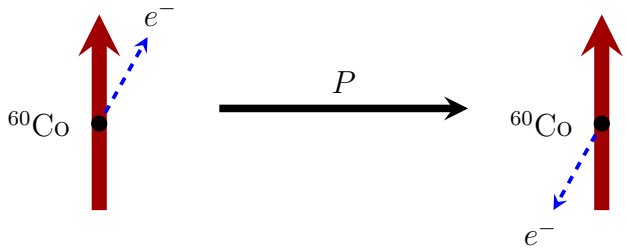

Figure 2.1: Cartoon of the action of P on the ^{60}Co nuclei in Wu's parity violation experiment. The spin of the nucleus is shown as a solid red arrow, while the electron momentum is depicted as a blue dashed arrow. The parity transformation reverses the direction of the electron's momentum without changing the direction of the nucleus' spin.

The parity operator doesn't alter the spin of the nuclei since angular momentum, and thus spin, is a pseudovector (even under parity). On the other hand, parity inverts the 3-momentum vectors of the emitted electrons, reversing the direction of emission. The principle of the experiment conducted by Wu is that, assuming parity is a perfect symmetry of the weak force, the electrons should have no preferred direction to be emitted in. If there was some predilection for a particular direction of emission, say in the same direction as the nuclear spin, then the parity transformed process in which electrons are emitted in the opposite direction to nuclear spin would be just as valid. In other words, if the weak interaction was invariant under parity, then there should have been equal rates for both processes in Figure 2.1 and so a uniform angular distribution of electron emission. But Wu observed that the

electrons tended to be emitted in the direction *opposite* to the nuclear spin, giving rise to the left-right asymmetry, and this was the first direct evidence of parity violation!

2.2.2 Charge Conjugation Violation in the Decays of Pions

With the fall of parity as a symmetry of weak interactions, one might question whether charge conjugation is similarly violated; it turns out that indeed it is. In a letter accompanying that of Wu and her team [12], Garwin, Lederman and Weinrich reported their findings in the two stage weak decay process

$$\pi^+ \to \mu^+ + \nu_\mu \,, \qquad \mu^+ \to e^+ + \nu_e + \bar{\nu}_\mu \,. \tag{2.24}$$

They found that the positrons were emitted predominantly in one direction and this had immediate consequences for the polarisation of the muons [12]. Consider that the π^+ has spin-0 and decays at rest so the μ^+ and ν_μ necessarily come out back-to-back with opposite spin projections along the momentum axis. Hence they are both either left- or right-handed. However, right-handed neutrinos and left-handed anti-neutrinos don't exist (or at least we haven't been able to observe them so far) and so the μ^+ is necessarily left-handed to match its accompanying neutrino.

The μ^+ goes on to decay to the positron, neutrino and anti-neutrino. Taking the high energy, relativistic limit of this process, the neutrino and anti-neutrino are emitted in the same direction, opposite to the positron [9]. Then, since the neutrino and anti-neutrino have opposite handedness, their spin projections along the momentum axis cancel. As a result, the positron must have the same component of spin as the muon to conserve angular momentum. Finally, since relativistic positrons are always right-handed (just as antineutrinos are always observed to be right-handed) [9], the positron *must* be emitted in the same direction as the μ^+ spin. The exact same arguments hold for the charge conjugated process whereby the μ^- emits an electron in the direction opposite to its spin.

The simplest way to see that C and P are both violated in this overall process is to perform the parity and charge conjugation transformations shown in Figure 2.2. Clearly, starting from either of the two allowed cases and applying either C or P we obtain a helicity forbidden emission, so both C and P are violated. This is in fact what was observed experimentally; the positrons produced were preferentially emitted in a particular direction with a noticeable suppression of the helicity forbidden regime attained by the relativistic limit. This immediately meant that invariance under parity was violated.

In concurrent work by Lee, Oehme and Yang, it was proven that for decays in which the final states were incapable of interacting strongly (as is the case for the purely leptonic final states in this decay chain), left-right asymmetries which give rise to P violation are not possible if C is conserved [13]. So when Garwin *et. al.* measured an asymmetry in the emission of the positrons in the final state, this meant that not only was parity violated, but so too was charge conjugation [12].

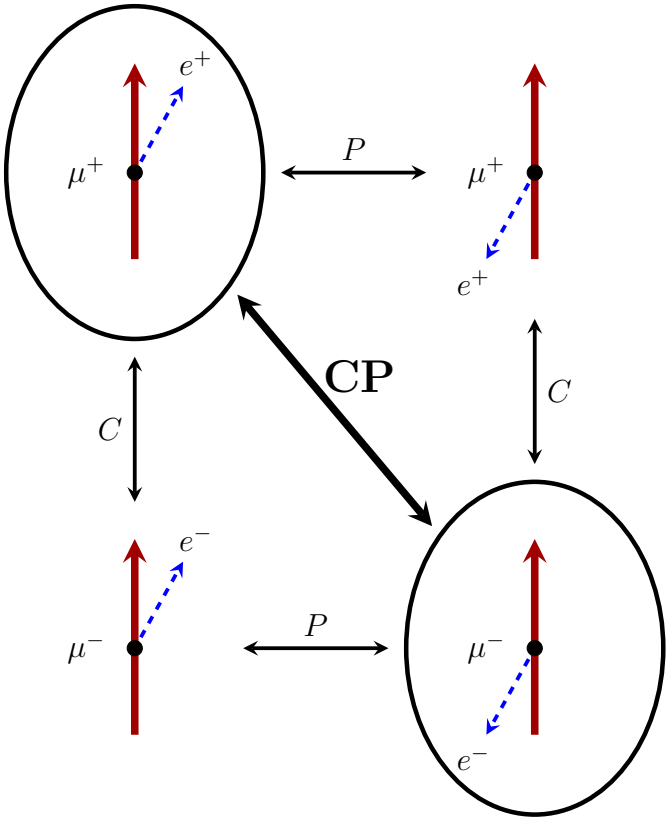

Figure 2.2: Flow chart showing the way C and P transform the decay of the muons. The helicity allowed states are circled and connected by an overall CP transformation. C acts to interchange particles with antiparticles ($e^+ \leftrightarrow e^-$ and $\mu^+ \leftrightarrow \mu^-$) while P acts to invert the 3-momentum of the emitted electron/positron (shown as a dashed blue line). The spin direction of the muon/anti-muon (shown as a thick red arrow) is unaffected by either transformation.

A final thing to note about Figure 2.2 is that the two observable emission processes are connected by a CP transformation, that is, applying the two transformations C and P consecutively. This then is an example where the individual symmetries C and P are violated, yet the system respects invariance under the CP operator. So it seems that although these individual symmetries may break down in weak interactions, this composite operator may still provide a valid symmetry. It turns out though that CP symmetry is also violated in some weak processes.

2.2.3 Time Reversal and CPT

In addition to the parity and charge conjugation operators, we can also construct the time reversal operator, which is defined by

$$T : (t, \boldsymbol{x}) \to (-t, \boldsymbol{x})\,. \tag{2.25}$$

We won't go into much more detail here, other than to say that one of the requirements of any theory in the SM is that it is CPT invariant [1,8,14]. This leads to the equality of masses and the equal magnitude but opposite sign of charge for particles and antiparticles, both of which have been rigorously tested [1]. All measurements have been in strong agreement with CPT invariance.

As a result of CPT invariance and the violation of C and P, there are cases then where T symmetry is also violated. In fact, one necessarily finds that the degree to which T invariance is violated is equal but opposite to that of the combined CP symmetry such that CPT remains invariant.

2.3 CP Violation

Although C and P symmetries are violated in weak processes, if one considers the combined CP symmetry this is in many circumstances a stronger symmetry than either C or P individually. However, one can find examples of CP violation as well, typically in the decays of kaons, and more recently in those of B mesons and D mesons.

2.3.1 CP Violation in Kaons

The first direct measurement of CP violation was made in the decays of neutral kaons. The neutral kaons K^0 and $\bar{K}^0$ are flavour eigenstates and not CP eigenstates since the CP operator acts on them in the following way:

$$CP\left|K^0(t,\boldsymbol{p})\right\rangle = -C\left|K^0(t,-\boldsymbol{p})\right\rangle = -\left|\bar{K}^0(t,-\boldsymbol{p})\right\rangle , \tag{2.26}$$

$$CP\left|\bar{K}^0(t,\boldsymbol{p})\right\rangle = -C\left|\bar{K}^0(t,-\boldsymbol{p})\right\rangle = -\left|K^0(t,-\boldsymbol{p})\right\rangle . \tag{2.27}$$

One typically forms CP eigenstates from the neutral kaons by defining

$$K_1 \equiv \frac{K^0 - \bar{K}^0}{\sqrt{2}} , \qquad K_2 \equiv \frac{K^0 + \bar{K}^0}{\sqrt{2}} . \tag{2.28}$$

Clearly K_1 is even under CP while K_2 is odd. Then, if CP is an exact symmetry of the SM, K_1 should decay to a 2π state (which is also CP even) and K_2 will decay to a 3π state (which is CP odd) [9]. CP being an exact symmetry means there would be no $K_1 \to 3\pi$ or $K_2 \to 2\pi$ decays. Since the allowed phase space is less for the 3π final state compared to the 2π final state, we would then expect that K_2 is longer lived than K_1.

In 1964, Christenson *et. al.* observed that the longer lived K_2 could decay to the 2π final state, albeit only a minute fraction of the time [15]. Nevertheless, this showed that CP was not conserved in the weak decays of kaons. One can quantify the degree of CP violation by considering mass eigenstates. Consider that if CP was conserved then the commutator of CP with the weak Hamiltonian would be zero and K_1 and K_2 would be mass eigenstates as well as CP eigenstates. However, CP

is not conserved and so the commutator is non-zero and the K_1 and K_2 states are not mass eigenstates (they can mix with one another). The mass eigenstates are instead written as small deviations from the states K_1 and K_2

$$K_S = K_1 + \epsilon K_2\,, \qquad\qquad K_L = K_2 - \epsilon K_1\,, \tag{2.29}$$

read as "K-short" and "K-long" to denote the short and long lived states respectively. Here ϵ measures the degree of CP violation ($\epsilon = 0$ implies CP is conserved).

One type of CP violation we can assign to this example is that due to **mixing**; the K_1 and K_2 CP eigenstates are capable of mixing through processes such as that shown in Figure 2.3 to form the mass eigenstates K_L and K_S which then decay to otherwise CP forbidden final states. However, there is another type of CP violation which may occur whereby, say, the K_2 can decay directly to the 2π final state without first mixing with the K_1. This is known as **direct** CP violation, and this is typically characterised by a process and its CP conjugate process having different decay rates. A third type of CP violation can occur through the **interference between mixing and direct decay** [5, 8].

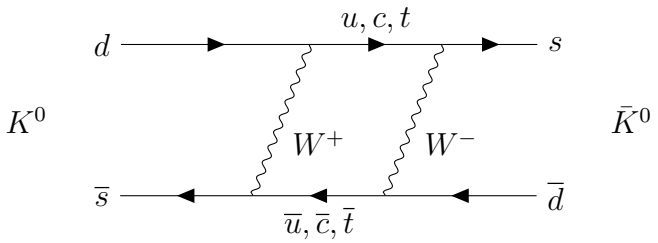

Figure 2.3: Feynman diagram showing the mixing between the neutral kaons.

The degree of violation measured for all three forms of CP violation in the kaon system is non-zero though still quite small [8]. However, the decays of kaons aren't the only sources of CP violation in the SM; B mesons and D mesons afford another avenue for sources of CP violation.

2.3.2 CP Violation in B Mesons

In analogy with the kaon mixing described above and shown in Figure 2.4, one can analyse the decays of the neutral B mesons through the mixing of the CP violating mass eigenstates B_L and B_H (L and H stand for "light" and "heavy"). These particles have very nearly identical lifetimes of about $1.5 \times 10^{-12} s$, which is significantly shorter than those of the kaon equivalents K_S and K_L [9]. This short a lifetime presents the biggest obstacle to B meson analyses for although it's predicted in the SM that the B mesons should be ideal laboratories for studying CP violation, it was historically difficult to produce and maintain a steady beam of B mesons without them decaying away too rapidly. This challenge was eventually solved by using Beauty/Bottom Factories.

As an aside, we've only addressed CP violation due to mixing in the B mesons. However, just as for the kaon example, one can measure direct CP violation by comparing the decay amplitudes for a B meson decaying to some final state as compared to a $\bar{B}$ meson decaying to the CP conjugate final state. We're exclusively interested in this type of CP violation and will explore it in more depth in chapter 4.

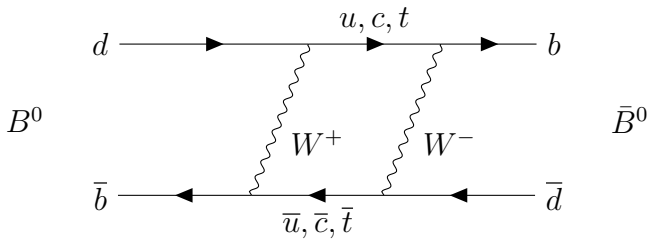

Figure 2.4: Feynman diagram showing the mixing between the neutral B mesons.

Beauty/Bottom Factories

In a naive experiment, one could have some source of B mesons but these would typically decay before we could begin any measurement, owing to their extremely short lifetimes. The novel realisation by physicists in the 1980's which allowed for the first detection of CP violation in B meson decays was to make use of the $\Upsilon(4S)$ resonance [16]. This $b\bar{b}$ state has the same quantum numbers as the photon so is typically produced at e^+e^- colliders. Furthermore, this particular resonance has a mass of 10.58 GeV, which is just at the threshold for $B - \bar{B}$ production. The result of all this is that the $\Upsilon(4S)$ is readily produced in e^+e^- colliders and decays almost exclusively to $B - \bar{B}$ pairs, with very little in the way of waste products. By tuning the e^+e^- beams, one is able to produce a large number of B mesons; enough that even though they decay rapidly, it is possible to maintain a steady beam of B mesons.

When they were first conceived, there were several proposals put forward for potential Beauty/Bottom factories (B-factories) and these were distilled to the current facilities at KEKB and PEP-II. These two laboratories consist of asymmetric-energy, circular e^+e^- colliders operating at the $\Upsilon(4S)$ resonance. The necessity of an asymmetric energy for the e^+e^- beams is a result of the time profile of the decays and the need for the $\Upsilon(4S)$ resonance to be produced not at rest in the laboratory frame [16].

The use of B-factories has allowed for a rich investigation into CP violation as well as other areas of flavour physics. These kinds of experiments allow physicists to explore some of the most complex and demanding questions in their field. The most relevant of these to CP violation is the matter-antimatter asymmetry present in the universe.

2.4 Matter-antimatter Asymmetry

At first glance, it might seem that CP being violated is a problem; it is in fact quite the opposite. It has been known for some time that there is an inherent predominance of matter over antimatter in the universe, although the exact reasons for this are still an open question. The groundwork for this avenue of research was laid by Sakharov when he postulated a model for **baryogenesis**, that is, the mechanism by which matter and antimatter density in the universe can fluctuate. In his 1966 paper, Sakharov proposed his famous three conditions for baryogenesis [17, 18]. Assuming an initial baryon-symmetric universe, baryogenesis occurs for interactions satisfying 1) baryon number B violation, 2) C and CP violation and 3) departure from thermal equilibrium.

The necessity for the first condition is somewhat obvious. Supposing that just after the Big Bang there was an equal number of baryons and anti-baryons ($B = 0$) then, if at some later point in time, there was an imbalance in the baryonic density ($B \neq 0$), there has clearly been a violation of baryon number along the way.

The violation of C in the second condition is necessary so that if there is a process which generates an excess of baryons, it is not counterbalanced by an exactly opposite process which generates the same excess of anti-baryons (which would leave the total baryon number unchanged). CP violation is then necessary for the same reasons but for left and right-handed baryons and anti-baryons.

The need for the third condition is not as immediately clear, although the proof is somewhat trivial. Starting from the equilibrium average for the baryon number operator at some temperature $T = 1/\beta$

$$\begin{aligned}\langle B\rangle &= Tr(e^{-\beta H}B)\\ &= Tr((CPT)(CPT)^{-1}e^{-\beta H}B)\\ &= Tr((CPT)^{-1}e^{-\beta H}B(CPT))\\ &= Tr(e^{-\beta H}(CPT)^{-1}B(CPT))\\ &= -Tr(e^{-\beta H}B)\end{aligned}$$

where we've used the cyclic property of the trace, $[CPT, H] = [(CPT)^{-1}, H] = 0$ and also the fact that B is odd under CPT [7]. Clearly, by comparing the first and second lines in the proof, the average baryon number is zero and so there is no matter-antimatter asymmetry if the interactions occur in thermal equilibrium (recall that thermal equilibrium was our initial assumption).

Although CP violation has been observed many times, in searches guided by the SM, the degree of violation hasn't been sufficient to fully account for Sakharov's second condition for baryogenesis [8]. This presents a real dilemma for physicists; if the SM can't predict large enough CP violations, then one may need to propose an extension to the theory or even come up with some entirely alternative explanation (such as dark matter). Fortunately, as we'll come to see, the Belle Collaboration had a recent measurement which reported an extremely large CP violation.

2.5 Belle Results

In their 2017 paper "Measurement of branching fraction and direct CP asymmetry in charmless $B^+ \to K^+K^-\pi^+$ decays at Belle", the Belle Collaboration reported an exceptionally significant CP violation. The study consisted of analysing data from the Belle detector at the KEKB collider, with 772×10^6 $B\bar{B}$ pairs in the data sample [19]. The Belle Collaboration reported their measurement of the CP violation in terms of the **CP asymmetry** for B^+ decays compared to B^- decays. This is quantified as

$$\mathcal{A}_{CP} = \frac{N^- - N^+}{N^- + N^+} \tag{2.30}$$

where $N^\pm$ refers to the number of $B^\pm \to K^+K^-\pi^\pm$ decays. They found an asymmetry of

$$\mathcal{A}_{CP} = -0.90 \pm 0.17 \pm 0.03 \tag{2.31}$$

in the K^+K^- invariant mass region $0.8 \leq m_{KK} \leq 1.1$ GeV/c^2 [19] where the invariant mass is define by $m^2_{KK} \equiv (p_{K^+} + p_{K^-})^2$. This means there was an excess of B^+ decays compared with B^- decays. This corresponds with the condition for direct CP violation, that is that the amplitudes for the decays are different,

$$A(B^+ \to K^+K^-\pi^+) \neq A(B^- \to K^+K^-\pi^-)\,. \tag{2.32}$$

The asymmetry is plotted in Figure 2.5 for various bins in m_{KK} the K^+K^- invariant mass, with the value quoted in equation (2.31) corresponding to the lowest m_{KK} bin. Clearly, an asymmetry of zero is indicative of CP conservation rather than violation. However, in general the asymmetry can take extreme values of ± 1, so the result obtained by Belle is highly significant.

While the Belle Collaboration suggested further studies by Belle and LHCb involving Dalitz analyses, we will investigate this ourselves, within the formalism of CP asymmetries arising from so called tree and penguin diagrams. Our analysis is guided by an effective Hamiltonian, to be discussed in the chapter immediately following this. Our goal is to produce a theoretical result for the CP asymmetry which is comparable to equation (2.31) and/or Figure 2.5.

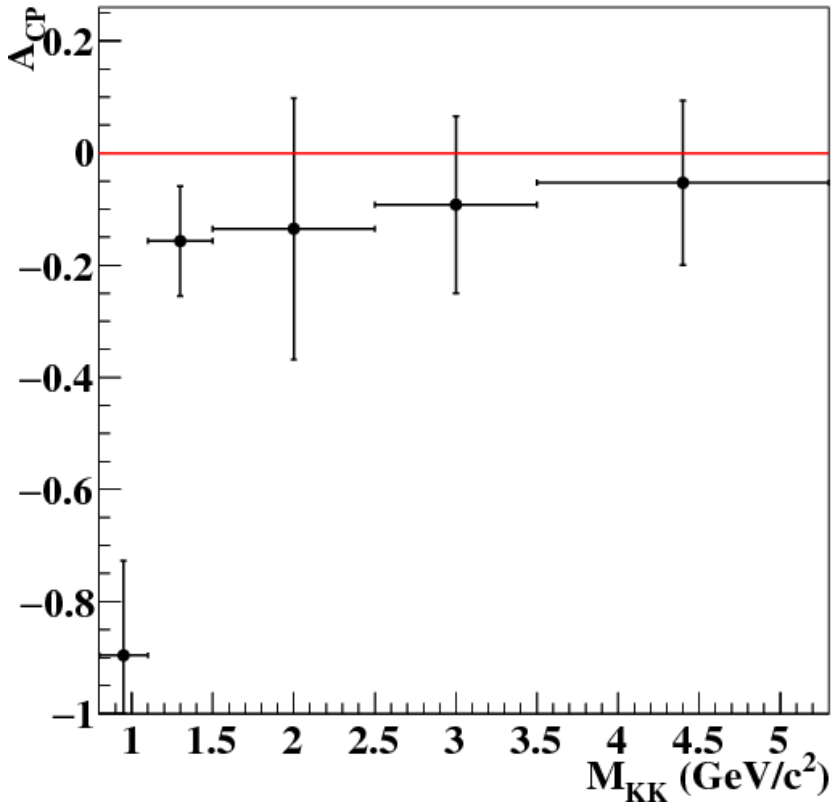

Figure 2.5: Plot of the CP violating asymmetry reported by Belle for five bins across the K^+K^- invariant mass range $0.8 \leq m_{KK} \leq 5.3$ GeV/c^2. The first bin $0.8 \leq m_{KK} \leq 1.1$ GeV/c^2 shows a significant CP asymmetry in the vicinity of $m_{KK} \sim 1$ GeV/c^2.

Chapter 3

Effective Hamiltonian

When calculating the CP asymmetry for a particular decay, one inevitably needs to compute the amplitudes for two types of processes known as tree and penguin decays and this is typically handled through an effective Hamiltonian approach. We begin by introducing the CKM quark matrix and the theory of four-fermion interactions and use these ideas, along with an Operator Product Expansion (OPE), to develop an effective Hamiltonian to describe the weak interaction. As part of this, we define the corresponding tree and penguin operators which appear in the Hamiltonian and the relevant Feynman diagrams. We conclude the chapter with a discussion of the Wilson coefficients in the OPE.

3.1 CKM Matrix

In the previous chapter we provided an overview of CP violation and the experiments which verified it. We return now to a discussion of the SM; specifically, we're interested in how the SM incorporates CP violation. From the historical observations of CP violation we know that it only occurs in weak interactions. As such, we'll delve exclusively into a discussion of this force.

In chapter 1 we introduced the three generations of quarks, and went on to describe the weak force which allows interaction between the quarks and leptons through the W and Z bosons. We also note that weak interactions are the only cases of flavour changing interactions in the standard model. In particular, the mixing of quark flavours through the W bosons is governed by a construction known as the Cabibbo-Kobayashi-Maskawa (CKM) matrix. We will go through the derivation of this matrix here, although we assume some prior familiarity with the relevant quantum field theory (a more fundamental derivation would take too long and would deviate from the intended scope of this work).

Starting from the mass terms in the Yukawa Lagrangian of the SM [8] we have

$$\mathcal{L}_{mass} = -Y^d_{ij}\bar{Q}^i H d^j_R - Y^u_{ij}\bar{Q}^i \tilde{H} u^j_R + h.c. \quad , \tag{3.1}$$

where *h.c.* are higher order corrections, Y^u and Y^d are Yukawa matrices, i and j are flavour indices, Q^i are the quark SU(2) doublets given by

$$Q^i = \begin{pmatrix} u_L \\ d_L \end{pmatrix}, \begin{pmatrix} c_L \\ s_L \end{pmatrix}, \begin{pmatrix} t_L \\ b_L \end{pmatrix}, \tag{3.2}$$

H is the Higgs multiplet ($\tilde{H} \equiv i\sigma_2 H$ where σ_2 is the second Pauli matrix) and $u_R^i \equiv (u_R, c_R, t_R)$ and likewise for d_R^i. After spontaneous symmetry breaking, the Higgs gains a vacuum expectation value (vev) and so the quark mass terms become

$$\mathcal{L}_{mass} = -\frac{v}{\sqrt{2}} Y_{ij}^d \bar{d}_L^i d_R^j - \frac{v}{\sqrt{2}} Y_{ij}^u \bar{u}_L^i u_R^j + h.c. \quad . \tag{3.3}$$

Writing this in terms of matrices, we have

$$\mathcal{L}_{mass} = -\frac{v}{\sqrt{2}} \big(\bar{d}_L Y_d d_R + \bar{u}_L Y_u u_R \big) + h.c. \quad . \tag{3.4}$$

We can then introduce two diagonal mass matrices M_u and M_d via the following arguments. First, note that $Y_d Y_d^\dagger$ and $Y_u Y_u^\dagger$ are clearly both hermitian ($YY^\dagger = (YY^\dagger)^\dagger$). Then clearly these matrices are also normal, that is, they commute with their hermitian conjugates. This is enough then to say that it is possible to diagonalise them by two different unitary similarity transformations [20]. We write these transformations as

$$U_d^\dagger Y_d Y_d^\dagger U_d = M_d^2 \,, \qquad U_u^\dagger Y_u Y_u^\dagger U_u = M_u^2 \,, \tag{3.5}$$

and we note that the diagonal mass matrices M_d and M_u introduced here are squared only for convenience; clearly if M is diagonal then so too is M^2. Then, using the unitarity of U_d and U_u, we rewrite equations (3.5) as

$$Y_d Y_d^\dagger = U_d M_d^2 U_d^\dagger \,, \qquad Y_u Y_u^\dagger = U_u M_u^2 U_u^\dagger \,. \tag{3.6}$$

We then write the Yukawa matrices explicitly as

$$Y_d = U_d M_d K_d^\dagger \,, \qquad Y_u = U_u M_u K_u^\dagger \,, \tag{3.7}$$

where we've introduced two new unitary matrices K_d and K_u. Clearly these definitions satisfy equation (3.6). Finally then, we can substitute these definitions for the Yukawa matrices into equation (3.4) and we get

$$\mathcal{L}_{mass} = -\frac{v}{\sqrt{2}} \Big(\bar{d}_L U_d M_d K_d^\dagger d_R + \bar{u}_L U_u M_u K_u^\dagger u_R \Big) + h.c. \quad . \tag{3.8}$$

At this point we perform a change of basis (to the **mass basis**) for each of the quark spinors

$$d_R \to K_d d_R\,, \qquad u_R \to K_u u_R\,, \tag{3.9}$$
$$d_L \to U_d d_L\,, \qquad u_L \to U_u u_L\,. \tag{3.10}$$

Substituting these in to our Lagrangian and leaving out the higher order terms for now, we get

$$\begin{aligned}
\mathcal{L}_{mass} &= -\frac{v}{\sqrt{2}}\Big(d_L^\dagger \gamma^0 U_d M_d K_d^\dagger d_R + u_L^\dagger \gamma^0 U_u M_u K_u^\dagger u_R\Big) \\
&\to\ -\frac{v}{\sqrt{2}}\Big((U_d d_L)^\dagger \gamma^0 U_d M_d K_d^\dagger K_d d_R + (U_u u_L)^\dagger \gamma^0 U_u M_u K_u^\dagger K_u u_R\Big) \\
&= -\frac{v}{\sqrt{2}}\Big(\bar{d}_L U_d^\dagger U_d M_d K_d^\dagger K_d d_R + \bar{u}_L U_u^\dagger U_u M_u K_u^\dagger K_u u_R\Big) \\
&= -\frac{v}{\sqrt{2}}\big(\bar{d}_L M_d d_R + \bar{u}_L M_u u_R\big)\,.
\end{aligned}$$

where we've made use of the definition of the "bar" notation as well as the unitarity of both U and K. This allows us to then write the mass terms in the mass basis as

$$\mathcal{L}_{mass} = -m_i^d \bar{d}_L^i d_R^i - m_i^u \bar{u}_L^i u_R^i + h.c. \quad , \tag{3.11}$$

where m_i^u are the diagonal elements of M_u and m_i^d are the diagonal elements of M_d. In other words

$$M_u = \frac{\sqrt{2}}{v}\begin{pmatrix} m_u & 0 & 0 \\ 0 & m_c & 0 \\ 0 & 0 & m_t \end{pmatrix}\,, \qquad M_d = \frac{\sqrt{2}}{v}\begin{pmatrix} m_d & 0 & 0 \\ 0 & m_s & 0 \\ 0 & 0 & m_b \end{pmatrix}\,. \tag{3.12}$$

So far, we've exclusively considered the mass terms in the electroweak Lagrangian, but there are also kinetic terms which may be altered under the change of basis we've imposed. Writing the full Lagrangian in the old flavour basis we have [8]

$$\begin{aligned}
\mathcal{L}_{flavour} = &\begin{pmatrix}\bar{u}_L & \bar{d}_L\end{pmatrix}^i \left[i\partial\!\!\!/ + \gamma_\mu \begin{pmatrix} \frac{g'}{6}B_\mu + \frac{g}{2}W_\mu^3 & \frac{g}{\sqrt{2}}W_\mu^+ \\ \frac{g}{\sqrt{2}}W_\mu^- & \frac{g'}{6}B_\mu - \frac{g}{2}W_\mu^3 \end{pmatrix}\right] \begin{pmatrix} u_L \\ d_L \end{pmatrix}^i \\
&+ \bar{u}_R^i\Big(i\partial\!\!\!/ + g'\frac{2}{3}B\!\!\!/\Big)u_R^i + \bar{d}_R^i\Big(i\partial\!\!\!/ - g'\frac{1}{3}B\!\!\!/\Big)d_R^i \\
&- \frac{v}{\sqrt{2}}\left[\bar{d}_L^i\Big(U_d M_d K_d^\dagger\Big)^{ij} d_R^j + \bar{u}_L^i\big(U_u M_u K_u^\dagger\big)^{ij} u_R^j + h.c.\right].
\end{aligned} \tag{3.13}$$

Here, i, j are flavour indices; g, g' are couplings in the electroweak theory; $B_\mu, W_\mu^3, W_\mu^\pm$ are the gauge fields corresponding to the weak bosons. The last line above consists of the mass terms we saw previously and we already know how these will transform under the change of basis to the mass basis. Now we just need to determine if and

how the kinetic terms (all the other terms) change under the same change of basis. In the second line of equation (3.13) we have the terms

$$\bar{u}_R^i\left(i\not{\partial}+\frac{2}{3}g'\not{B}\right)u_R^i+\bar{d}_R^i\left(i\not{\partial}-\frac{1}{3}g'\not{B}\right)d_R^i\,. \tag{3.14}$$

Under the change of basis to the mass basis, consider the transformations in equations (3.9) and (3.10). These can be written with their explicit indices as

$$\begin{aligned} u_R^i &\to K_u^{ij}u_R^j\,, & \bar{u}_R^i &\to \bar{u}_R^k(K_u^\dagger)^{ki}\,,\\ d_R^i &\to K_d^{ij}d_R^j\,, & \bar{d}_R^i &\to \bar{d}_R^k(K_d^\dagger)^{ki}\,, \end{aligned}$$

where we've used the property $(AB)^\dagger = B^\dagger A^\dagger$ to derive the transformations for $\bar{u}_R$ and $\bar{d}_R$. Substituting these transformations into expression (3.14), we notice that all the terms in brackets will commute with the K's (since the K's are constant and aren't affected by either $\not{\partial}$ or $\not{B}$) and so we can commute the K's through. We also note that the unitarity of K_u and K_d implies that

$$(K_u^\dagger)^{ki}K_u^{ij}=\delta^{kj}=(K_d^\dagger)^{ki}K_d^{ij}\,. \tag{3.15}$$

Putting this all together, the second line of equation (3.13) transforms in the following way when we change to the mass basis:

$$\begin{aligned} &\bar{u}_R^i\left(i\not{\partial}+g'\frac{2}{3}\not{B}\right)u_R^i+\bar{d}_R^i\left(i\not{\partial}-g'\frac{1}{3}\not{B}\right)d_R^i\\ &\to \bar{u}_R^k(K_u^\dagger)^{ki}K_u^{ij}\left(i\not{\partial}+\frac{2}{3}g'\not{B}\right)u_R^j+\bar{d}_R^k(K_d^\dagger)^{ki}K_d^{ij}\left(i\not{\partial}-\frac{1}{3}g'\not{B}\right)d_R^j\\ &=\bar{u}_R^j\left(i\not{\partial}+g'\frac{2}{3}\not{B}\right)u_R^j+\bar{d}_R^j\left(i\not{\partial}-g'\frac{1}{3}\not{B}\right)d_R^j\,. \end{aligned} \tag{3.16}$$

Hence the second line in equation (3.13) is invariant under the change of basis.

Turning our attention to the first line of equation (3.13) we can quickly see which pieces will be invariant. When we perform the change of basis for the left-handed quark spinors, the B_μ and W_μ^3 couplings don't change since these fields only couple two left quark spinors of the same handedness and up/down-type flavour. However, the couplings to $W_\mu^\pm$ *are* affected by the change of basis. We thus write the first line of the Lagrangian (in the mass basis) as

$$\frac{e}{\sqrt{2}\sin\theta_W}\left[W_\mu^+\bar{u}_L^i\gamma^\mu(V)^{ij}d_L^j+W_\mu^-\bar{d}_L^i\gamma^\mu(V^\dagger)^{ij}u_L^j\right], \tag{3.17}$$

where we've defined $V\equiv U_u^\dagger U_d$ and used $g=\frac{e}{\sin\theta_W}$ where e is the charge of an electron and θ_W is the weak mixing angle [8]. The matrix V has a special name, the **Cabibbo-Kobayashi-Maskawa (CKM) matrix**, named after the three physicists who discovered it. As we'll see shortly, the CKM matrix is required to be a

3×3 unitary matrix (so it explicitly requires three generations of quarks) in order to incorporate CP violation into the SM. The CKM matrix has the following form

$$V = \begin{pmatrix} V_{ud} & V_{us} & V_{ub} \\ V_{cd} & V_{cs} & V_{cb} \\ V_{td} & V_{ts} & V_{tb} \end{pmatrix} . \tag{3.18}$$

The CKM matrix is a 3×3 complex matrix. From the outset it has nine elements, each with a real and imaginary part, so a total of 18 potential degrees of freedom. However, the fact that it is unitary means that half of these are eliminated straight away. We see this by noting that the unitarity condition $V^\dagger V = \mathbb{I}$ leads to two types of equations; we'll denote these by *diagonal* equations, and *off-diagonal* equations.

The three diagonal equations are of the same form, for example

$$V_{ud}^* V_{ud} + V_{cd}^* V_{cd} + V_{td}^* V_{td} = 1 \,. \tag{3.19}$$

These are clearly real equations so give us just three constraints. The six off-diagonal equations are of a different form, for example

$$V_{ud}^* V_{us} + V_{cd}^* V_{cs} + V_{td}^* V_{ts} = 0 \,. \tag{3.20}$$

Of note though, is another of these equations

$$V_{us}^* V_{ud} + V_{cs}^* V_{cd} + V_{ts}^* V_{td} = 0 \,. \tag{3.21}$$

This is just the complex conjugate of equation (3.20) and so we don't get any new information. In fact, writing out all six off-diagonal equations one finds that they all come in pairs such as this and so we really only have three equations to work with. Clearly, these are complex equations and so we can solve each for a real and imaginary part. Hence, each of these three equations gives two equations, one for the real part, one for the imaginary part. Putting all this together, we see that the unitarity condition accounts for $3 + 3(2) = 9$ constraints and so the total number of degrees of freedom of V is reduced to nine.

We can go a step further though; we can take

$$d_L^j \to e^{i\alpha_j} d_L^j \,, \qquad d_R^j \to e^{i\alpha_j} d_R^j \,, \qquad u_L^j \to e^{i\beta_j} u_L^j \,, \qquad u_R^j \to e^{i\beta_j} u_R^j \,, \tag{3.22}$$

where $j = 1, 2, 3$, without affecting terms in the mass basis. Thus there is a global $\mathrm{U}(1)^6$ symmetry within the definitions of our quark spinors. Under these phase transformations, V will transform in some way. However, if one sets all the phases to be equal ($\alpha_j = \beta_j = \theta,\ j = 1, 2, 3$) then V will remain invariant. Clearly then, we can absorb five of these phases into the quark spinors, leaving a single overall phase in the CKM matrix, along with three as of yet unaccounted for degrees of freedom. We recognise these final three parameters as rotation angles by noting that if V was real, it would be an orthogonal matrix with three rotation angles.

In the **standard parametrisation** [8] one considers the rotation angles to describe rotations in the ij-flavour planes and we write $\theta_{12}\,, \theta_{23}$ and θ_{13} to denote these. The single phase of the CKM matrix is written as δ. Introducing the shorthand $c_{ij} \equiv \cos\theta_{ij}$ and $s_{ij} \equiv \sin\theta_{ij}$ one writes

$$V = \begin{pmatrix} c_{12}c_{13} & s_{12}c_{13} & s_{13}e^{-i\delta} \\ -s_{12}c_{23} - c_{12}s_{23}s_{13}e^{i\delta} & c_{12}c_{23} - s_{12}s_{23}s_{13}e^{i\delta} & s_{23}c_{13} \\ s_{12}s_{23} - c_{12}c_{23}s_{13}e^{i\delta} & -c_{12}s_{23} - s_{12}c_{23}s_{13}e^{i\delta} & c_{23}c_{13} \end{pmatrix}, \tag{3.23}$$

where $\theta_{12} = 13.02^\circ \pm 0.04^\circ$, $\theta_{23} = 2.36^\circ \pm 0.08^\circ$, $\theta_{13} = 0.20^\circ \pm 0.02^\circ$, $\delta = 69^\circ \pm 5^\circ$ [8]. Since all three rotation angles are quite small, the mass and flavour bases are only separated by a small degree. This leads to the CKM matrix having an almost diagonal structure. Additionally, since both θ_{23} and θ_{13} are far smaller than θ_{12}, one can redefine the matrix in terms of $\lambda \equiv \sin\theta_{12}$ using the **Wolfenstein parametrisation**. In this parametrisation the degrees of freedom are described by the parameters $\lambda\,, A\,, \rho$ and η. The matrix is written

$$\begin{pmatrix} 1 - \frac{1}{2}\lambda^2 & \lambda & A\lambda^3(\rho - i\eta) \\ -\lambda & 1 - \frac{1}{2}\lambda^2 & A\lambda^2 \\ A\lambda^3(1 - \rho - i\eta) & -A\lambda^2 & 1 \end{pmatrix} + \mathcal{O}(\lambda^4)\,, \tag{3.24}$$

where the new parameters are related to the old by

$$s_{12} = \lambda\,, \qquad s_{23} = A\lambda^2\,, \qquad s_{13}e^{-i\delta} = A\lambda^3(\rho - i\eta)\,. \tag{3.25}$$

The current estimates of the Wolfenstein parameters, taken from [21] are

$$\lambda = 0.22506 \pm 0.00050\,, \tag{3.26}$$
$$A = 0.811 \pm 0.026\,, \tag{3.27}$$
$$\rho = 0.124^{+0.019}_{-0.018}\,, \tag{3.28}$$
$$\eta = 0.356 \pm 0.011\,. \tag{3.29}$$

The Wolfenstein parametrisation will be used later when we start calculating the CP violating asymmetry. In particular, note that the parameter δ in the standard parametrisation is referred to as the CP violating phase (the same role is played by η in the Wolfenstein parametrisation). This phase is the single source of CP violation in the SM and the requirement of incorporating CP violation in the SM in a gauge invariant way was what prompted Kobayashi and Maskawa to posit the existence of a third generation of quarks, extending the work done by Cabibbo. CP violation arises through the **Jarlskog constant** which is defined as

$$J = \mathrm{Im}(V_{ud}V_{tb}V_{td}^*V_{ub}^*) \tag{3.30}$$

with CP violation occurring for $J \neq 0$. Current measurements place the value of J at $(3.18 \pm 0.15) \times 10^{-5}$ [21].

The CKM matrix provides one of the most promising avenues of research into physics beyond the Standard Model. For instance, were the universe to have a fourth generation of quarks available to it, then the CKM matrix would not be unitary [8]. Hence, by measuring the elements of the CKM matrix, one can test for unitarity and thus test the SM. The current best measurements for these elements are, according to [8],

$$\begin{aligned} |V| &= \begin{pmatrix} |V_{ud}| & |V_{us}| & |V_{ub}| \\ |V_{cd}| & |V_{cs}| & |V_{cb}| \\ |V_{td}| & |V_{ts}| & |V_{tb}| \end{pmatrix} \\ &= \begin{pmatrix} 0.97 \pm 0.0001 & 0.22 \pm 0.001 & 0.0039 \pm 0.0004 \\ 0.23 \pm 0.01 & 1.02 \pm 0.04 & 0.0041 \pm 0.001 \\ 0.0084 \pm 0.0006 & 0.039 \pm 0.002 & 0.88 \pm 0.07 \end{pmatrix} . \end{aligned} \tag{3.31}$$

3.2 Four Fermion Interactions

We've already come across a description of the weak interaction in equation (3.17) in our derivation of the CKM matrix. Now we'll try to develop a description we can use in our calculations of the CP asymmetry. Our approach is based on four-fermion interactions.

Early Forms

Four-fermion interactions were first proposed by Enrico Fermi in 1933 to describe nuclear β decay through the weak force [22]. When Fermi first put forward his description of the weak interaction, he framed it as

$$\mathcal{H}_{int}(x) = G\{\bar{\psi}_1(x)\gamma_\mu\psi_2(x)\}\{\bar{\psi}_3(x)\gamma_\mu\psi_4(x)\}\,, \tag{3.32}$$

with some overall interaction strength G. We interpret this as a four-fermion theory where each of the ψ's denotes a fermion field and they interact at the point x. Hence the theory is inherently *local* and encapsulates the short range of the weak interaction.

Equation (3.32) is in fact a specific case of a much more general interaction involving four fermions. Motivated by the form of the electromagnetic force, we've implicitly assumed that only vector currents contribute to the interaction, but these are only one of the five types of Dirac bilinears available to us. More generally, a four fermion interaction could be comprised of any of the five Dirac bilinears seen previously (S, P, V, A or T). Then, generalising equation (3.32) to include all such bilinears and requiring that the Hamiltonian remains Lorentz invariant, we obtain

$$\mathcal{H}^{(1)}_{int}(x) = \sum_i C_i(\bar{\psi}_1\Gamma_i\psi_2)(\bar{\psi}_3\Gamma_i\psi_4) + h.c. \quad , \tag{3.33}$$

where Γ_i is one of the Dirac bilinear forms ($i = S, P, V, A$ or T) and the C_i are possibly complex coupling constants [23]. This is known as the general four-fermion interaction; however, it is still not as general as it could be. If we simply require the Hamiltonian to be invariant under the proper orthochronous Lorentz group, we can include the following interactions in our Hamiltonian

$$\mathcal{H}^{(2)}_{int}(x) = \sum_i C'_i(\bar{\psi}_1\Gamma_i\psi_2)(\bar{\psi}_3\Gamma_i\gamma_5\psi_4) + h.c. \quad . \tag{3.34}$$

Then our four-fermion interaction Hamiltonian is just

$$\mathcal{H}_{int}(x) = \mathcal{H}^{(1)}_{int}(x) + \mathcal{H}^{(2)}_{int}(x)\,. \tag{3.35}$$

In the case of the weak interactions, we construct our effective Hamiltonian subject to the constraints that it must allow for both C and P violation separately (remember, we are trying to produce a theory of the weak interactions which we know violate both C and P). In particular, by considering chiral symmetry, we are led to the structures

$$\left[\bar{\psi}_1\gamma_\mu(1 \pm \gamma_5)\psi_2\right]\left[\bar{\psi}_3\gamma_\mu(1 \pm \gamma_5)\psi_4\right]. \tag{3.36}$$

The $\gamma_\mu(1 \pm \gamma_5)$ structure is composed of a vector and axial vector current in equal proportions and is known as a $V \pm A$ current. This is the most general combination of Dirac bilinears which correspond to the exchange of spin-1 bosons (the W and Z bosons) and which also allows for C and P violation [23]. The experimental measurements of parity and charge conjugation violation were pivotal in determining the form of the weak interaction in that they indicated a $V - A$ structure in order to account for symmetry violating effects[1]. In the following section, we'll use a quantum field theoretic approach to arrive at the same form, although we'll place more emphasis on the coupling constants.

Quantum Field Theory

The weak interactions are mediated by the $W^\pm$ and Z bosons (for our purposes, we're just interested in the flavour changes effected by the $W^\pm$ bosons). The $W^\pm$ couple to the following left handed currents

$$J^+_\mu = \bar{\nu}_{eL}\gamma^\mu e_L + \bar{\nu}_{\mu L}\gamma^\mu\mu_L + \bar{\nu}_{\tau L}\gamma^\mu\tau_L + V_{ij}\bar{u}^i_L\gamma^\mu d^j_L\,, \tag{3.37}$$

$$J^-_\mu = \bar{e}_L\gamma^\mu\nu_{eL} + \bar{\mu}_L\gamma^\mu\nu_{\mu L} + \bar{\tau}_L\gamma^\mu\nu_{\tau L} + V^\dagger_{ij}\bar{d}^i_L\gamma^\mu u^j_L\,, \tag{3.38}$$

where we can clearly see the contributions from the three generations of leptons and neutrinos, as well as the up-type quark and down-type quark interaction which enters with an additional coupling due to the V_{ij} elements of the CKM quark mixing matrix [8]. The coupling between these currents and the $W^\pm$ is described by the

[1] One can show that other combinations, such as just V or A individually, can't give rise to C and P violation. This is the basis for CP conservation in QED and QCD.

interaction Lagrangian

$$\mathcal{L} = \frac{e}{\sqrt{2}\sin\theta_w}(W^{\mu}_{+}J^{+}_{\mu} + W^{\mu}_{-}J^{-}_{\mu})\,. \tag{3.39}$$

Equation (3.39) should look familar since it is the same as equation (3.17), we've just bundled all the quark and lepton currents into the currents $J^{\pm}_{\mu}$. We can then read off the Feynman diagrams and we obtain the vertices shown in Figure 3.1.

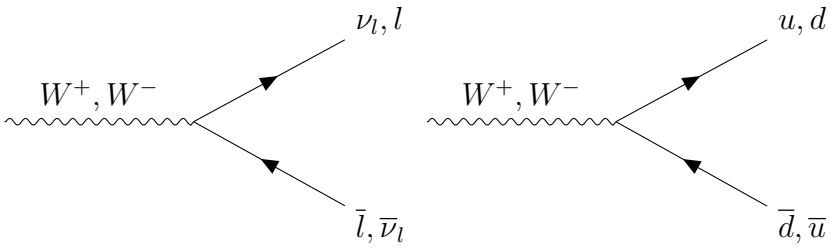

Figure 3.1: Feynman diagrams showing the interaction vertices involving fermions and the weak bosons $W^{\pm}$. l denotes an electron, muon or tau lepton, with ν_l the corresponding neutrino. u and d denote up- and down-type quarks respectively ($u = u\,, c\,, t$ and $d = d\,, s\,, b$). Both vertices get a factor of $\frac{e}{\sqrt{2}\sin\theta_w}$, although the quark vertex gets an extra factor of either V_{ij} or V^*_{ij}.

Since we are just interested in the $B^{\pm} \to K^+K^-\pi^{\pm}$ decays observed by Belle, and these have purely hadronic final states, we can disregard the contributions from the lepton and neutrino vertices and write the quark currents as

$$J^{+}_{\mu} \sim V_{ij}\bar{u}^i_L\gamma^{\mu}d^j_L\,, \qquad\qquad J^{-}_{\mu} \sim V^{\dagger}_{ij}\bar{d}^i_L\gamma^{\mu}u^j_L\,. \tag{3.40}$$

For our investigation of weak decays, we'll be interested in transitions such as $b \to u\bar{u}d$. We write the matrix element for this decay as

$$i\mathcal{M} = \left(\frac{ie}{\sqrt{2}\sin\theta_w}\right)^2 \left(V^*_{ud}\bar{d}_L\gamma^{\mu}u_L\right)\left(\frac{-i\left(g_{\mu\nu} - \frac{p_\mu p_\nu}{m^2_W}\right)}{p^2 - m^2_W}\right)\left(V_{ub}\bar{u}_L\gamma^{\nu}b_L\right).$$

Note that we've used the full propagator for the W boson where p is its 4-momentum. Taking the limit that $p^2 \ll m^2_W$ we see that the second term in the propagator is negligible once we pull out a $g_{\mu\nu}$. This then gives

$$\begin{aligned} i\mathcal{M} &= \left(\frac{ie}{\sqrt{2}\sin\theta_w}\right)^2 (V^*_{ud}V_{ub})\left(\bar{d}_L\gamma^{\mu}u_L\right)\left(\frac{-ig_{\mu\nu}}{-m^2_W}\right)(\bar{u}_L\gamma^{\nu}b_L) \\ &= \frac{-ie^2}{2m^2_W\sin^2\theta_w}(V^*_{ud}V_{ub})\left(\bar{d}_L\gamma^{\mu}u_L\right)g_{\mu\nu}(\bar{u}_L\gamma^{\nu}b_L)\,. \end{aligned}$$

Writing the left chiral projection operators explicitly ($P_L = \frac{1}{2}(1-\gamma_5)$) we obtain

$$\begin{aligned} i\mathcal{M} &= \frac{-ie^2}{2m_W^2 \sin^2\theta_w}(V_{ud}^* V_{ub})\left(\bar{d}\frac{\gamma^\mu(1-\gamma_5)}{2}u\right)g_{\mu\nu}\left(\bar{u}\frac{\gamma^\nu(1-\gamma_5)}{2}b\right) \\ &= \frac{-ie^2}{2m_W^2 \sin^2\theta_w}(V_{ud}^* V_{ub})\left(\bar{d}\frac{\gamma^\mu(1-\gamma_5)}{2}u\right)\left(\bar{u}\frac{\gamma_\mu(1-\gamma_5)}{2}b\right). \end{aligned}$$

Finally, including Fermi's constant G_F via the replacement

$$\frac{4G_F}{\sqrt{2}} \equiv \frac{e^2}{2m_W^2 \sin^2(\theta_w)}\,, \tag{3.41}$$

allows us to write this particular interaction as

$$\begin{aligned} \mathcal{L}_{4F} &= -\frac{4G_F}{\sqrt{2}}(V_{ud}^* V_{ub})\left(\bar{d}\frac{\gamma^\mu(1-\gamma_5)}{2}u\right)\left(\bar{u}\frac{\gamma_\mu(1-\gamma_5)}{2}b\right) \\ &= -\frac{G_F}{\sqrt{2}}(V_{ud}^* V_{ub})\big(\bar{d}\gamma^\mu(1-\gamma_5)u\big)(\bar{u}\gamma_\mu(1-\gamma_5)b)\,. \end{aligned} \tag{3.42}$$

This is the fundamental basis for the four-fermion interaction. This type of interaction is often thought of as having "shrunk down" to a single vertex; the idea is that when we take the limit of small momenta for the W boson, the propagator collapses down to a point. This effective vertex is of the same form as seen in equation (3.36). We've thus retrieved Fermi's four-fermion interaction from a quantum field theory approach. Importantly, we've included the CKM matrix elements in the coupling. Writing equation (3.42) for some generic quarks, we have the Feynman diagram shown in Figure 3.2 and thus the interaction Lagrangian is written as

$$\mathcal{L} = -\frac{G_F}{\sqrt{2}}\big(V^{(*)}_{q_1q_2}V^{(*)}_{q_3q_4}\big)(\bar{q}_2\gamma^\mu(1-\gamma_5)q_1)(\bar{q}_3\gamma_\mu(1-\gamma_5)q_4) \tag{3.43}$$

where

$$V^{(*)}_{q_iq_j} = \begin{cases} V_{q_iq_j} & \text{if } q_i \text{ is up-type and } q_j \text{ is down type} \\ V^*_{q_jq_i} & \text{if } q_j \text{ is up-type and } q_i \text{ is down type} \end{cases}\,. \tag{3.44}$$

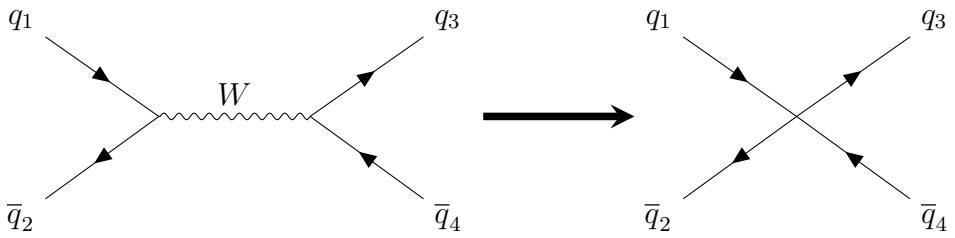

Figure 3.2: Feynman diagram showing a general four-fermion interaction in the limit that $p_W^2 \ll m_W^2$.

3.3 Operator Product Expansion

Now that we've constructed a description of the weak interaction at low momenta using four-fermion interactions, there is one more thing we need before we can construct our effective Hamiltonian for these weak decays. The last ingredient is the Operator Product Exansion (OPE) [14]. We'll discuss this from an abstract perspective first and then relate the OPE back to the weak effective Hamiltonian.

Typically one extracts information such as the amplitude for a decay from the corresponding Green's function. Consider a case where we have two operators $\mathcal{O}_1$ and $\mathcal{O}_2$ separated by some distance x, and with some additional fields $\phi(y_i)$ with the y_i far away from the origin at 0. The corresponding Green's function is then

$$G_{12}(x; y_1, \ldots, y_m) = \langle \mathcal{O}_1(x)\mathcal{O}_2(0)\phi(y_1)\ldots\phi(y_m)\rangle \,. \tag{3.45}$$

Now consider the operator product $\mathcal{O}_1(x)\mathcal{O}_2(0)$ with x small (corresponding to high energies); this composite operator could be the source for any general disturbance at 0. However, any such disturbance in general could be induced by a single local operator at 0 and this local operator must, by necessity, have the same global symmetry quantum numbers (baryon number, lepton number and electric charge) as the composite operator $\mathcal{O}_1(x)\mathcal{O}_2(0)$ [14]. We can write this general operator as a linear combination of a basis of operators, where the complex coefficients in the linear combination are functions of the separation x [14]. Putting all these statements together, one arrives at the formal proposal of the OPE put forward by Wilson in 1969

$$\mathcal{O}_1(x)\mathcal{O}_2(0) \to \sum_n C_{12}^n(x)\mathcal{O}'_n(0) \,, \tag{3.46}$$

where all the separation dependence has been placed in the complex valued Wilson coefficients $C_{12}^n(x)$ and the $\mathcal{O}'_n$ are a basis of composite local operators. This trivially means we can rewrite the Green's function in equation (3.45) as

$$G_{12}(x; y_1, \ldots, y_m) = \sum_n C_{12}^n(x)\langle \mathcal{O}'_n(0)\phi(y_1)\ldots\phi(y_m)\rangle \tag{3.47}$$

so now all the x dependence is in the Wilson coefficients, rather than the Green's functions. The real crux of the OPE lies in the separation x (or equivalently the energy scale used). For high energy processes, QCD exhibits asymptotic freedom since the running coupling $\alpha_s(Q^2)$ tends to decrease for higher and higher energies [1, 6]. In weak processes involving the W boson the separation of currents goes like $x \sim 1/m_W$ and is thus small. This corresponds to a region where QCD is asymptotically free and so the Wilson coefficients which appear in the OPE of weak currents can be calculated in QCD perturbation theory. The coefficients can then be evolved to the required scale using the renormalisation group equation [24]. As a note, there may be some scale dependence μ which needs to be accounted for.

When we apply the OPE to the weak interaction we write the product of currents as

$$\lim_{x\to 0} \mathcal{O}_i(x)\mathcal{O}_j(0) = \sum_n C_{ij}^n(x)\mathcal{O}'_n(0) \tag{3.48}$$

where the local currents $\mathcal{O}_i$ and $\mathcal{O}_j$ are just the $V-A$ quark terms which appear in the weak current. The composite operators $\mathcal{O}'_n$ are of two different forms, either **tree** or **penguin** operators. We discuss these in more detail below.

As a final remark, we can interpret the limit $x \to 0$ in two equivalent ways. We can view this as the separation approaching zero just as for the four-fermion interaction interpretation of the weak interaction, or we can say that the energy/-momentum transfer between the currents approaches infinity (becomes large).

3.4 Tree and Penguin Operators

The following section is one of the most important points of reference for the remainder of the thesis. We'll come to find that we need processes constructed from the following operators to observe any CP violating asymmetry.

3.4.1 Tree Operators

For our work involving the decays $B^\pm \to K^+K^-\pi^\pm$ we are interested in the quark decays $b \to du\bar{u}$ in so called **tree** diagrams, and $b \to dq\overline{q}$ (with $q = u, d, s$) in **penguin** diagrams [19]. Starting with the tree operators, consider Figure 3.3 which shows an example of the kinds of decays we'll be considering. In this case, we have two local currents

$$\mathcal{O}_1 = \bar{d}\gamma_\mu(1-\gamma_5)u \tag{3.49}$$
$$\mathcal{O}_2 = \bar{u}\gamma^\mu(1-\gamma_5)b \tag{3.50}$$

interacting in some large energy process. The composite operator describing their interaction is then

$$\mathcal{O}'_1 = \bar{d}\gamma_\mu(1-\gamma_5)u\bar{u}\gamma^\mu(1-\gamma_5)b\,. \tag{3.51}$$

However, there are really two possible ways of writing this since there is some ambiguity over how we contract colour indices on the fermion spinors. Including the colour indices α and β explicitly, we have

$$\mathcal{O}'_1 = \bar{d}_\alpha\gamma_\mu(1-\gamma_5)u_\beta\bar{u}_\beta\gamma^\mu(1-\gamma_5)b_\alpha\,, \tag{3.52}$$
$$\mathcal{O}'_2 = \bar{d}_\alpha\gamma_\mu(1-\gamma_5)u_\alpha\bar{u}_\beta\gamma^\mu(1-\gamma_5)b_\beta\,. \tag{3.53}$$

Relabelling the composite operators without primes for convenience, we write

Tree Operators ($i = 1, 2$)

$$\mathcal{O}_1 = \bar{d}_\alpha \gamma_\mu (1-\gamma_5) u_\beta \bar{u}_\beta \gamma^\mu (1-\gamma_5) b_\alpha \,, \tag{3.54}$$

$$\mathcal{O}_2 = \bar{d}_\alpha \gamma_\mu (1-\gamma_5) u_\alpha \bar{u}_\beta \gamma^\mu (1-\gamma_5) b_\beta \,. \tag{3.55}$$

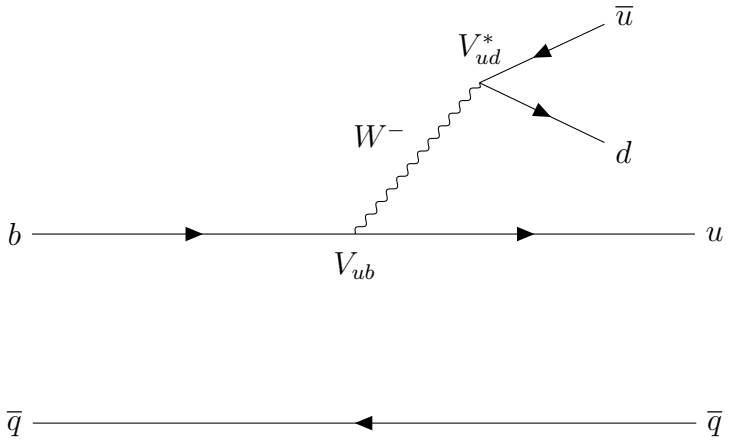

Figure 3.3: Tree diagram for $b \to u\bar{u}d$ decay via a W^- boson, with some spectator quark q.

3.4.2 Penguin Operators

In much the same way as for the tree operators, we can define a set of penguin operators corresponding to either a QCD or Electroweak penguin diagram (Figures 3.4 and 3.5 respectively). It should be noted that $(V-A)(V+A)$ transitions are allowed now owing to the presence of a gluon, Z boson or photon. Additionally, these operators include sums over quark flavours since the newly introduced bosons are capable of creating quark anti-quark pairs. For the penguins involving gluons, we have

QCD Penguin Operators ($i = 3, ..., 6$)

$$\mathcal{O}_3 = \bar{d}\gamma_\mu (1-\gamma_5) b \sum_q \bar{q}\gamma^\mu (1-\gamma_5) q \,, \tag{3.56}$$

$$\mathcal{O}_4 = \bar{d}_\alpha \gamma_\mu (1-\gamma_5) b_\beta \sum_q \bar{q}_\beta \gamma^\mu (1-\gamma_5) q_\alpha \,, \tag{3.57}$$

$$\mathcal{O}_5 = \bar{d}\gamma_\mu (1-\gamma_5) b \sum_q \bar{q}\gamma^\mu (1+\gamma_5) q \,, \tag{3.58}$$

$$\mathcal{O}_6 = \bar{d}_\alpha \gamma_\mu (1-\gamma_5) b_\beta \sum_q \bar{q}_\beta \gamma^\mu (1+\gamma_5) q_\alpha \,, \tag{3.59}$$

where α and β are colour indices, μ is a Lorentz index, and $q = u\,, d\,, s$ are the quarks available for the penguin processes.

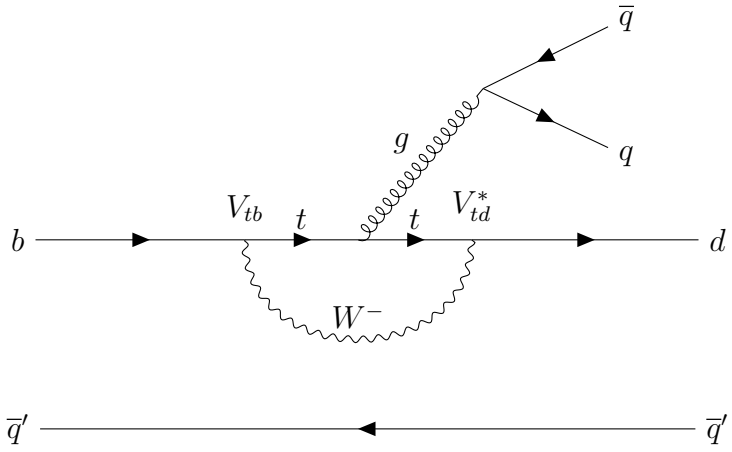

Figure 3.4: QCD penguin diagram for the decay $b \to dq\overline{q}$ with some spectator quark q'. Note that the top quark t is present in our model since this gives access to the CKM matrix element V_{tb}. The significance of this in the CP asymmetry will be discussed in chapter 4.

Turning our attention to the final set of operators, we consider that now we could have the same W loop with a Z boson or photon being emitted through either of the cases depicted in Figure 3.5. In this case we need to include the charge e_q of the various quark spinors produced by the Z, γ. The overall factor of $3/2$ is introduced as a convention [25].

Electroweak Penguin Operators ($i = 7, ..., 10$)

$$\mathcal{O}_7 = \frac{3}{2}\bar{d}\gamma_\mu(1-\gamma_5)b\sum_q e_q\bar{q}\gamma^\mu(1+\gamma_5)q\,, \tag{3.60}$$

$$\mathcal{O}_8 = \frac{3}{2}\bar{d}_\alpha\gamma_\mu(1-\gamma_5)b_\beta\sum_q e_q\bar{q}_\beta\gamma^\mu(1+\gamma_5)q_\alpha\,, \tag{3.61}$$

$$\mathcal{O}_9 = \frac{3}{2}\bar{d}\gamma_\mu(1-\gamma_5)b\sum_q e_q\bar{q}\gamma^\mu(1-\gamma_5)q\,, \tag{3.62}$$

$$\mathcal{O}_{10} = \frac{3}{2}\bar{d}_\alpha\gamma_\mu(1-\gamma_5)b_\beta\sum_q e_q\bar{q}_\beta\gamma^\mu(1-\gamma_5)q_\alpha\,, \tag{3.63}$$

3.5 Effective Hamiltonian

To recap what we've done so far, we've realised that the decays of interest to us happen at high energies, since the mass of the decaying b quark is so large. This limits the range of the interaction and so we argued that we could approximate the weak interaction with a four-fermion interaction. We then wrote down an effective

Lagrangian for the interactions in our system. Then we applied an Operator Product Expansion on the terms in this effective Lagrangian by carrying through the limit of small separation to the product of currents. This allowed us to write the terms in our Lagrangian with all the long range (hadronic) physics in the Wilson coefficients, which are calculable in perturbation theory, and the short range (weak) physics in the operators $\mathcal{O}_i'(0)$.

Combining all these pieces together, and using the fact that $\mathcal{L}_{int} = -\mathcal{H}_{int}$, we obtain the effective Hamiltonian for charmless hadronic decays of B mesons via the weak force,

$$\mathcal{H}_{\text{eff}} = \frac{G_F}{\sqrt{2}}\left\{ V_{ub}V_{uq}^*(c_1\mathcal{O}_1 + c_2\mathcal{O}_2) - V_{tb}V_{tq}^*\sum_{i=3}^{10} c_i\mathcal{O}_i \right\},$$

where the operators $\mathcal{O}_i$ now denote the tree and penguin operators in equations (3.54) to (3.63). The c_i are Wilson coefficients evaluated at some scale μ, the V_{ij} are entries from the CKM matrix appearing at the vertices in either the tree or penguin diagrams. Finally, G_F is the Fermi constant. With this key structure in place, we can finally begin to calculate the CP asymmetry of interest to us.

3.6 Wilson Coefficients

With our effective Hamiltonian constructed, there is one subtlety we've ignored thus far. When we calculate the Wilson coefficients and scale them as desired, this incurs a corresponding scaling of the matrix elements which is renormalisation scheme dependent. Hence, we should really have written our final effective Hamiltonian with some explicit scale dependences. However, we'd rather keep our matrix elements as simple as possible so one tends to define a collection of effective Wilson coefficients c_i' [5, 26] satisfying

$$c_i\langle\mathcal{O}_i(m_b)\rangle = c_i'\langle\mathcal{O}_i\rangle^{tree}, \tag{3.64}$$

where $\langle\mathcal{O}_i(m_b)\rangle$ is the matrix element for the operator $\mathcal{O}_i$ evaluated at the scale $\mu = m_b$ (the mass of the b quark). $\langle\mathcal{O}_i\rangle^{tree}$ is the matrix element for the operator $\mathcal{O}_i$ at tree level and so all the scale dependence is kept within these new effective Wilson coefficients.

The effective Wilson coefficients are calculated from known Wilson coefficients by the relations [5, 26]

$$\begin{aligned}
c_1' &= c_1\,, & c_2' &= c_2\,,\\
c_3' &= c_3 - P_s/3\,, & c_4' &= c_4 + P_s\,,\\
c_5' &= c_5 - P_s/3\,, & c_6' &= c_6 + P_s\,,\\
c_7' &= c_7 + P_e\,, & c_8' &= c_8\,,\\
c_9' &= c_9 + P_e\,, & c_{10}' &= c_{10}\,,
\end{aligned}$$

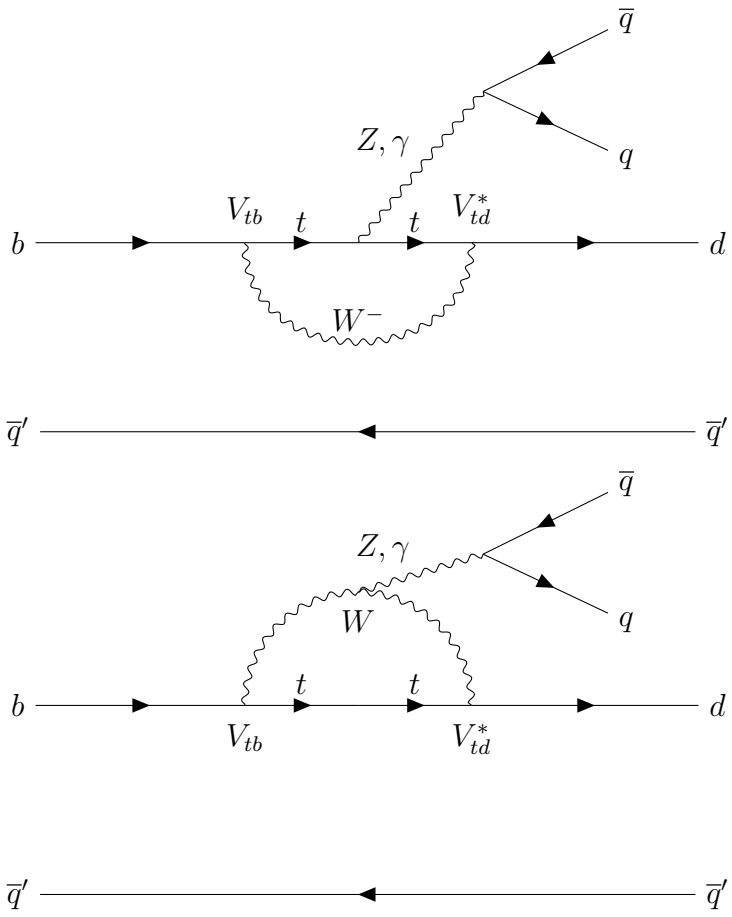

Figure 3.5: (Top) Electroweak penguin diagram for the decay $b \to dq\overline{q}$ with a Z boson or photon radiated by the top quark. (Bottom) Electroweak penguin diagram for the decay $b \to dq\overline{q}$ with a Z boson or photon radiated by the W boson. The q' is just some spectator quark.

where

$$P_s = \left(\frac{\alpha_s}{8\pi}\right) c_2 \left(\frac{10}{9} + G(m_c, \mu, q^2)\right), \tag{3.65}$$

$$P_e = \left(\frac{\alpha_{em}}{9\pi}\right) (3c_1 + c_2) \left(\frac{10}{9} + G(m_c, \mu, q^2)\right), \tag{3.66}$$

and

$$G(m_c, \mu, q^2) = 4 \int_0^1 x(x-1) \ln \frac{m_c^2 - x(1-x)q^2}{\mu^2} dx\,. \tag{3.67}$$

In $G(m_c, \mu, q^2)$, m_c is the mass of the charm quark, μ is the scale set at $\mu = m_b$ where m_b is the mass of the bottom quark, and q^2 is the momentum transfer of the intermediate gluon, photon or Z boson in the penguin diagram. $G(m_c, \mu, q^2)$ is

complex, having real and imaginary parts

$$\mathrm{Re}\, G = \frac{2}{3}\left\{ \ln\left(\frac{m_c^2}{\mu^2}\right) - \frac{5}{3} - 4\frac{m_c^2}{q^2} + \left(1 + 2\frac{m_c^2}{q^2}\right)\sqrt{1 - 4\frac{m_c^2}{q^2}}\, \ln\left(\frac{1 + \sqrt{1 - 4\frac{m_c^2}{q^2}}}{1 - \sqrt{1 - 4\frac{m_c^2}{q^2}}}\right)\right\}, \tag{3.68}$$

$$\mathrm{Im}\, G = -\frac{2}{3}\left(1 + 2\frac{m_c^2}{q^2}\right)\sqrt{1 - 4\frac{m_c^2}{q^2}}\,. \tag{3.69}$$

All the quantities in these last two equations are known, except the momentum transfer q^2. Simple quark level arguments[2] allow us to choose values for q^2 in the range $0.3 < q^2/m_b^2 < 0.5$. The effective Wilson coefficients are then calculable, given some initial Wilson coefficients; the effective Wilson coefficients are given in Table 3.1 and reproduced in Appendix C for easy reference, along with a table of the initial Wilson coefficients.

c_i'	$q^2/m_b^2 = 0.3$	$q^2/m_b^2 = 0.5$
c_1'	-0.3125	-0.3125
c_2'	1.1502	1.1502
c_3'	$2.433 \times 10^{-2} + 1.543 \times 10^{-3} i$	$2.120 \times 10^{-2} + 2.174 \times 10^{-3} i$
c_4'	$-5.808 \times 10^{-2} - 4.628 \times 10^{-3} i$	$-4.869 \times 10^{-2} - 1.552 \times 10^{-2} i$
c_5'	$1.733 \times 10^{-2} + 1.543 \times 10^{-3} i$	$1.420 \times 10^{-2} + 5.174 \times 10^{-3} i$
c_6'	$-6.668 \times 10^{-2} - 4.628 \times 10^{-3} i$	$-5.729 \times 10^{-2} - 1.552 \times 10^{-2} i$
c_7'	$-1.435 \times 10^{-4} - 2.963 \times 10^{-5} i$	$-8.340 \times 10^{-5} - 9.938 \times 10^{-5} i$
c_8'	3.839×10^{-4}	3.839×10^{-4}
c_9'	$-1.023 \times 10^{-2} - 2.963 \times 10^{-5} i$	$-1.017 \times 10^{-2} - 9.938 \times 10^{-5} i$
c_{10}'	1.959×10^{-3}	1.959×10^{-3}

Table 3.1: Table of effective Wilson coefficients calculated at the kinematic endpoints $q^2/m_b^2 = 0.3$ and $q^2/m_b^2 = 0.5$ [5, 26].

[2] See Appendix A for details.

Chapter 4

CP Asymmetry

At the end of chapter 2 we introduced the idea of a CP violating asymmetry. This was done very much in an ad hoc manner but now we develop this concept more formally. Throughout this chapter we work under the framework of the effective Hamiltonian established in chapter 3. We start by considering the most general case for B decays where the B meson decays to some final state F. Then we work through the more specific case of the CP asymmetry in the $B^{\pm} \to K^+K^-\pi^{\pm}$ case. The rest of the chapter is devoted to prescribing relevant decay processes with which we hope to replicate the CP asymmetry result from Belle, and then describing the initial calculation of the relevant Feynman diagrams.

4.1 Formalism

Recall the definition of direct CP violation given in chapter 2b was that the decay amplitudes for a particle decay differs from that of the CP conjugate decay. This is typically quantified in terms of the decay rates Γ as a **CP asymmetry**,

$$\mathcal{A}_{CP} \equiv \frac{\Gamma(B \to F) - \Gamma(\bar{B} \to \bar{F})}{\Gamma(B \to F) + \Gamma(\bar{B} \to \bar{F})}\,. \tag{4.1}$$

We then recognise that the decay rate is equal to the mod square of the amplitude up to some phase space factors and additional constants [8]. Assuming the additional factors are the same and that the amplitudes are approximately constant across the entire region of phase space[1], one typically rewrites this as

$$\mathcal{A}_{CP} = \frac{|A(B \to F)|^2 - \left|\bar{A}(\bar{B} \to \bar{F})\right|^2}{|A(B \to F)|^2 + \left|\bar{A}(\bar{B} \to \bar{F})\right|^2}\,, \tag{4.2}$$

where $A(B \to F)$ is the amplitude for the decay of a meson B to some final state F. $\bar{A}(\bar{B} \to \bar{F})$ is just the amplitude for the conjugate decay of the antiparticle $\bar{B}$ to the final state $\bar{F}$.

[1] This is possibly an oversimplification. We will investigate the full integration across the phase space in chapter 6, after having performed this simpler calculation.

General B Meson Decay

We write the amplitude for the weak decay $B \to F$ as

$$A(B \to F) = \langle F|\mathcal{H}|B\rangle \ ,$$

and for the corresponding antiparticle process

$$\bar{A}(\bar{B} \to \bar{F}) = \left\langle \bar{F}\middle|\mathcal{H}\middle|\bar{B}\right\rangle \ ,$$

where $\mathcal{H}$ is the effective Hamiltonian developed in chapter 3. We can also separate the individual amplitudes into their different contributions. We write

$$A(B \to F) = |A_1|e^{i\delta_1 + i\phi_1} + |A_2|e^{i\delta_2 + i\phi_2} \ , \tag{4.3}$$

where the two terms correspond to a particular (set of) Feynman diagram(s). The ϕ_i are weak phases which change sign under the action of CP, and the δ_i are strong phases which do *not* change sign under CP.

Making note of the change of sign of the weak phase when writing $\bar{A}$ and using trigonometric addition formulae and the identity $e^{i\theta} = \cos\theta + i\sin\theta$, we substitute for A and $\bar{A}$ in equation (4.2) and obtain

$$\mathcal{A}_{CP} = -\frac{2|A_1||A_2|\sin(\delta_1 - \delta_2)\sin(\phi_1 - \phi_2)}{|A_1|^2 + |A_2|^2 + 2|A_1||A_2|\cos(\delta_1 - \delta_2)\cos(\phi_1 - \phi_2)} \ . \tag{4.4}$$

The derivation of $\mathcal{A}_{CP}$ for our specific decay process is explored in more detail below.

CP asymmetry in $B^\pm \to K^+K^-\pi^\pm$ decays

We start by recognising that the contributions of interest come from the previously introduced tree and penguin diagrams. The amplitude for $B^- \to K^+K^-\pi^-$ decays is then given by

$$A = \left\langle K^+K^-\pi^-\middle|\mathcal{H}^T\middle|B^-\right\rangle + \left\langle K^+K^-\pi^-\middle|\mathcal{H}^P\middle|B^-\right\rangle \tag{4.5}$$

where $\mathcal{H}^T$ and $\mathcal{H}^P$ are tree and penguin Hamiltonians respectively. Note that this is just a specific case of the form given in equation (4.3). We define r as the magnitude of the ratio of the tree and penguin diagrams, and we define as well δ the strong phase difference and ϕ the weak phase difference between the tree and penguin amplitudes. The formal definition is then

$$re^{i\delta}e^{i\phi} \equiv \frac{\langle K^+K^-\pi^-|H^P|B^-\rangle}{\langle K^+K^-\pi^-|H^T|B^-\rangle} \ . \tag{4.6}$$

Comparing this with the work in the previous section, this is equivalent to the mappings

$$\frac{|A_1|}{|A_2|} \to r\,, \qquad (\delta_1 - \delta_2) \to \delta\,, \qquad (\phi_1 - \phi_2) \to \phi\,.$$

We can now rewrite equation (4.5) as

$$A = \left\langle K^+K^-\pi^-\middle|\mathcal{H}^T\middle|B^-\right\rangle [1 + re^{i\delta}e^{i\phi}] \tag{4.7}$$

and similarly for the CP conjugate decay

$$\bar{A} = \left\langle K^+K^-\pi^+\middle|\mathcal{H}^T\middle|B^+\right\rangle [1 + re^{i\delta}e^{-i\phi}]. \tag{4.8}$$

The CP asymmetry is calculated by

$$\mathcal{A}_{CP} = \frac{|A|^2 - \left|\bar{A}\right|^2}{|A|^2 + \left|\bar{A}\right|^2} \tag{4.9}$$

where

$$\begin{aligned} |A|^2 &= \left|\left\langle K^+K^-\pi^-\middle|\mathcal{H}^T\middle|B^-\right\rangle\right|^2 [1 + re^{i\delta}e^{i\phi}][1 + re^{-i\delta}e^{-i\phi}] \\ &= \left|\left\langle K^+K^-\pi^-\middle|\mathcal{H}^T\middle|B^-\right\rangle\right|^2 [1 + 2r\cos\delta\cos\phi - 2r\sin\delta\sin\phi + r^2] \end{aligned}$$

and

$$\begin{aligned} \left|\bar{A}\right|^2 &= \left|\left\langle K^+K^-\pi^+\middle|\mathcal{H}^T\middle|B^+\right\rangle\right|^2 [1 + re^{i\delta}e^{-i\phi}][1 + re^{-i\delta}e^{i\phi}] \\ &= \left|\left\langle K^+K^-\pi^+\middle|\mathcal{H}^T\middle|B^+\right\rangle\right|^2 [1 + 2r\cos\delta\cos\phi + 2r\sin\delta\sin\phi + r^2]\,. \end{aligned}$$

For our purposes, the only form of CP violation we are considering is direct and this arises only through the interference of the tree and penguin diagram phases [5,19,26]. Hence, the tree amplitude taken on its own is CP invariant and we have

$$\left|\left\langle K^+K^-\pi^-\middle|\mathcal{H}^T\middle|B^-\right\rangle\right|^2 = \left|\left\langle K^+K^-\pi^+\middle|\mathcal{H}^T\middle|B^+\right\rangle\right|^2.$$

Therefore, we can write equation (4.9) as

$$\mathcal{A}_{CP} = \frac{-4r\sin\delta\sin\phi}{2 + 4r\cos\delta\cos\phi + 2r^2}\,,$$

$$\therefore \mathcal{A}_{CP} = -\frac{2r\sin\delta\sin\phi}{1 + 2r\cos\delta\cos\phi + r^2}\,. \tag{4.10}$$

We recognise that this is equivalent to equation (4.4) under the transformations introduced at the beginning of this subsection. One of the key features of the asymmetry is that it shows maximal CP violation when it is either 1 or -1. This

can only occur when r , $\sin\delta$, $\sin\phi$ are all close to 1. As such, we'll end up choosing specific decay processes which we suspect satisfy these conditions for a large CP asymmetry, and then proceed with calculating the resultant CP asymmetry. In particular, the values of r and $\sin\delta$ are the main sources of uncertainty in the calculation, and will require the most work to determine.

4.2 Choice of Diagrams

In order to calculate the CP asymmetry as given in equation (4.10), we require the parameters r, δ and ϕ (the ratio of the amplitudes, the strong phase difference and the weak phase difference between two tree and penguin diagrams). Recall equation (4.6)

$$re^{i\delta}e^{i\phi} \equiv \frac{\langle K^+K^-\pi^-|H^P|B^-\rangle}{\langle K^+K^-\pi^-|H^T|B^-\rangle}\,.$$

We need to evaluate this quantity if we are to find the CP asymmetry. To begin, we'll digress to a discussion of the two matrix elements; one for the tree Hamiltonian and one for the penguin Hamiltonian. Consider the tree and penguin processes for which the proposed Feynman diagrams are given in Figures 4.1 and 4.2. The motivation for these particular diagrams is as follows.

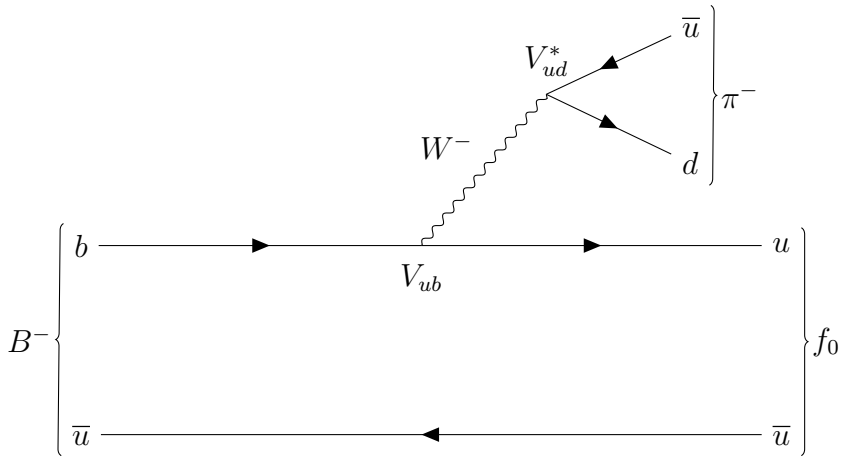

Figure 4.1: Tree diagram for the decay $B^- \to K^+K^-\pi^-$. The f_0 can subsequently decay to a K^+K^- pair.

First, the region of interest for us is the K^+K^- invariant mass range $0.8 \leq m_{KK} \leq 1.1$ GeV[2]. This is where the large CP asymmetry was reported by Belle and so we consider the following two-step decay processes involving K^+K^- resonances at around 1 GeV:

$$B^- \to f_0(980)\pi^- \to K^+K^-\pi^- \qquad B^- \to \phi(1020)\pi^- \to K^+K^-\pi^-\,. \tag{4.11}$$

[2]This is the bin used by Belle. However, the lower bound is unphysical since $m_{KK} \geq 0.986$ (twice the mass of the charged kaons). We comment on the physical realisation of this bin later.

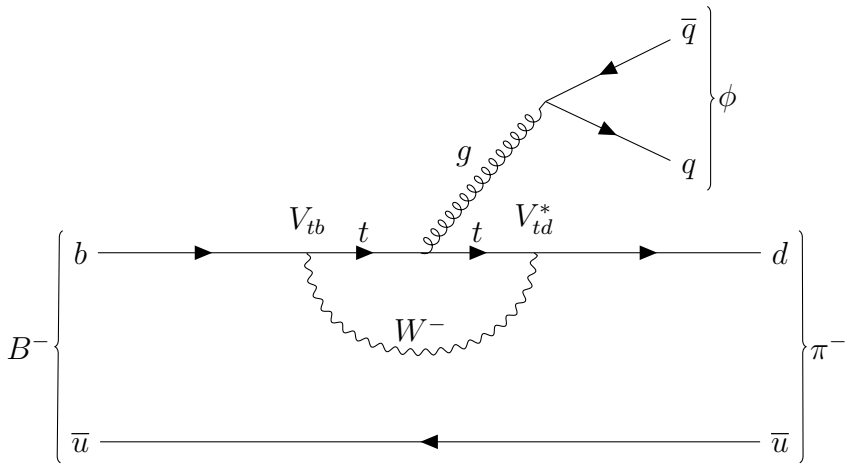

Figure 4.2: QCD penguin diagram for the decay $B^- \to K^+K^-\pi^-$. The ϕ can subsequently decay to a K^+K^- pair. Note that the $\bar{q}q$ pair can be u, d or s quarks although the ϕ is primarily composed of $\bar{s}s$.

In naive quark models the $f_0(980)$ scalar meson is composed of combinations of up, down and strange $q\bar{q}$ pairs although the exact structure, as with many of the scalar mesons below 1 GeV, is not well understood [27]. In our model, we propose that the f_0 can couple to the tree diagram through the $u\bar{u}$ pair shown in Figure 4.1. Having a mass of about 980 MeV, the f_0 resonance is just below threshold for K^+K^- production. However, the decay width is estimated to be $10 - 100$ MeV [21], more than enough to allow for a heavier f_0 to produce the kaon pair.

Turning our attention to the penguin diagram, shown in Figure 4.2, we initially explore the contribution of the $\phi(1020)$ vector meson in this process. It would do so through the emission of the $s\bar{s}$ pair from the gluon (see Appendix B). The ϕ meson has a narrow width of about 4 MeV centred at 1020 MeV, right within the m_{KK} region in which Belle reported the large CP violation. However, the narrow width of the ϕ means the amplitude for the decay may fall off quickly and so only be significant over a small range of invariant mass. This will be something to keep in mind as we proceed with our analysis.

The bottom to top quark flavour change in the penguin, which is Cabibbo favoured, provides the mechanism for a large CP violation through the CKM matrix element V_{tb}. Also, the electroweak penguin diagrams are excluded and we take them to be background contributions in accordance with [19].

We also note that in constructing the relevant Feynman diagrams, we need different intermediate states for the tree and penguin processes since there would be no phase differences otherwise, and thus no CP violation. Finally, as noted from equation (4.10), a large CP asymmetry occurs for large r and $\sin\delta$ close to unity. This further justifies our choice of processes since the chosen diagrams enhance the magnitude of the penguin process relative to the tree (typically the penguin amplitude is much smaller compared to the tree). One can see this by comparing the magnitudes of the CKM matrix elements V_{tb}, V_{td}, V_{ub} and V_{ud} in equation (3.31)

or by recalling that the CKM matrix is near diagonal. Finally, the strong phase difference between the two resonances varies rapidly and passes through 90^0.

To explain our calculations more explicitly, we simplify the full Feynman diagrams in Figures 4.1 and 4.2 to those in Figures 4.3 and 4.4. This allows us to write

$$\left\langle K^+K^-\pi^-\middle|H^T\middle|B^-\right\rangle = \frac{g_f}{s_f}t_f \tag{4.12}$$

where g_f is the $f_0 \to K^+K^-$ coupling, t_f is the amplitude to produce an f_0 through a tree diagram in which a π^- is also produced, and s_f is the inverse propagator for the f_0 meson

$$s_f = s - m_f^2 + im_f\Gamma_f \tag{4.13}$$

where $\sqrt{s} = m_{KK}$ is the invariant mass of the K^+K^- pair, m_f is the mass of the f_0 meson and Γ_f is the decay width of the f_0 meson. Further discussion of propagators for unstable particles is given in Appendix A.

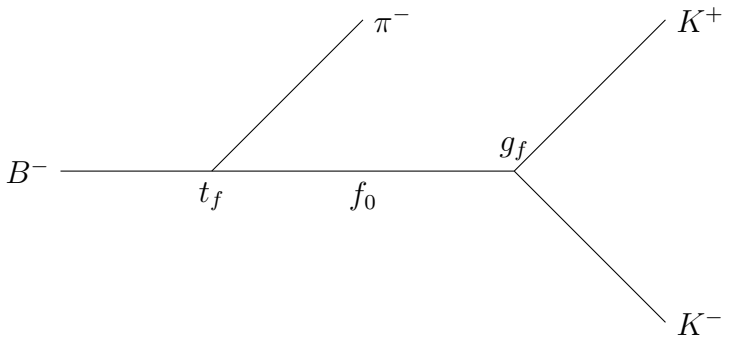

Figure 4.3: Simplified tree diagram for $B^- \to f_0(980)\pi^- \to K^+K^-\pi^-$. The decay progresses left to right.

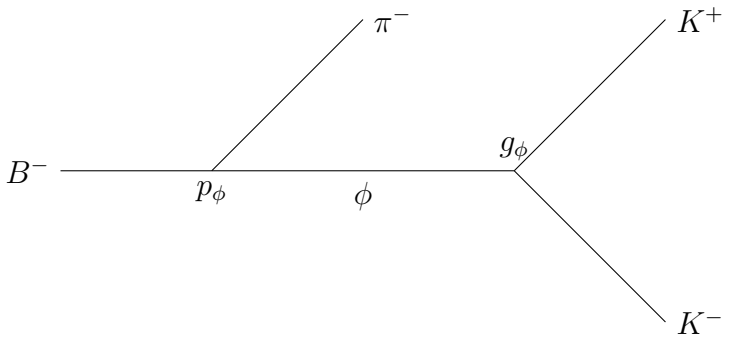

Figure 4.4: Simplified penguin diagram for $B^- \to \phi(1020)\pi^- \to K^+K^-\pi^-$. The decay progresses left to right.

Similarly, one can show that for the simplified penguin diagram in Figure 4.4, the corresponding matrix element can be written as

$$\left\langle K^+K^-\pi^-\middle|H^P\middle|B^-\right\rangle = \frac{g_\phi}{s_\phi}p_\phi \tag{4.14}$$

where the quantities are analogous to those in the tree amplitude. We can then take the ratio of equations (4.12) and (4.14) and write

$$re^{i\delta}e^{i\phi} = \frac{g_\phi p_\phi s_f}{g_f t_f s_\phi}\,. \tag{4.15}$$

Then, in the vein of similar studies [26] we make the following substitution. Define the ratio

$$r'e^{i(\delta_q+\phi)} \equiv \frac{p_\phi}{t_f} \tag{4.16}$$

where δ_q is a strong phase and ϕ the weak phase between the penguin and tree diagrams as previously defined. Then, substituting this into equation (4.15), we obtain

$$re^{i\delta}e^{i\phi} = \frac{g_\phi s_f}{g_f s_\phi}\left(\frac{p_\phi}{t_f}\right) = r'e^{i\delta_q}e^{i\phi}\frac{g_\phi s_f}{g_f s_\phi}\,, \tag{4.17}$$

and hence

$$re^{i\delta} = r'e^{i\delta_q}\frac{g_\phi s_f}{g_f s_\phi}\,. \tag{4.18}$$

We now have an expression for the ratio r and the strong phase difference δ. This will require the calculation of the tree and penguin amplitudes, covered in the next section. The final piece is just that due to the weak phase difference ϕ. We use the following parametrisation

$$\sin\phi = \frac{\eta}{\sqrt{[\rho(1-\rho)-\eta^2]^2+\eta^2}}\,, \qquad \cos\phi = \frac{\rho(1-\rho)-\eta^2}{\sqrt{[\rho(1-\rho)-\eta^2]^2+\eta^2}}\,, \tag{4.19}$$

where ρ and η are parameters in the Wolfenstein parametrisation of the CKM matrix. We use the values given in chapter 3 which we recall are

$$\lambda = 0.22506 \pm 0.00050\,, \tag{4.20}$$
$$A = 0.811 \pm 0.026\,, \tag{4.21}$$
$$\rho = 0.124^{+0.019}_{-0.018}\,, \tag{4.22}$$
$$\eta = 0.356 \pm 0.011\,, \tag{4.23}$$

and these allow us to compute the contributions to the CP asymmetry from the weak phase ϕ.

4.3 Tree and Penguin Amplitudes

At the end of the previous section we were able to fully account for the weak phase contribution to the CP asymmetry. We now continue with our calculation of the contributions due to r and δ, keeping equations (4.16) and (4.18) in mind. The amplitude for a given B meson decay to the final state F is generally written as [5]

$$A(B \to F) = \frac{G_F}{\sqrt{2}} \sum_{i=1}^{10} V^{T,P} a_i \langle F|O_i|B\rangle \ , \tag{4.24}$$

where G_F is the Fermi constant and $V^{T,P}$ are combinations of CKM matrix elements given by

$$V^T = |V_{ub}V_{ud}^*| \quad \text{for } i = 1, 2\,, \qquad V^P = |V_{tb}V_{td}^*| \quad \text{for } i = 3, \ldots, 10\,.$$

Note that in taking the ratio of penguin and tree diagrams, we need to calculate the quantity

$$\left|\frac{V_{tb}V_{td}^*}{V_{ub}V_{ud}^*}\right| .$$

Using the Wolfenstein parameterisation, one can show that

$$\left|\frac{V_{tb}V_{td}^*}{V_{ub}V_{ud}^*}\right| = \frac{\sqrt{(1-\rho)^2+\eta^2}}{(1-\lambda^2/2)\sqrt{\rho^2+\eta^2}}\,, \tag{4.25}$$

where the values of the various parameters in the Wolfenstein parametrisation are given at the end of the previous section. The a_i's in equation (4.24) are combinations of effective Wilson coefficients given by

$$a_{2j} = c'_{2j} + \frac{1}{N_c} c'_{2j-1}\,, \qquad a_{2j-1} = c'_{2j-1} + \frac{1}{N_c} c'_{2j}\,, \qquad j = 1, ..., 5\,.$$

The $\mathcal{O}_i$'s are the operators given in the OPE. More explicitly, we implement our proposed mechanism for the interaction of the two Feynman diagrams given in Figure 4.2 by writing

$$t_f \equiv A(B^- \xrightarrow{tree} f_0\pi^-) = \frac{G_F}{\sqrt{2}} \sum_{i=1}^{2} V^T a_i \left\langle f_0\pi^-\middle|\mathcal{O}_i\middle|B^-\right\rangle \tag{4.26}$$

$$p_\phi \equiv A(B^- \xrightarrow{penguin} \phi\pi^-) = -\frac{G_F}{\sqrt{2}} \sum_{i=3}^{6} V^P a_i \left\langle \phi\pi^-\middle|\mathcal{O}_i\middle|B^-\right\rangle \ . \tag{4.27}$$

Then, in order to calculate the last pieces for the asymmetry, those due to r and δ, equations (4.16) and (4.18) tell us that we simply need to compute the tree and penguin amplitudes in equations (4.26) and (4.27). The method we will use for this is that of a factorisation approximation, to be discussed in the next chapter.

Chapter 5

Hadronic Matrix Elements

The matrix elements identified at the end of the previous chapter are historically non-trivial to calculate since they involve QCD. Several schemes exist for carrying out the calculation, namely factorisation approaches and Lattice QCD. We use the approach of Naive Factorisation for its simplicity. This entails the use of Fierz identities and form factors, and we conclude the chapter with an initial result for the CP asymmetry.

5.1 Naive Factorisation

Naive Factorisation is a technique used to simplify hadronic matrix elements in the case of heavy meson decays. To justify this approximation, consider that the b quark decays are highly energetic, since the b quark has $m_b \approx 5$ GeV $\gg m_u$. This means any final state particles produced by the highly localised weak interaction move away very quickly and so become isolated. Hadronisation of the quark-antiquark pair then occurs at some sufficiently distant point so that the meson can be factorised out.

The approximation itself is as follows [5]; for a B meson decaying to a final state consisting of mesons M_1 and M_2 through some current operator $\mathcal{O}_i$, we can factorise the matrix elements

$$\langle M_1 M_2|\mathcal{O}_i|B\rangle = \langle M_2|J_{2i}|0\rangle \, \langle M_1|J_{1i}|B\rangle \ , \tag{5.1}$$

$$\text{or } \langle M_1 M_2|\mathcal{O}_i|B\rangle = \langle M_1|J_{4i}|0\rangle \, \langle M_2|J_{3i}|B\rangle \ , \tag{5.2}$$

where the J_{ki} are transition currents. Hence, we are able to approximate such matrix elements as products of simpler matrix elements. In general, the first factor corresponds to one of the final state particles being formed from the vacuum, while the second represents the other final state particle being produced from the B meson. Up to this point there is no reason we couldn't take one combination over the other, however in our calculations the choice of factorisation is determined by the flavours of the spinors in the transition currents. We require, for example, that the vacuum can only form a π^- through a $\bar{d}\gamma^\mu(1-\gamma_5)u$ current, since the π^- has quark content $\bar{u}d$. This means there is no ambiguity in how we should factorise our hadronic matrix elements and that the procedure is well defined.

The effects of hadronization are incorporated into the number of effective colours N_c which is taken to be the same for each operator $\mathcal{O}_i$. It has the following general form

$$\frac{1}{N_c} = \frac{1}{3} + \xi$$

where ξ is a parameter describing the non-factorizable colour octet contribution. Thus, in our model, we have N_c as a free parameter. As a note, the value of the gluon momentum transfer q^2 influences the allowed values for N_c. For $q^2/m_b^2 = 0.3$, we take values for N_c of 0.98 and 2.01, while for $q^2/m_b^2 = 0.5$ the equivalent values are $N_c = 0.94$ and 1.95 [5,26]. In both cases we also investigate $N_c = 3$ which is the physical limit of the number of colours.

5.1.1 Fierz Identities

The application of the Naive Factorisation is fairly straight forward, especially since we are neglecting the electroweak penguin diagrams. However, in one of the computations to follow, we require a useful tool called a Fierz identity (also known as a Fierz Reordering Theorem).

The Fierz identities allow for products of Dirac matrices and spinors to be rearranged. There are a number of these identities, although the only one we will need is

$$\bar{\psi}_1\gamma_\mu(1-\gamma_5)\psi_2\bar{\psi}_3\gamma^\mu(1+\gamma_5)\psi_4 = -2\bar{\psi}_1(1+\gamma_5)\psi_4\bar{\psi}_3(1-\gamma_5)\psi_2\,. \tag{5.3}$$

This will allow us to calculate the matrix elements for the penguin operators in which there are mixed chiral states and we need to rearrange the spinors using the cyclic property of traces. Here we will provide an outline for the proof of equation (5.3).

To start, we'll consider the case for spinors u_i which commute. The case for anticommuting spinors introduces an overall minus sign so we want to prove

$$\bar{u}_1\gamma_\mu(1-\gamma_5)u_2\bar{u}_3\gamma^\mu(1+\gamma_5)u_4 = 2\bar{u}_1(1+\gamma_5)u_4\bar{u}_3(1-\gamma_5)u_2\,. \tag{5.4}$$

In general, we can decompose a product of two Dirac bilinears in terms of the basis $\Gamma^A = \{1,\ \gamma_5,\ \gamma^\mu,\ \gamma^\mu\gamma_5,\ \sigma^{\mu\nu}\}$ [28]. We write this expansion as

$$\bar{u}_1\Gamma^A u_2\bar{u}_3\Gamma^B u_4 = \sum_{C,D} c_{CD}^{AB}\bar{u}_1\Gamma^C u_4\bar{u}_3\Gamma^D u_2 \tag{5.5}$$

with

$$c_{CD}^{AB} = \frac{1}{16}\,\mathrm{tr}\big(\Gamma^C\Gamma^A\Gamma^D\Gamma^B\big)\,. \tag{5.6}$$

To prove equation (5.6), consider

$$\bar{u}_{1\alpha}\Gamma^A u_{2\beta}\bar{u}_{3\gamma}\Gamma^B u_{4\delta} = \sum_{C,D} c_{CD}^{AB}\bar{u}_{1\alpha}u_{4\delta}\bar{u}_{3\gamma}u_{2\beta}\Gamma^C_{\alpha\delta}\Gamma^D_{\gamma\beta}$$

and so

$$\Gamma^A_{\alpha\beta}\Gamma^B_{\gamma\delta} = \sum_{C,D} \Gamma^C_{\alpha\delta}\Gamma^D_{\gamma\beta}\,.$$

Multiplying through by $\Gamma^E_{\delta\alpha}\Gamma^F_{\beta\gamma}$ on both sides, we obtain

$$\Gamma^E_{\delta\alpha}\Gamma^A_{\alpha\beta}\Gamma^F_{\beta\gamma}\Gamma^B_{\gamma\delta} = \sum_{C,D} \Gamma^C_{\alpha\delta}\Gamma^E_{\delta\alpha}\Gamma^D_{\gamma\beta}\Gamma^F_{\beta\gamma} = 16c^{AB}_{EF}\,,$$

where we've recognised the two traces $\mathrm{tr}\big(\Gamma^C\Gamma^E\big) = \Gamma^C_{\alpha\delta}\Gamma^E_{\delta\alpha}$ and $\mathrm{tr}\big(\Gamma^F\Gamma^D\big) = \Gamma^F_{\beta\gamma}\Gamma^D_{\gamma\beta}$, and used the fact that $\mathrm{tr}\big(\Gamma^A\Gamma^B\big) = 4\delta^{AB}$. Rewriting the left-hand side as a trace as well, we see that we've proven equation (5.6).

The decomposition shown in equation (5.5) is the foundation for the remainder of the proof, and all the hard work goes into computing the coefficients c^{AB}_{CD}. We will label the coefficients by the classification of the Dirac bilinears as scalar (S), pseudoscalar (P), vector (V), axial vector (A) or antisymmetric tensor (T).

Continuing to the main proof, we have

$$\begin{aligned}\bar{u}_1\gamma_\mu(1-\gamma_5)u_2\bar{u}_3\gamma^\mu(1+\gamma_5)u_4 = \bar{u}_1\gamma_\mu u_2\bar{u}_3\gamma^\mu u_4 - \bar{u}_1\gamma_\mu\gamma_5 u_2\bar{u}_3\gamma^\mu\gamma_5 u_4 \\ - \bar{u}_1\gamma_\mu\gamma_5 u_2\bar{u}_3\gamma^\mu u_4 + \bar{u}_1\gamma_\mu u_2\bar{u}_3\gamma^\mu\gamma_5 u_4\,. \qquad (5.7)\end{aligned}$$

Then we apply equation (5.5) to each of these four terms. The first term is expanded as

$$\begin{aligned}\bar{u}_1\gamma_\mu u_2\bar{u}_3\gamma^\mu u_4 = c^{VV}_{SS}\,\bar{u}_1 u_4\bar{u}_3 u_2 + c^{VV}_{PP}\bar{u}_1\gamma_5 u_4\bar{u}_3\gamma_5 u_2 \\ + c^{VV}_{VV}\bar{u}_1\gamma_\mu u_4\bar{u}_3\gamma^\mu u_2 + c^{VV}_{AA}\bar{u}_1\gamma_\mu\gamma_5 u_4\bar{u}_3\gamma^\mu\gamma_5 u_2 \\ + c^{VV}_{TT}\bar{u}_1\sigma_{\mu\nu}u_4\bar{u}_3\sigma^{\mu\nu}u_2\end{aligned}$$

where we note that we can only have bilinears with the same overall Lorentz structure as the left-hand side, and only those bilinears which give an even number of gamma matrices will survive when we take the trace to get the coefficients c^{AB}_{CD}.

Then, it's just a matter of calculating the coefficients c^{AB}_{CD} from the traces of gamma matrices. For example

$$\begin{aligned}c^{VV}_{SS} &= \frac{1}{16}\,\mathrm{tr}(1.\gamma_\mu.1.\gamma^\mu) = \frac{1}{16}\,\mathrm{tr}(4\mathbb{I}_4) = 1\,,\\ c^{VV}_{PP} &= \frac{1}{16}\,\mathrm{tr}(\gamma_5\gamma_\mu\gamma_5\gamma^\mu) = -\frac{1}{16}\,\mathrm{tr}(\gamma_5\gamma_5\gamma_\mu\gamma^\mu) = -\frac{1}{16}\,\mathrm{tr}(4\mathbb{I}_4) = -1\,.\end{aligned}$$

This is the general process, but rather than doing this for each term, one typically looks up the coefficients from the following equation, from [28]

$$\begin{pmatrix} S \\ V \\ T \\ A \\ P \end{pmatrix} = \frac{1}{4} \begin{pmatrix} 1 & 1 & 1 & 1 & 1 \\ 4 & -2 & 0 & 2 & -4 \\ 6 & 0 & -2 & 0 & 6 \\ 4 & 2 & 0 & -2 & -4 \\ 1 & -1 & 1 & -1 & 1 \end{pmatrix} \begin{pmatrix} S' \\ V' \\ T' \\ A' \\ P' \end{pmatrix} , \tag{5.8}$$

where the primed indices indicate the reordered spinors. This accounts for the first two terms of equation (5.7). For the last two terms, we have mixed bilinear classifications and so we need to compute the traces of the gamma matrices explicitly.

It is a straightforward but tedious matter then of writing out all the expanded terms in equation (5.7) using equation (5.5), collecting like terms and cancelling until one eventually ends up with

$$\bar{u}_1\gamma_\mu(1-\gamma_5)u_2\bar{u}_3\gamma^\mu(1+\gamma_5)u_4 = 2\bar{u}_1(1+\gamma_5)u_4\bar{u}_3(1-\gamma_5)u_2\,. \tag{5.9}$$

Then, replacing the u_i spinors with fermion spinors, one obtains the required Fierz identity.

5.2 Factorisation Approximation

In the following calculation, we make use of Naive Factorisation and the Fierz identity in equation (5.3) to compute the hadronic matrix elements identified at the end of the previous chapter. The expressions for the operators $\mathcal{O}_i$ are given in equations (3.54) to (3.63).

For $\mathcal{O}_1$, we get

$$\begin{aligned} \langle f_0\pi^-|\mathcal{O}_1|B^-\rangle &= \langle f_0\pi^-|\bar{d}_\alpha\gamma_\mu(1-\gamma_5)u_\beta\bar{u}_\beta\gamma^\mu(1-\gamma_5)b_\alpha|B^-\rangle \\ &= \langle f_0\pi^-|\bar{d}\gamma_\mu(1-\gamma_5)b\bar{u}\gamma^\mu(1-\gamma_5)u)|B^-\rangle \\ &= \langle f_0|\bar{u}\gamma_\mu(1-\gamma_5)u|0\rangle\ \langle\pi^-|\bar{d}\gamma^\mu(1-\gamma_5)b|B^-\rangle\ . \end{aligned}$$

Similarly, for $\mathcal{O}_2$ we obtain

$$\begin{aligned} \langle f_0\pi^-|\mathcal{O}_2|B^-\rangle &= \langle f_0\pi^-|\bar{d}\gamma_\mu(1-\gamma_5)u\bar{u}\gamma^\mu(1-\gamma_5)b|B^-\rangle \\ &= \langle f_0|\bar{u}\gamma_\mu(1-\gamma_5)b|B^-\rangle\ \langle\pi^-|\bar{d}\gamma^\mu(1-\gamma_5)u|0\rangle\ . \end{aligned}$$

Now consider the penguin operator contributions. For $\mathcal{O}_3$ we have

$$\begin{aligned} &\langle\phi\pi^-|\mathcal{O}_3|B^-\rangle = \langle\phi\pi^-|\bar{d}\gamma_\mu(1-\gamma_5)b\sum_{q'}\bar{q}'\gamma^\mu(1-\gamma_5)q'|B^-\rangle \\ &= \langle\phi\pi^-|\bar{d}\gamma_\mu(1-\gamma_5)b\big(\bar{u}\gamma^\mu(1-\gamma_5)u + \bar{d}\gamma^\mu(1-\gamma_5)d + \bar{s}\gamma^\mu(1-\gamma_5)s\big)|B^-\rangle \\ &= \langle\phi|\bar{u}\gamma_\mu(1-\gamma_5)u + \bar{d}\gamma_\mu(1-\gamma_5)d + \bar{s}\gamma_\mu(1-\gamma_5)s|0\rangle\ \langle\pi^-|\bar{d}\gamma^\mu(1-\gamma_5)b|B^-\rangle\ . \end{aligned}$$

For $\mathcal{O}_4$,

$$\begin{aligned}
\langle\phi\pi^-|\mathcal{O}_4|B^-\rangle &= \langle\phi\pi^-|\bar{d}_\alpha\gamma_\mu(1-\gamma_5)b_\beta\sum_{q'}\bar{q'}_\beta\gamma^\mu(1-\gamma_5)q'_\alpha|B^-\rangle \\
&= \langle\phi\pi^-|\bar{d}_\alpha\gamma_\mu(1-\gamma_5)b_\beta\big(\bar{u}_\beta\gamma^\mu(1-\gamma_5)u_\alpha+\bar{d}_\beta\gamma^\mu(1-\gamma_5)d_\alpha+\bar{s}_\beta\gamma^\mu(1-\gamma_5)s_\alpha\big)|B^-\rangle \\
&= \langle\phi\pi^-|\bar{d}_\alpha\gamma_\mu(1-\gamma_5)b_\beta\big(\bar{u}_\beta\gamma^\mu(1-\gamma_5)u_\alpha+\bar{d}_\beta\gamma^\mu(1-\gamma_5)d_\alpha\big)|B^-\rangle \\
&= \langle\phi\pi^-|\bar{d}\gamma^\mu(1-\gamma_5)u\bar{u}\gamma_\mu(1-\gamma_5)b+\bar{d}\gamma^\mu(1-\gamma_5)d\bar{d}\gamma_\mu(1-\gamma_5)b|B^-\rangle \\
&= \langle\phi\pi^-|\bar{d}\gamma^\mu(1-\gamma_5)u\bar{u}\gamma_\mu(1-\gamma_5)b|B^-\rangle+\langle\phi\pi^-|\bar{d}\gamma^\mu(1-\gamma_5)d\bar{d}\gamma_\mu(1-\gamma_5)b|B^-\rangle \\
&= \langle\phi|\bar{u}\gamma_\mu(1-\gamma_5)b|B^-\rangle\,\langle\pi^-|\bar{d}\gamma^\mu(1-\gamma_5)u|0\rangle \\
&\qquad + \langle\phi|\bar{d}\gamma^\mu(1-\gamma_5)d|0\rangle\,\langle\pi^-|\bar{d}\gamma_\mu(1-\gamma_5)b|B^-\rangle\,.
\end{aligned}$$

For $\mathcal{O}_5$,

$$\begin{aligned}
\langle\phi\pi^-|\mathcal{O}_5|B^-\rangle &= \langle\phi\pi^-|\bar{d}\gamma_\mu(1-\gamma_5)b\sum_{q'}\bar{q'}\gamma^\mu(1+\gamma_5)q'|B^-\rangle \\
&= \langle\phi\pi^-|\bar{d}\gamma_\mu(1-\gamma_5)b\big(\bar{u}\gamma^\mu(1+\gamma_5)u+\bar{d}\gamma^\mu(1+\gamma_5)d+\bar{s}\gamma^\mu(1+\gamma_5)s\big)|B^-\rangle \\
&= \langle\phi|\bar{u}\gamma^\mu(1+\gamma_5)u+\bar{d}\gamma^\mu(1+\gamma_5)d+\bar{s}\gamma^\mu(1+\gamma_5)s|0\rangle\,\langle\pi^-|\bar{d}\gamma_\mu(1-\gamma_5)b|B^-\rangle\,.
\end{aligned}$$

The final calculation makes use of the Fierz identity in equation (5.3).

$$\begin{aligned}
\langle\phi\pi^-|\mathcal{O}_6|B^-\rangle &= \langle\phi\pi^-|\bar{d}_\alpha\gamma_\mu(1-\gamma_5)b_\beta\sum_{q'}\bar{q'}_\beta\gamma^\mu(1+\gamma_5)q'_\alpha|B^-\rangle \\
&= \langle\phi\pi^-|\bar{d}_\alpha\gamma_\mu(1-\gamma_5)b_\beta\big(\bar{u}_\beta\gamma^\mu(1+\gamma_5)u_\alpha+\bar{d}_\beta\gamma^\mu(1+\gamma_5)d_\alpha+\bar{s}_\beta\gamma^\mu(1+\gamma_5)s_\alpha\big)|B^-\rangle \\
&= -2\,\langle\phi\pi^-|\bar{d}_\alpha(1+\gamma_5)\big[u_\alpha\bar{u}_\beta+d_\alpha\bar{d}_\beta+s_\alpha\bar{s}_\beta\big](1-\gamma_5)b_\beta|B^-\rangle \\
&= -2\big(\langle\phi\pi^-|\bar{d}(1+\gamma_5)u\bar{u}(1-\gamma_5)b|B^-\rangle+\langle\phi\pi^-|\bar{d}(1+\gamma_5)d\bar{d}(1-\gamma_5)b|B^-\rangle \\
&\qquad + \langle\phi\pi^-|\bar{d}(1+\gamma_5)s\bar{s}(1-\gamma_5)b|B^-\rangle\big) \\
&= -2\big(\langle\pi^-|\bar{d}(1+\gamma_5)u|0\rangle\,\langle\phi|\bar{u}(1-\gamma_5)b|B^-\rangle \\
&\qquad + \langle\phi|\bar{d}(1+\gamma_5)d|0\rangle\,\langle\pi^-|\bar{d}(1-\gamma_5)b|B^-\rangle\big)\,.
\end{aligned}$$

To summarise, we have the 6 matrix elements

$$\langle f_0\pi^-|\mathcal{O}_1|B^-\rangle = \langle f_0|\bar{u}\gamma_\mu(1-\gamma_5)u|0\rangle \langle \pi^-|\bar{d}\gamma^\mu(1-\gamma_5)b|B^-\rangle , \tag{5.10}$$

$$\langle f_0\pi^-|\mathcal{O}_2|B^-\rangle = \langle f_0|\bar{u}\gamma_\mu(1-\gamma_5)b|B^-\rangle \langle \pi^-|\bar{d}\gamma^\mu(1-\gamma_5)u|0\rangle , \tag{5.11}$$

$$\begin{aligned}\langle \phi\pi^-|\mathcal{O}_3|B^-\rangle = {} & \langle \phi|\bar{u}\gamma_\mu(1-\gamma_5)u + \bar{d}\gamma_\mu(1-\gamma_5)d + \bar{s}\gamma_\mu(1-\gamma_5)s|0\rangle \\ & \times \langle \pi^-|\bar{d}\gamma^\mu(1-\gamma_5)b|B^-\rangle ,\end{aligned} \tag{5.12}$$

$$\begin{aligned}\langle \phi\pi^-|\mathcal{O}_4|B^-\rangle = {} & \langle \phi|\bar{u}\gamma_\mu(1-\gamma_5)b|B^-\rangle \langle \pi^-|\bar{d}\gamma^\mu(1-\gamma_5)u|0\rangle \\ & + \langle \phi|\bar{d}\gamma^\mu(1-\gamma_5)d|0\rangle \langle \pi^-|\bar{d}\gamma_\mu(1-\gamma_5)b|B^-\rangle ,\end{aligned} \tag{5.13}$$

$$\begin{aligned}\langle \phi\pi^-|\mathcal{O}_5|B^-\rangle = {} & \langle \phi|\bar{u}\gamma^\mu(1+\gamma_5)u + \bar{d}\gamma^\mu(1+\gamma_5)d + \bar{s}\gamma^\mu(1+\gamma_5)s|0\rangle \\ & \times \langle \pi^-|\bar{d}\gamma_\mu(1-\gamma_5)b|B^-\rangle ,\end{aligned} \tag{5.14}$$

$$\begin{aligned}\langle \phi\pi^-|\mathcal{O}_6|B^-\rangle = -2\big(& \langle \pi^-|\bar{d}(1+\gamma_5)u|0\rangle \langle \phi|\bar{u}(1-\gamma_5)b|B^-\rangle \\ & + \langle \phi|\bar{d}(1+\gamma_5)d|0\rangle \langle \pi^-|\bar{d}(1-\gamma_5)b|B^-\rangle \big) .\end{aligned} \tag{5.15}$$

Now that we have the required matrix elements in a factorised form, we need some way of computing them. To meet this need, we introduce some form factors.

5.3 Form Factors

Form factors are of widespread use in nuclear and particle physics. They are typically used for describing the complex interactions between particles and describing features of their structure. We briefly introduce their formalism here and then detail the required form factors for our calculation of the matrix elements.

5.3.1 Motivation

Consider the matrix element $\langle P|J^\mu|B\rangle$ for the transition from a B meson to some pseudoscalar meson P through a $V-A$ current J^μ. By considering Lorentz covariance, we know that this matrix element behaves like a Lorentz four-vector so can be written in terms of a basis for the Lorentz four-vector space. We thus need to choose a convenient basis from the available four-vectors P_P and P_B. We choose as our basis vectors $P_B + P_P$ and $P_B - P_P = k$ since these are manifestly linearly independent and span the available space [23].

We write our matrix element as a linear combination of the basis vectors and have

$$\langle P|J^\mu|B\rangle = (P_B + P_P)^\mu f_+(k^2) + (P_B - P_P)^\mu f_-(k^2) , \tag{5.16}$$

where $f_{\pm}(k^2)$ are scalar functions of the momentum transfer. These are our form factors. We can then introduce another set of form factors $F_0(k^2)\,, F_1(k^2)$ to obtain

$$\langle P|J^{\mu}|B\rangle = \left(P_B + P_P - \frac{M_B^2 - M_P^2}{k^2}k\right)^{\mu} F_1(k^2) + \left(\frac{M_B^2 - M_P^2}{k^2}k^{\mu}\right)F_0(k^2)\,. \quad (5.17)$$

Clearly we have the following equations relating the form factors

$$F_1(k^2) = f_+(k^2)\,, \quad (5.18)$$

$$F_0(k^2) = f_+(k^2) + \frac{k^2}{M_1^2 - M_2^2}f_-(k^2)\,. \quad (5.19)$$

It is typical in such calculations to take the nearest pole dominance assumption [5, 26, 29] in which the form factors are described by

$$f_{\pm}(k^2) = \frac{f_{\pm}(0)}{\left(1 - k^2/M_{pole}^2\right)^n}\,. \quad (5.20)$$

Here, M_{pole} is a pole mass and n denotes the order of the pole. The motivation behind this form is that resonances appear as poles in the S-matrix for the decays [21]. These are just the physical poles and the unphysical poles which are nearby may influence the dependence on k^2.

In [5, 26, 29] several models are used, such as $n = 1$ and $n = 2$ monopole dominance (for a single pole close to the resonance) and also dipole dominance (for two poles close to the resonance). For our case, we start with the $n = 1$ monopole dominance assumption. Later calculations will investigate the influence of the $n = 2$ monopole and dipole dominance assumptions on the final CP asymmetry. In all cases, we use values for the pole masses and form factor coefficients given in [5,26,29]. For the monopole dominance assumption, we have

$$F_1(k^2) = \frac{h_1}{\left(1 - \dfrac{k^2}{m_1^2}\right)^n} \quad (5.21)$$

with $f_+(0) = f_-(0) = h_1 = 0.330$, $m_1 = 5.320$ GeV/c^2 and $F_1(0) = F_0(0)$.

5.3.2 Matrix Element Parameterisation

With this motivation, it should come as no surprise that we can similarly parameterise the other matrix elements in terms of form factors and 4-momenta. For completeness, the relevant expressions for the B meson transitions are [26, 30]

$$\langle P|\hat{V}_{\mu}|B\rangle = \left(P_B + P_P - \frac{m_B^2 - m_P^2}{k^2}k\right)_{\mu} F_1(k^2) + \frac{m_B^2 - m_P^2}{k^2}k_{\mu}F_0(k^2)\,, \quad (5.22)$$

$$\langle V|\hat{V}_\mu - \hat{A}_\mu|B\rangle = \frac{2}{m_B+m_V}\epsilon_{\mu\nu\rho\sigma}\varepsilon^\nu P_B^\rho P_V^\sigma \mathcal{V}(k^2) + i\Bigg(\varepsilon_\mu(m_B+m_V)A_1(k^2) - \frac{\varepsilon\cdot k}{m_B+m_V}(P_B+P_V)_\mu A_2(k^2) - \frac{\varepsilon\cdot k}{k^2}2m_V k_\mu\big(A_3(k^2)-A_0(k^2)\big)\Bigg), \tag{5.23}$$

$$\langle S|\hat{A}_\mu|B\rangle = -i\left[\left(P_B+P_S-\frac{m_B^2-m_S^2}{k^2}k\right)_\mu F_1(k^2) + \frac{m_B^2-m_S^2}{k^2}k_\mu F_0(k^2)\right]. \tag{5.24}$$

Here, for $X = P$ or V, m_X and P_X are the mass and 4-momentum of the particle X and $k \equiv P_B - P_X$ is the momentum transfer. $F_0(k^2)$ and $F_1(k^2)$ are $B \to P$ and $B \to S$ transition form factors. ε^μ is the polarisation 4-vector for the vector meson, and $\mathcal{V},\ A_0,\ A_1,\ A_2,\ A_3$ are $B \to V$ transition form factors. $\epsilon_{\mu\nu\rho\sigma}$ is the Levi-Cevita antisymmetric tensor with $\epsilon_{0123} = +1$. We will come to find that the $\mathcal{V}$, A_1, A_2, and A_3 form factors won't contribute (see Appendix A). The form factor A_0 is given in [5, 26, 29] as

$$A_0(k^2) = \frac{h_{A_0}}{\left(1-\frac{k^2}{m_0^2}\right)^n} \tag{5.25}$$

with $h_{A_0} = 0.28$ and $m_0 = 5.27\ \text{GeV}/c^2$.

The vacuum transitions are much simpler and read

$$\langle P(p')|\hat{A}_\mu|0\rangle = -if_P p'_\mu, \tag{5.26}$$

$$\langle V(p')|\hat{V}_\mu|0\rangle = f_V m_V \varepsilon_\mu, \tag{5.27}$$

$$\langle S(p')|\hat{V}_\mu|0\rangle = f_S p'_\mu. \tag{5.28}$$

At this point it looks like we haven't made our lives a whole lot easier, however we note that we never need to calculate a matrix element on its own; they always come as fully contracted pairs after applying Naive Factorisation. This significantly simplifies the computations once we recognise the simple forms of the pairs of contracted matrix elements. This is the topic of the following section.

5.4 Matrix Element Contraction

With expressions (5.22) to (5.28) for the matrix elements in hand, we return to looking at the expressions for the factorised matrix elements in equations (5.10) to (5.15). We begin by applying parity and charge conjugation symmetries to find that the first matrix element, corresponding to $\mathcal{O}_1$, is zero [31].

We further note that the last matrix element, corresponding to $\mathcal{O}_6$, must also vanish since it involves vector mesons in the final states. These vector mesons require a current with either a vector or pseudovector component to form the vector meson polarisation vector. Since the Fierz transformed current has only scalar

and pseudoscalar components, this gives zero contribution so the matrix element corresponding to $\mathcal{O}_6$ vanishes.

We are now in a position to make use of equations (5.22) to (5.28). To calculate the $\mathcal{O}_2$ matrix element, we modify the general result for a $B \to P_1P_2$ transition where P_1 and P_2 are two pseudoscalar mesons,

$$\langle P_2|J^\mu|0\rangle \ \langle P_1|J'_\mu|B\rangle = if_{P_2}(m_B^2 - m_{P_1}^2)F_0(m_{P_2}^2)\,. \tag{5.29}$$

Making the replacement $P_1 \to S$ we just get an additional factor of i (see equations (5.22) and (5.24)) and we obtain the general result for a $B \to PS$ transition:

$$\langle P|J^\mu|0\rangle \ \langle S|J'_\mu|B\rangle = -f_P(m_B^2 - m_S^2)F_0(m_P^2)\,. \tag{5.30}$$

Likewise, we compute the inner product of pairs of matrix elements in the general cases involving a B meson transitioning to a pseudoscalar or vector final state. The results are

$$\langle V|J_\mu|0\rangle \ \langle P|J'^\mu|B\rangle = 2f_V m_B p_c F_1(m_V^2)\,, \tag{5.31}$$
$$\langle P|J_\mu|0\rangle \ \langle V|J'^\mu|B\rangle = 2f_P m_B p_c A_0(m_P^2)\,, \tag{5.32}$$

where P is a pseudoscalar meson, V is a vector meson, B is a B meson; J^μ and J'^μ are $V-A$ currents; f_i is the decay constant for the $i = P, V$ meson; m_j is the mass of the $j = P, V$ or B meson; F_1 is a form factor for the pseudoscalar meson and A_0 is a form factor for the vector meson; p_c is the magnitude of the 3-momentum in the centre of momentum frame

$$p_c = |\boldsymbol{p}_P| = |\boldsymbol{p}_V| = \frac{\sqrt{(m_B^2 - (m_P + m_V)^2)(m_B^2 - (m_P - m_V)^2)}}{2m_B}\,. \tag{5.33}$$

The proofs of equations (5.29) to (5.33) are given in Appendix A. These general results allow us to quickly compute the matrix elements corresponding to the operators $\mathcal{O}_2$, $\mathcal{O}_3$, $\mathcal{O}_4$ and $\mathcal{O}_5$. Comparing with equations (5.10) to (5.15), the results are given below:

$$\left\langle f_0\pi^-\middle|O_2\middle|B^-\right\rangle = -f_\pi(m_B^2 - m_f^2)F_0(m_\pi^2)\,, \tag{5.34}$$
$$\left\langle \phi\pi^-\middle|O_3\middle|B^-\right\rangle = 2f_\phi m_B p_c F_1(m_\phi^2)\,, \tag{5.35}$$
$$\left\langle \phi\pi^-\middle|O_4\middle|B^-\right\rangle = 2m_B p_c\big(f_\pi A_0(m_\pi^2) + f_\phi F_1(m_\phi^2)\big)\,, \tag{5.36}$$
$$\left\langle \phi\pi^-\middle|O_5\middle|B^-\right\rangle = 2f_\phi m_B p_c F_1(m_\phi^2)\,. \tag{5.37}$$

With these expressions in mind, we write the expressions for the tree and penguin amplitudes t_f and p_ϕ

$$t_f = \frac{G_F}{\sqrt{2}} V_{ub}V_{ud}^* a_2 \left\langle f_0\pi^-\middle|O_2\middle|B^-\right\rangle\,, \tag{5.38}$$

$$p_\phi = -\frac{G_F}{\sqrt{2}} V_{tb} V_{td}^* \left(a_3 \left\langle \phi\pi^- \middle| O_3 \middle| B^- \right\rangle + a_4 \left\langle \phi\pi^- \middle| O_4 \middle| B^- \right\rangle + a_5 \left\langle \phi\pi^- \middle| O_5 \middle| B^- \right\rangle \right) . \quad (5.39)$$

Then we can use equations (5.34) to (5.37) to calculate t_f and p_ϕ and thus calculate the ratio p_ϕ/t_f. To summarise, recall that the process we're using to find the CP asymmetry is

$$\mathcal{A}_{CP} \equiv \frac{|A(B^- \to K^+K^-\pi^-)|^2 - |A(B^+ \to K^+K^-\pi^+)|^2}{|A(B^- \to K^+K^-\pi^-)|^2 + |A(B^+ \to K^+K^-\pi^+)|^2}$$

which can be shown to be equivalent to

$$\mathcal{A}_{CP} = -\frac{2r \sin\delta \sin\phi}{1 + 2r\cos\delta\cos\phi + r^2} \quad (5.40)$$

where

$$re^{i\delta}e^{i\phi} = \frac{\langle K^+K^-\pi^-|H^P|B^-\rangle}{\langle K^+K^-\pi^-|H^T|B^-\rangle} . \quad (5.41)$$

We then parametrised equation (5.41) using t_f and p_ϕ as

$$\frac{\langle K^+K^-\pi^-|H^P|B^-\rangle}{\langle K^+K^-\pi^-|H^T|B^-\rangle} = \frac{g_\phi p_\phi}{g_f t_f} \frac{s_f}{s_\phi}$$

Next we used equation (4.16) to separate out the strong and weak phase contributions; the weak phase contribution was calculated using the Wolfenstein parametrisation of the CKM matrix while the strong phase contribution and ratio of the tree and penguin diagrams was calculated through the Naive Factorisation approximation. Note that the quantities g_ϕ, g_f, p_ϕ and t_f amount to an overall constant multiplying the propagators which we recall have the form

$$s_M = s - m_M^2 + i m_M \Gamma_M . \quad (5.42)$$

We use values for the relevant quantities in s_f and s_ϕ from the Particle Data Group as well as the following [32, 33]

$$g_\phi = 4.5 , \text{ GeV} \qquad g_f = 7.8 \text{ GeV} . \quad (5.43)$$

Then it is a simple matter of extracting the relevant pieces for the asymmetry

$$r = \left| re^{i\delta} \right| , \qquad r\cos\delta = Re(re^{i\delta}) , \qquad r\sin\delta = Im(re^{i\delta}) , \quad (5.44)$$

and plotting the asymmetry as a function of $s = m_{KK}$, the invariant mass of the K^+K^- pair.

5.5 Initial Results

Recall that we have several parameters in our model such as N_c, η, ρ and q^2/m_b^2. For this initial calculation, we choose $q^2/m_b^2 = 0.3\,,\ N_c = 0.98\,,\ \rho = \rho_{max}\,,\ \eta = \eta_{max}$. The result of our initial work is shown in Figure 5.1.

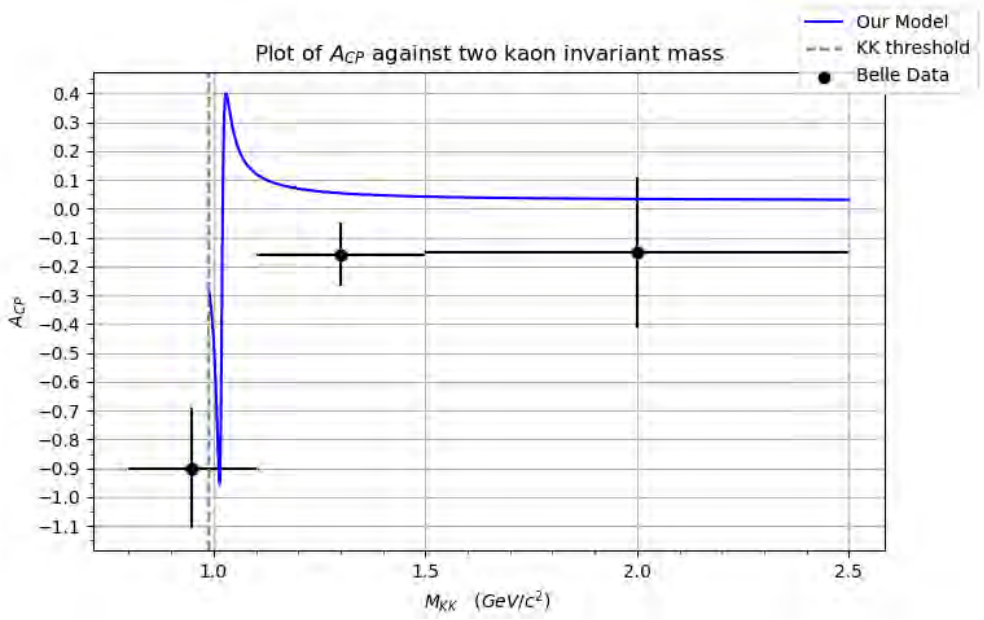

Figure 5.1: Plot of the CP asymmetry against the two kaon invariant mass. The Belle data is shown as well for comparison.

There are several important features to observe in Figure 5.1. First, we note that although the Belle Collaboration label the first bin as $0.8 - 1.1$ GeV/c^2 in the K^+K^- invariant mass, their measurement is achieved by averaging across this bin. The threshold for K^+K^- production is about 0.988 GeV/c^2 or twice the mass of the kaon at $m_K = 0.494$ GeV/c^2. This is indicated by the dashed line on Figure 5.1. For our purely theoretical calculation of the asymmetry, the threshold is a hard cutoff for the allowed decays. Taking this into account, we see that our curve predicts a large CP asymmetry in the $0.8 - 1.1$ GeV/c^2 bin, in agreement with the Belle data.

Second, we note that just after the downward spike at 1.0 GeV/c^2, there is a sharp upward peak in the asymmetry. This clearly doesn't agree with the Belle data in either of the two lowest bins.

Finally, the tail of the asymmetry is almost negligible and this is important. Recall that when we outlined our choice of the $\phi(1020)$ meson for the penguin diagram, we noted that it had a narrow width of about 4 MeV/c^2. As such, we should expect the interference between the penguin and tree diagrams to fall off rapidly away from the mass of the ϕ. This is evident in the right hand tail approaching zero.

Although we've reproduced a significant asymmetry in the first Belle bin, clearly the result of our calculation is not sufficient to fully explain the result seen at

Belle. In particular, we'd really like to have some way of calculating an averaged asymmetry across the bin. A naive average of the asymmetry involves integrating $\mathcal{A}_{CP}$ as a function of m_{KK} across the first Belle bin. The two opposite spikes in the asymmetry lead to an integrated asymmetry of $\mathcal{A}_{CP} = -0.00464$, which seems almost negligible. So, despite the promising minimum in the asymmetry in the region of interest, it appears our model doesn't reproduce the result from Belle as is. The following chapter contains a discussion of improvements made to the calculation and its extension.

Chapter 6

Revised Calculation

With the plot obtained at the end of the previous chapter, we see that there is some agreement with the Belle findings. However, there are several discrepancies which need to be addressed. The purpose of this chapter is to revise our definition of the CP asymmetry to allow us to integrate over the available phase space. We begin by introducing this phase space and construct it using Dalitz plot parameters, and we also introduce the Breit Wigner and Flatté parametrisations of the meson propagators. We then report results from our original model before moving on to a new model involving non-resonant processes.

6.1 Lorentz Invariant Phase Space

Fundamentally, our approach thus far has been one contrived from pure theory. As such, it doesn't make complete sense to compare this directly with the experimentally measured findings from Belle. For example, there is a finite resolution to any physical measurement whereas we quote our predicted curve for the CP asymmetry with infinite resolution. In other words, we need some way to make our prediction more realistic.

To do this, we need to be more careful in our derivation of the CP asymmetry. Recall equation (4.2) which had

$$\mathcal{A}_{CP} \equiv \frac{\Gamma(B^- \to K^+K^-\pi^-) - \Gamma(B^+ \to K^+K^-\pi^+)}{\Gamma(B^- \to K^+K^-\pi^-) + \Gamma(B^+ \to K^+K^-\pi^+)}\,. \tag{6.1}$$

In chapter 4 we went on to say that the asymmetry could be written as

$$\mathcal{A}_{CP} = \frac{|A(B^- \to K^+K^-\pi^-)|^2 - |A(B^+ \to K^+K^-\pi^+)|^2}{|A(B^- \to K^+K^-\pi^-)|^2 + |A(B^+ \to K^+K^-\pi^+)|^2}\,. \tag{6.2}$$

Rather than jumping straight to this equation, we write the explicit definition of the decay rate Γ as

$$\Gamma = \int d\Gamma\,, \tag{6.3}$$

where the **differential decay rate** $d\Gamma$ is defined as [8]

$$d\Gamma = \frac{1}{2m_B}|A|^2 d\Pi\,. \tag{6.4}$$

Here, m_B is the mass of the B meson, $|A|^2$ is the amplitude squared for the given decay and $d\Pi$ is the **Lorentz Invariant Phase Space** (LIPS) [8] defined by

$$\begin{aligned} d\Pi &= (2\pi)^4\delta^4\Big(\sum p\Big)\prod_{i=1}^{3}\frac{d^3p_i}{(2\pi)^3}\frac{1}{2E_{p_i}} \\ &= (2\pi)^4\delta^4\Big(\sum p\Big)\frac{d^3p}{(2\pi)^3}\frac{d^3k_1}{(2\pi)^3}\frac{d^3k_2}{(2\pi)^3}\frac{1}{2E_p}\frac{1}{2E_{k_1}}\frac{1}{2E_{k_2}}\,. \end{aligned} \tag{6.5}$$

Note that in equation (6.5) the delta function contains a sum of 4-momenta to enforce 4-momentum conservation, and the product over the index i is over all the final particle states (corresponding to the final momenta for the $\pi^\pm$, K^+ and K^-; p, k_1 and k_2 respectively).

Now, if we substitute equation (6.4) into equation (6.3) and then use this in equation (6.1), we obtain

$$\begin{aligned} \mathcal{A}_{CP} &= \frac{\int \frac{1}{2m_B}|A_-|^2 d\Pi - \int \frac{1}{2m_B}|A_+|^2 d\Pi}{\int \frac{1}{2m_B}|A_-|^2 d\Pi + \int \frac{1}{2m_B}|A_+|^2 d\Pi} \\ &= \frac{\int |A_-|^2 d\Pi - \int |A_+|^2 d\Pi}{\int |A_-|^2 d\Pi + \int |A_+|^2 d\Pi}\,, \end{aligned} \tag{6.6}$$

where we've introduced the notation $A_\pm \equiv A(B^\pm \to K^+K^-\pi^\pm)$. Now, we note that the LIPS is the same for both types of decay so we simplify this to

$$\mathcal{A}_{CP} = \frac{\int |A(B^- \to K^+K^-\pi^-)|^2 - |A(B^+ \to K^+K^-\pi^+)|^2 \; d\Pi}{\int |A(B^- \to K^+K^-\pi^-)|^2 + |A(B^+ \to K^+K^-\pi^+)|^2 \; d\Pi}\,. \tag{6.7}$$

Recall that we previously averaged the asymmetry by just integrating over it. We prefaced this by saying the average was naive, and hopefully it is clear why. We integrated over the asymmetry as a whole whereas, by equation (6.7), we see that we need to integrate both the numerator and denominator individually in order to produce an integrated asymmetry.

Additionally, equation (6.7) looks almost like we have the expression given in equation (6.2). However, we can only simplify to this if the amplitudes inside the integrals have no phase space dependence. It is not immediately clear whether they do, and if they do, how strong the dependence is. So we will compute integrated asymmetries directly, to be sure.

6.2 Dalitz Phase Space

We are now left with the problem of how to perform the integral over the phase space. Our approach is to integrate over a region of the Dalitz plot phase space. The Kinematics chapter of [21] gives a succinct review of Dalitz plots but for completeness we describe the formalism here.

6.2.1 Kinematics

Consider a three-body decay with parent particle of mass M and four momentum P which decays to three daughter particles with masses and momenta m_i, p_i where $i = 1, 2, 3$, shown in Figure 6.1. Clearly 4-momentum conservation implies that $P = p_1 + p_2 + p_3$. We go on to define the **invariant mass** of a pair of particles by

$$m_{ij}^2 = p_{ij}^2 \qquad \text{where } p_{ij} \equiv p_i + p_j \,. \tag{6.8}$$

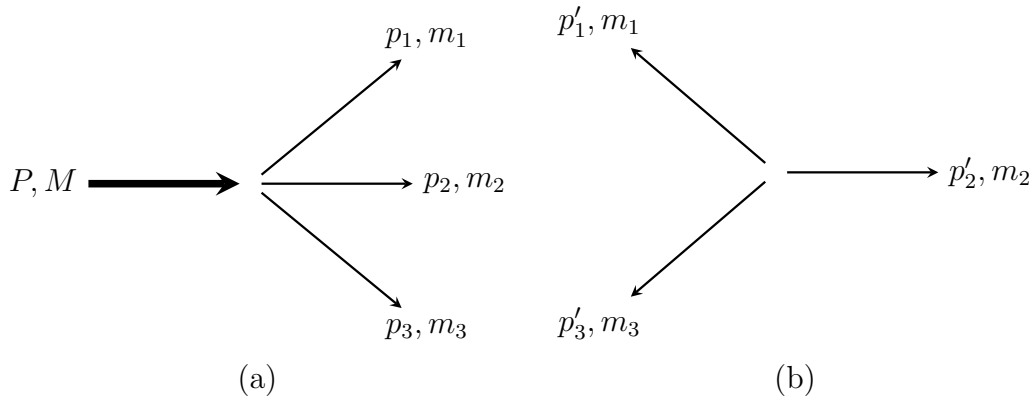

Figure 6.1: Three body decay in the (a) lab frame, and (b) parent particle rest frame.

We note that in the rest frame of the parent particle (see Figure 6.1) the decay products' 3-momenta lie in a plane. In fact, one can define three Euler angles α, β and γ which describe the exact configuration of the particles, given their energies [21]. Then, since knowing two of the energies is enough to know the third, we can change our phase space variables from momenta to $d\alpha, d(\cos\beta), d\gamma, dE_1, dE_3$. We can then write the differential decay rate as

$$d\Gamma = \frac{1}{(2\pi)^5}\frac{1}{16M}|\mathcal{M}|^2 dE_1 dE_3 d\alpha d(\cos\beta) d\gamma \,. \tag{6.9}$$

At a quick glance we see that the delta function has been integrated over to simplify the original nine dimensional phase space down to just five dimensions. The factors of 2π and 2 follow from equation (6.5).

Now, if we integrate over the Euler angles and average over the spins of the parent particle, we have

$$\begin{aligned} d\Gamma &= \frac{1}{(2\pi)^5}\frac{1}{16M}\overline{|\mathcal{M}|^2}dE_1dE_3\int_0^{2\pi}d\alpha\int_{-1}^{1}d(\cos\beta)\int_0^{2\pi}d\gamma \\ &= \frac{1}{(2\pi)^5}\frac{1}{16M}2(2\pi)^2\overline{|\mathcal{M}|^2}dE_1dE_3 \\ \therefore\ d\Gamma &= \frac{1}{(2\pi)^3}\frac{1}{8M}\overline{|\mathcal{M}|^2}dE_1dE_3\,. \end{aligned}$$

Here $\overline{|\mathcal{M}|^2}$ denotes the spin-averaged matrix element squared for the decay (which we take to be our $|A_\pm|^2$ from previously). This is close to what we want but recall that we would like to be integrating over the K^+K^- invariant mass at some point. Hence, we need to perform a change of variables.

From the definition of the invariant mass and conservation of 4-momentum, we write

$$m_{12}^2 = (p_1+p_2)^2 = (P-p_3)^2 = M^2+m_3^2-2ME_3\,, \tag{6.10}$$

and likewise

$$m_{23}^2 = (P-p_1)^2 = M^2+m_1^2-2ME_1\,. \tag{6.11}$$

To complete our change of variables from $(E_1, E_3) \to (m_{23}, m_{12})$ we take partial derivatives and construct the Jacobian matrix as

$$J = \begin{pmatrix} \dfrac{\partial E_1}{\partial m_{23}} & \dfrac{\partial E_1}{\partial m_{12}} \\ \dfrac{\partial E_3}{\partial m_{23}} & \dfrac{\partial E_3}{\partial m_{12}} \end{pmatrix} = \begin{pmatrix} -\dfrac{m_{23}}{M} & 0 \\ 0 & -\dfrac{m_{12}}{M} \end{pmatrix}\,. \tag{6.12}$$

The Jacobian factors which enter the integrand upon our change of variables are simply given by the determinant of the matrix above and so we write the differential decay rate as

$$d\Gamma = \frac{1}{(2\pi)^3}\frac{1}{8M^3}\overline{|\mathcal{M}|^2}m_{12}m_{23}dm_{12}dm_{23}\,. \tag{6.13}$$

The factors of 2π and $8M^3$ are irrelevant for us since we'll take the ratio of the sum and difference of the decay rates; the key feature is that there is some explicit dependence on the phase space parameters m_{12} and m_{23} along with any dependence which lies within the matrix element itself. As a note, if the matrix elements have no dependence on the phase space parameters, then integrating over the phase space will just produce a constant, which will again drop out of the ratio. What we find however, is that the matrix elements do in fact depend on the phase space and so the reduction of the CP asymmetry to equation (6.2) is not immediately justified.

Now we make the identifications $m_1 \equiv m_{K^+}$, $m_2 \equiv m_{K^-}$ and $m_3 \equiv m_{\pi^\pm}$. Since all the constants drop out when we take the ratio in the asymmetry, we then write

equation (6.7) as

$$\mathcal{A}_{CP} = \frac{\int \left(|A_-|^2 - |A_+|^2\right) m_{KK} m_{K\pi} dm_{KK} dm_{K\pi}}{\int \left(|A_-|^2 + |A_+|^2\right) m_{KK} m_{K\pi} dm_{KK} dm_{K\pi}} \,. \tag{6.14}$$

Then we can make use of results which led us to equation (4.10), and we obtain

$$\mathcal{A}_{CP} = -\frac{\int m_{KK} m_{K\pi} (2r \sin\delta \sin\phi) |A_T|^2 dm_{KK} dm_{K\pi}}{\int m_{KK} m_{K\pi} (1 + 2r \cos\delta \cos\phi + r^2) |A_T|^2 dm_{KK} dm_{K\pi}} \,. \tag{6.15}$$

Previously the tree amplitude terms $|A_T|^2$ cancelled since weren't integrating them. However, with the full phase space integrals we need to keep these. For completeness we recall that the tree amplitude is written

$$A_T \equiv \frac{t_f g_f}{s_f} \,. \tag{6.16}$$

6.2.2 Dalitz Plots

Our next step is to construct the phase space in such a way that it is simple to compute. Plots of the phase space for three-body decays in terms of the invariant masses are known as **Dalitz plots** [21]. For a given value of m_{12}, we can place bounds on the value of m_{23} by considering when the momenta of the particles are aligned or anti-aligned. These are given by

$$(m_{23}^2)_{\max} = (E_2^* + E_3^*)^2 - \left(\sqrt{E_2^{*2} - m_2^2} - \sqrt{E_3^{*2} - m_3^2}\right)^2 , \tag{6.17}$$

and

$$(m_{23}^2)_{\min} = (E_2^* + E_3^*)^2 - \left(\sqrt{E_2^{*2} - m_2^2} + \sqrt{E_3^{*2} - m_3^2}\right)^2 . \tag{6.18}$$

Here, we use the $*$ notation to denote energies in the rest frame of m_{12}. These energies are given by

$$E_2^* = \frac{m_{12}^2 - m_1^2 + m_2^2}{2m_{12}} \,, \tag{6.19}$$

and

$$E_3^* = \frac{M^2 - m_3^2 - m_{12}^2}{2m_{12}} \,. \tag{6.20}$$

The bounds of the Dalitz plot are then restricted purely by enforcing conservation of 4-momentum and are determined by the masses of the particles. For instance, m_{12} has minimal value $(m_{12})_{\min} = m_1 + m_2$ (the particles m_1 and m_2 are at rest) while its maximum is $(m_{12})_{\max} = M - m_3$ (when M and m_3 are at rest). Equations (6.17) and (6.18) along with the maximal and minimal values for m_{12} and m_{23} allow us to generate plots such as that shown in Figure 6.2.

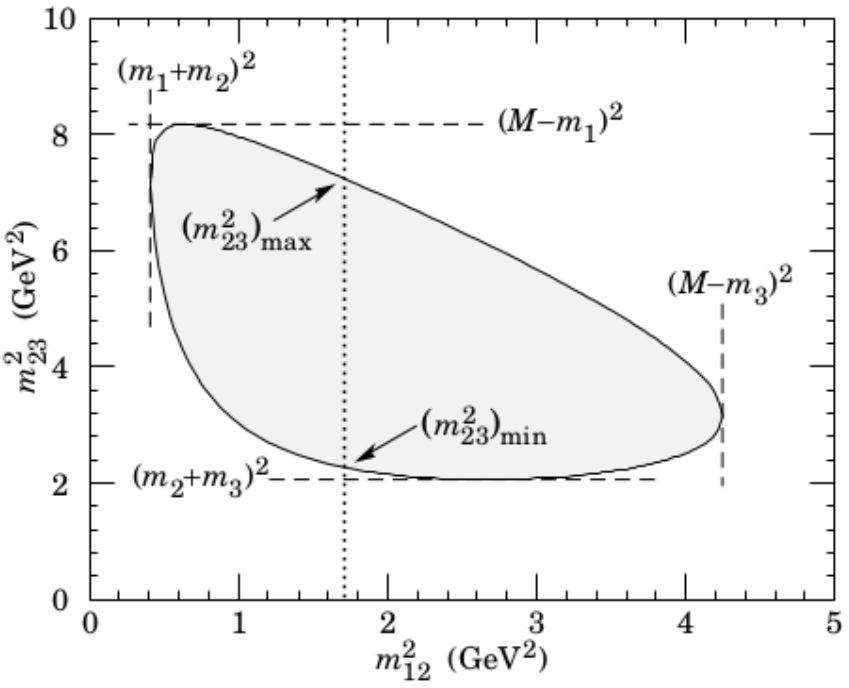

Figure 6.2: Dalitz plot for a general three-body decay, taken from [21]. The dotted line shows all possible values of m_{23}^2 for a given value of m_{12}^2.

For the case of $B^\pm \to K^+K^-\pi^\pm$ decays, the allowed phase space is bounded by $(m_{K\pi})_{\max}$ and $(m_{K\pi})_{\min}$ which are both functions of m_{KK}, as well as m_{KK} in the range

$$m_{K^+} + m_{K^-} = 2m_K \leq m_{KK} \leq m_B - m_\pi \,, \tag{6.21}$$

or

$$0.986 \leq m_{KK} \leq 5.14 \text{ GeV}/c^2 \,. \tag{6.22}$$

Although we've now mapped out the entire phase space available in the decays, we are only interested in a small fraction of this space. Recall that the bin where Belle measured the significant asymmetry was the first bin, $0.8 \leq m_{KK} \leq 1.1$ GeV/c^2. The other bins all showed negligible, or at least less significant, CP asymmetry and so we aren't interested in these. In fact, since our model only incorporates resonances at ~ 1 GeV/c^2, we aren't justified in extending beyond this first Belle bin. Recalling that the lower bound on the Belle bin is unphysical, we thus take our limits of integration to be 0.986 GeV/c^2 and 1.1 GeV/c^2 in the m_{KK} variable, with the corresponding limits on $m_{K\pi}$ determined by equations (6.17) and (6.18).

Once we've chosen the end points of our integration, we can proceed with one of two integration schemes. In the first, we take the bin $0.986 \leq m_{KK} \leq 1.1$ GeV/c^2 and integrate over it. This should then be directly comparable to the Belle data. In the second case, we subdivide this bin and perform the integration over these smaller bins. In particular, by taking the number of bins to infinity and making

each bin width infinitesimally small, we expect to produce purely theoretical curves similar to those seen in chapter 5.

6.3 Couplings and Partial Widths

Although we can calculate the asymmetry at this point, we note that there is some implicit phase space dependence in the propagators which we haven't addressed; specifically in the Γ_M term. The form of the propagator in equation (5.42) is more explicitly written as

$$s_M(m_{KK}) = m_{KK} - m_M^2 + im_M\Gamma_M(m_{KK})\,, \tag{6.23}$$

where the width of the propagating meson M is in principle dependent on the K^+K^- invariant mass. Typically, one writes the full width as

$$\Gamma_R(s) = \sum_c \Gamma_{R\to c}\left(\frac{q_c}{q_{Rc}}\right)^{2L_c+1}\left(\frac{m_R}{\sqrt{s}}\right)\left(\frac{F_{L_c}(q_c,q_0)}{F_{L_c}(q_{Rc},q_0)}\right)^2, \tag{6.24}$$

where R denotes the resonance in question, c denotes the available decay channels and $\sqrt{s}$ is the invariant mass of the final states [21]. The momenta q_c is given by

$$q_c = \frac{1}{2m_{ab}}\sqrt{(m_{ab}^2-(m_a+m_b)^2)(m_{ab}^2-(m_a-m_b)^2)} \tag{6.25}$$

where a and b denote the particles in the two-particle final state. One arrives at this form by considering conservation of 3-momentum, as in the earlier case of p_c for the centre of mass momentum (see Appendix A for derivation). We then have, for a Breit Wigner pole mass m_{BW} [21]

$$q_{Rc} = \frac{1}{2m_{BW}}\sqrt{(m_{BW}^2-(m_a+m_b)^2)(m_{BW}^2-(m_a-m_b)^2)} \tag{6.26}$$

and if the final states have the same mass ($m_a = m_b = m_c$) then we get

$$q_{Rc} = \frac{1}{2}\sqrt{m_{BW}^2-4m_c^2}\,. \tag{6.27}$$

Returning back to equation (6.24), L_c is the angular momentum of the decay products, $s = m_c^2$ is the square of the invariant mass of the decay products. Finally, F_{L_c} are barrier factors. They are typically taken to be of the *Blatt-Weisskopf* form, given in Table 6.1. We note that there are other forms for the Blatt-Weisskopf functions; we've chosen the form in Table 6.1 so that we can explicitly write the centrifugal barrier factors as the ratio q_c/q_{Rc} [34].

This formalism comes with the caveat that it only applies for resonances which are isolated. This is the case for the $\phi(1020)$ but it does not apply for the $f_0(980)$

L_c	$F_{L_c}(q_c, q_0)$
0	1
1	$\sqrt{\frac{1+z_0}{1+z}}$
2	$\sqrt{\frac{(z_0-3)^2+9z_0}{(z-3)^2+9z}}$
where $z = (\lvert q_c\rvert d)^2$	and $z_0 = (\lvert q_0\rvert d)^2$

Table 6.1: Table of Blatt-Weisskopf form factors. q_c has already been defined previously and q_0 is the value of q_c when $m_{ab} = m_R$. d is the impact parameter (meson radius) which we take to be on the order of 1 fm [34].

since the $a_0(980)$ is also close to the $K\bar{K}$ threshold [34]. We instead need to introduce another parametrization for the mass dependent propagator of the $f_0(980)$.

6.3.1 Flatté Parametrization

In the Flatté parametrization [21,34,35], we write the mass dependent width of the $f_0(980)$ as

$$m_f \Gamma_f = \rho_{\pi\pi} g_{\pi\pi}^2 + \rho_{KK} g_{KK}^2 \tag{6.28}$$

where the phase space terms are

$$\rho_{\pi\pi} = \frac{2}{3}\sqrt{\frac{s - 4m_{\pi^\pm}^2}{s}} + \frac{1}{3}\sqrt{\frac{s - 4m_{\pi^0}^2}{s}}\,, \tag{6.29}$$

and

$$\rho_{KK} = \frac{1}{2}\sqrt{\frac{s - 4m_{K^\pm}^2}{s}} + \frac{1}{2}\sqrt{\frac{s - 4m_{K^0}^2}{s}}\,. \tag{6.30}$$

We take $g_{KK}/g_{\pi\pi} = 4.21 \pm 0.25 \pm 0.21$ and $g_{\pi\pi} = 0.165 \pm 0.010 \pm 0.015$ GeV/c^2 [35]. This then fully accounts for the mass dependence of the propagators and so we are able to compute the asymmetry. This is shown in the following section.

6.3.2 Results for the $f_0(980)$ Tree, $\phi(1020)$ Penguin Model

With the phase space fully defined, we compute the integrated CP asymmetry for the model using the $f_0(980)$ in the tree diagram and the $\phi(1020)$ in the penguin. In our preliminary calculation of the purely theoretical asymmetry we just set the values of $N_c = 0.98\,, q^2/m_b^2 = 0.3\,, \rho = \rho_{max}$ and $\eta = \eta_{max}$. Now, we allow each of these parameters to vary, with the results shown in Table 6.2 (the purely theoretical asymmetry curves are shown in Figure 6.3 for reference).

Unfortunately, the promising asymmetry we first observed with this model is not present in the integrated CP asymmetry, although it does appear again in the plots of the asymmetry. We suspect that, since the ϕ is produced by a gluon, it must be spin-1 and so when we integrate over the angular degrees of freedom in the phase space the penguin amplitude will be suppressed. Hence, although the plots suggest that there is a significant asymmetry around 1 GeV/c^2 in m_{KK}, the integrated asymmetry (the asymmetry which is measurable by Belle) appears to be negligible. We thus propose a second model with which we compute the asymmetry, in the hope that it performs better than the first model we've tested.

$q^2/m_b^2 = 0.3$		$q^2/m_b^2 = 0.5$	
$N_c = 0.98$		$N_c = 0.94$	
ρ_{max} , η_{max}	-0.0008	ρ_{max} , η_{max}	-0.0282
ρ_{min} , η_{min}	-0.0007	ρ_{min} , η_{min}	-0.0252
$N_c = 2.01$		$N_c = 1.95$	
ρ_{max} , η_{max}	-0.0020	ρ_{max} , η_{max}	-0.0449
ρ_{min} , η_{min}	-0.0018	ρ_{min} , η_{min}	-0.0403
$N_c = 3.00$		$N_c = 3.00$	
ρ_{max} , η_{max}	-0.0032	ρ_{max} , η_{max}	-0.0554
ρ_{min} , η_{min}	-0.0028	ρ_{min} , η_{min}	-0.0500

Table 6.2: The values for the integrated CP asymmetry for the $f_0(980)$ tree and $\phi(1020)$ penguin diagrams for $q^2/m_b^2 = 0.3\,, 0.5$. The integration is performed over the range $2m_K \leq m_{KK} \leq 1.1$ GeV and for both maximum and minimum values of ρ and η.

6.4 Non-Resonant Calculation

Since the ϕ meson has spin-1, we postulated that the interference between this contribution and that of the tree diagram would vanish once we integrated over the entire angular range of our phase space. Further, although we could potentially see an $a_0(980)$ from the tree/penguin diagram, with the $f_0(980)$ coming from the penguin/tree diagram, these would necessarily have orthogonal wavefunctions (they correspond to different isospins for the K^+K^- pair) so can not interfere as needed to observe significant CP violation.

The result of this is that we now take two new diagrams, although they still have the same general form as those in Figures 4.1 and 4.2. We replace the $\phi(1020)$

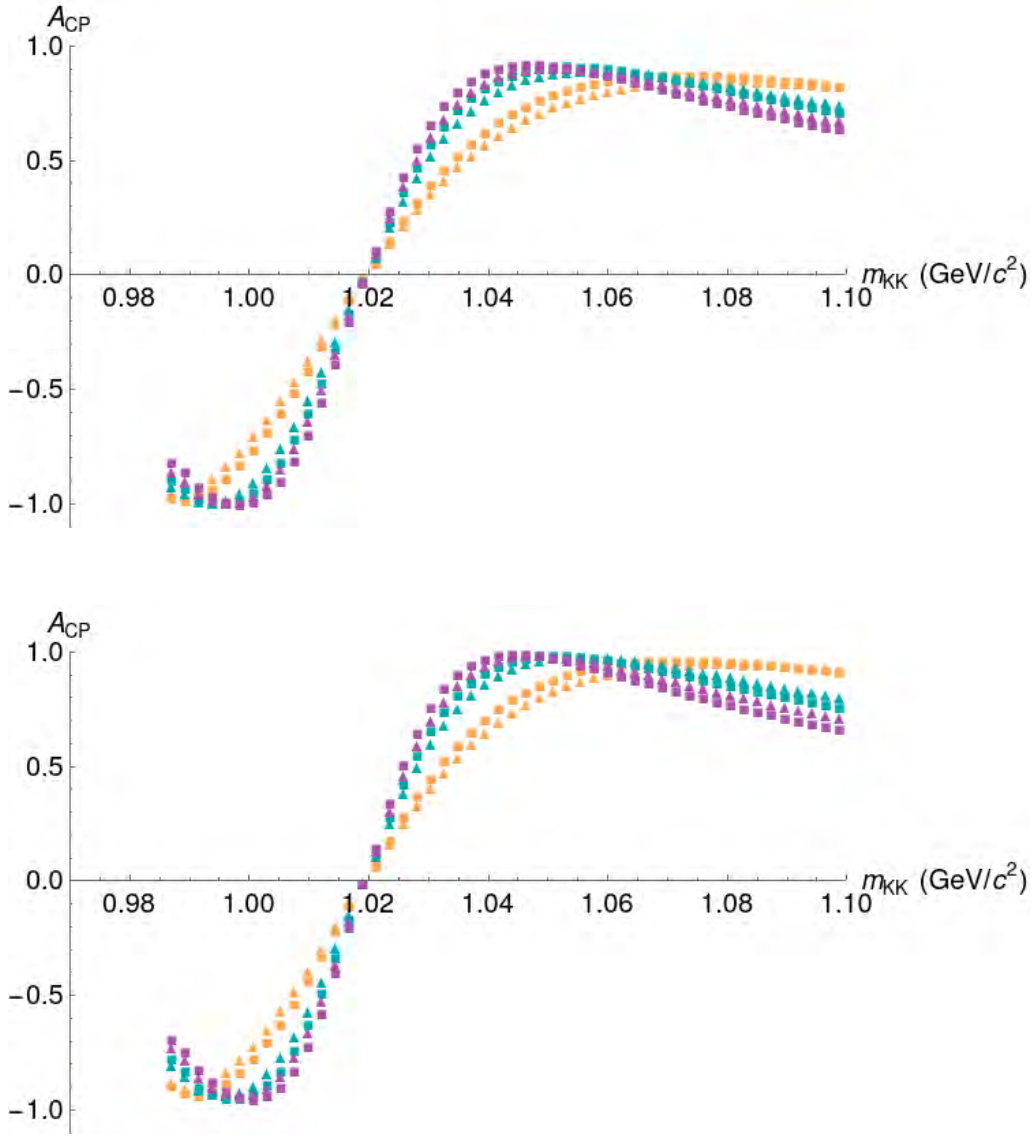

Figure 6.3: Plots of the integrated CP asymmetry for 50 bins over the range $2m_K \leq m_{KK} \leq 1.1$ GeV/c^2. The top (bottom) plot is for $q^2/m_b^2 = 0.3(0.5)$. Squares correspond to maximum values for ρ and η, while triangles correspond to minimum values for ρ and η. The numbers of effective colours correspond to the colours of the plots in the following way: $N_c = 0.98(0.94)$ is shown in orange, $N_c = 2.01(1.95)$ is shown in blue, $N_c = 3.00(3.00)$ is shown in purple.

produced in the penguin diagram with an $f_0(980)$ and the original $f_0(980)$ produced in the tree diagram is replaced with a non-resonant $q\bar{q}$ state. Figures 6.4 and 6.5 show these new diagrams.

In calculating the amplitudes for these two diagrams, we use the same methodology as before with some slight adjustments. The amplitudes for the two diagrams are written as

$$\left\langle K^+K^-\pi^-\middle|H^P\middle|B^-\right\rangle = \frac{g_f}{s_f}p_f \qquad \text{and} \qquad \left\langle K^+K^-\pi^-\middle|H^T\middle|B^-\right\rangle = t_{NR}\,, \tag{6.31}$$

and the ratio of these is just

$$re^{i\delta}e^{i\phi} = \frac{\langle K^+K^-\pi^-|H^P|B^-\rangle}{\langle K^+K^-\pi^-|H^T|B^-\rangle} = \frac{g_f p_f}{s_f t_{NR}}\,. \tag{6.32}$$

The key thing to note here is that the tree process has been condensed down to just the t_{NR} factor; there is no intermediate resonance in this non-resonant decay and so there is no propagator for the tree process, nor is there a separate coupling to the K^+K^- pair as we had previously. The factorisation approximation proceeds as usual, with the same definitions of the operators $\mathcal{O}_i$ found in equations (3.54) to (3.63). The results of the factorisation are given after a brief discussion of Heavy Meson Chiral Perturbation Theory.

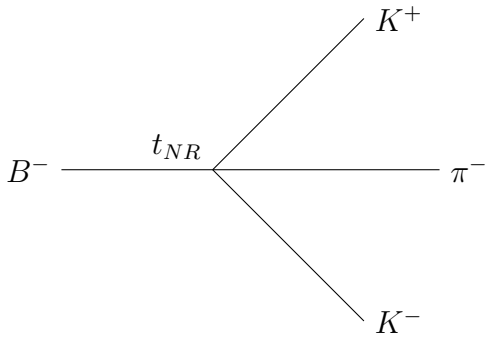

Figure 6.4: Simplified tree diagram for $B^- \to K^+K^-\pi^-$ through a non-resonant decay channel.

6.4.1 Heavy Meson Chiral Perturbation Theory

Our method for computing the matrix elements in the factorisation approximation is based on that found in [36]. Before we proceed though, one should be aware of the limitations of this method, in particular, the limitations of using heavy meson chiral perturbation theory (HMChPT). For HMChPT to be valid, we require two of the final state pseudoscalar mesons to be soft with momenta less than the chiral symmetry breaking scale $\Lambda_\chi \sim 0.83$ GeV [36]. As a result, HMChPT is applicable to only a small region of the Dalitz phase space and so we need to check if the range of m_{KK} values of interest lies within the region of validity for HMChPT.

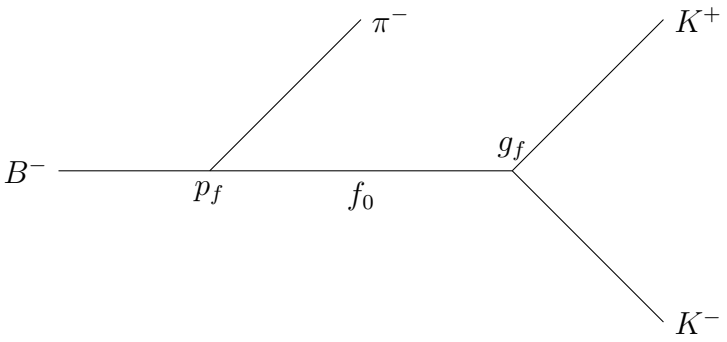

Figure 6.5: Simplified penguin diagram for $B^- \to f_0(980)\pi^- \to K^+K^-\pi^-$.

More specifically, we'll need HMChPT to describe the B^- to K^+K^- transition so we should consider the invariant mass of the kaons in the context of soft kaons; if the region we've investigated ($2m_K < m_{KK} < 1.1$ GeV/c^2) corresponds to soft kaons, then we are justified in using HMChPT.

In the following, we'll use a rough argument to investigate the validity of HMChPT. First, let's apply conservation of 4-momentum at the decay vertex. We have that

$$p_B^\mu = p_{K^+}^\mu + p_{K^-}^\mu + p_\pi^\mu \,. \tag{6.33}$$

Working in the rest frame of the B meson, we choose our axes such that the pion travels in the negative z direction while the kaons travel in the $x - z$ plane. We also assume that the kaons have the same magnitude for their momenta and define $|\boldsymbol{p}_{K^+}| = |\boldsymbol{p}_{K^-}| \equiv p_K$ so the angle θ between them is symmetric about the z-axis.

The zero component of momentum conservation then gives

$$\begin{aligned} p_B^0 &= p_{K^+}^0 + p_{K^-}^0 + p_\pi^0 \\ \Rightarrow\ m_B &= 2\sqrt{m_K^2 + p_K^2} + \sqrt{m_\pi^2 + |\boldsymbol{p}_\pi|^2} \\ \therefore\ |\boldsymbol{p}_\pi| &= \sqrt{\left(m_B - 2\sqrt{m_K^2 + p_K^2}\right)^2 - m_\pi^2} \,. \end{aligned} \tag{6.34}$$

The conservation of 3-momentum gives only one meaningful equation (in the z direction) from which we get

$$\begin{aligned} \boldsymbol{p}_B &= \boldsymbol{p}_{K^+} + \boldsymbol{p}_{K^-} + \boldsymbol{p}_\pi \\ \Rightarrow\ 0 &= 2p_K \cos\theta - |\boldsymbol{p}_\pi| \\ \therefore\ \theta &= \cos^{-1}\left(\frac{|\boldsymbol{p}_\pi|}{2p_K}\right) . \end{aligned} \tag{6.35}$$

Combining these results, we can plot the values of θ as a function of the magnitude of the kaon momenta. This is shown in Figure 6.6.

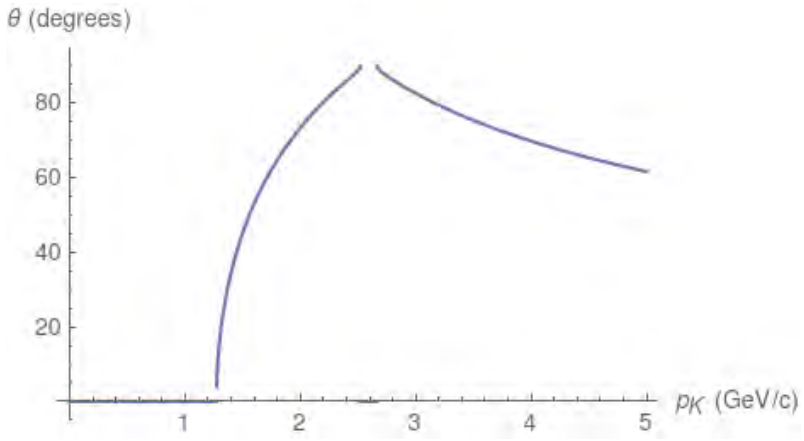

Figure 6.6: Plot of the values for θ the angle between the kaons as a function of p_K, the magnitude of their momenta. This assumes the kaons have the same magnitude for their momenta.

We note that there are two types of region where this function is undefined. The first case is when the square roots in equation (6.34) give an imaginary result. Clearly the term $\sqrt{m_K^2 + p_K^2}$ is always real and so we just need to check the overall square root. In other words, θ is undefined if

$$\left(m_B - 2\sqrt{m_K^2 + p_K^2}\right)^2 < m_\pi^2 \tag{6.36}$$

which is equivalent to

$$0 < m_B - 2\sqrt{m_K^2 + p_K^2} < m_\pi \,. \tag{6.37}$$

where we note that the terms in brackets in inequality (6.36) are equal to the pion energy and so cannot be negative. Rearranging these inequalities and substituting values for the relevant masses, one finds that the square roots lead to the function being undefined in the region

$$2.52 < p_K < 2.59 \text{ GeV}/c \,. \tag{6.38}$$

The second cause for the $\theta(p_K)$ function being undefined is to do with the inverse cosine function. Since $\cos(x)$ has values within $-1 \leq \cos(x) \leq 1$, the $\cos^{-1}(x)$ function is only defined on the interval from -1 to 1. So, we need to check if there are any places where the argument of the $\cos^{-1}$ function is outside this range. Starting with the inequality

$$-1 \leq \frac{|p_\pi|}{2p_K} \leq 1 \,, \tag{6.39}$$

one can show that $\theta(p_K)$ is undefined for $p_K \leq 1.273$ GeV/c. These two regions where θ is undefined correspond to the flat lines shown in Figure 6.6 along the p_K-axis.

Immediately, we can see a problem. We wanted to show that the pseudoscalars K^+ and K^- are soft, with momenta smaller than 0.83 GeV/c. However, this is physically untenable with our assumptions, since there is no value of θ for which the kaons can have this low a value for their momenta and still conserve momentum. So the question is, should we be using HMChPT to evaluate the matrix elements? Strictly speaking, we shouldn't. However, we stress an important part of the recommendations from [36]; the main cause for concern with using chiral perturbation theory in these heavy meson decays is that the phase space is quite large and yet chiral perturbation theory is only applicable to a small portion of it. Problems arise when one attempts to calculate, say, the total decay rate across the *entire* phase space, since this entails extending HMChPT well beyond its region of applicability. In our case however, we are only interested in the lower end of the phase space, with the region of interest being $2m_K \leq m_{KK} \leq 1.1$ GeV/c^2.

The question then arises; how far away from the region of validity might we be extending in our investigation? In our rough approximation where the kaons have equal momenta, we actually showed that the kaons cannot both have $p_K < 0.83$ GeV/c in any region of the phase space. However, we can still check what our range in m_{KK} corresponds to in p_K. Starting from the definition of the kaon pair's invariant mass

$$\begin{aligned} m_{KK}^2 &\equiv (p_{K^+} + p_{K^-})^2 \\ &= 2m_K^2 + 2p_{K^+}^{\mu} p_{\mu}^{K^-} \\ &= 2m_K^2 + 2\Big(p_{K^+}^0 p_0^{K^-} - \boldsymbol{p}_{K^+} \cdot \boldsymbol{p}_{K^-}\Big) \\ &= 2m_K^2 + 2\sqrt{\left(|\boldsymbol{p}_{K^+}|^2 + m_K^2\right)\left(|\boldsymbol{p}_{K^-}|^2 + m_K^2\right)} - 2|\boldsymbol{p}_{K^+}||\boldsymbol{p}_{K^-}|\cos\theta\,, \end{aligned}$$

we can then substitute the condition that $|\boldsymbol{p}_{K^+}| = |\boldsymbol{p}_{K^+}| = p_K$ and use the resulting form for θ given in equation (6.35). This gives us an expression for m_{KK} in terms of p_K

$$m_{KK}^2 = 4m_K^2 + 2p_K^2\left(1 - \frac{\sqrt{\left(m_B - 2\sqrt{m_K^2 + p_K^2}\right)^2 - m_\pi^2}}{2p_K}\right). \tag{6.40}$$

Hence, in our investigation of the invariant mass region $0.986 \leq m_{KK} \leq 1.1$ GeV/c^2 we in fact have kaons with approximately $1.27 \leq p_K \leq 1.32$ GeV/c (assuming the kaons have the same magnitude for their 3-momenta).

In these rough calculations, we've shown that the kaons are not "soft" (we want $p_K < 0.83$ GeV/c), and so we can only treat the remainder of the calculation of the asymmetry as approximate.

6.4.2 Factorisation Approximation

With this interlude complete, we perform the calculation of the tree and penguin amplitudes following the method of [36]. We begin by considering the tree amplitude t_{NR} defined as

$$t_{NR} \equiv \frac{G_F}{\sqrt{2}} V_{ud} V_{ub}^* \big(a_1 \left\langle K^+ K^- \pi^- \middle| \mathcal{O}_1 \middle| B^- \right\rangle + a_2 \left\langle K^+ K^- \pi^- \middle| \mathcal{O}_2 \middle| B^- \right\rangle \big) \,. \tag{6.41}$$

We propose that the total non-resonant contribution to the $B^- \to K^+ K^- \pi^-$ decay is tree dominated and also that the $\mathcal{O}_1$ contribution is dominant [36]. Focusing on the $\mathcal{O}_1$ contribution, we obtain

$$\begin{aligned}
&\left\langle K^+ K^- \pi^- \middle| \mathcal{O}_1 \middle| B^- \right\rangle \\
&= \left\langle K^+ K^- \pi^- \middle| (\bar{d}u)_{V-A} (\bar{u}b)_{V-A} \middle| B^- \right\rangle \\
&= \left\langle \pi^- \middle| (\bar{d}u)_{V-A} \middle| 0 \right\rangle \left\langle K^+ K^- \middle| (\bar{u}b)_{V-A} \middle| B^- \right\rangle + \left\langle K^+ K^- \pi^- \middle| (\bar{d}u)_{V-A} \middle| 0 \right\rangle \left\langle 0 \middle| (\bar{u}b)_{V-A} \middle| B^- \right\rangle \\
&= \left\langle \pi^- \middle| (\bar{d}u)_{V-A} \middle| 0 \right\rangle \left\langle K^+ K^- \middle| (\bar{u}b)_{V-A} \middle| B^- \right\rangle \,,
\end{aligned}$$

where we've used the fact that, after factorising, the second pair of matrix elements is helicity suppressed so vanishes [36]. We thus have the result

$$\left\langle K^+ K^- \pi^- \middle| \mathcal{O}_1 \middle| B^- \right\rangle = \left\langle \pi^- \middle| (\bar{d}u)_{V-A} \middle| 0 \right\rangle \left\langle K^+ K^- \middle| (\bar{u}b)_{V-A} \middle| B^- \right\rangle \,. \tag{6.42}$$

The matrix element involving the pion is exactly what we had previously and is calculated in the same manner. However, we need to make use of a new set of form factors in order to compute the second matrix element. We write

$$\begin{aligned}
\left\langle K^+(p_2) K^-(p_1) \middle| (\bar{u}b)_{V-A} \middle| B^-(p_B) \right\rangle = {} & ir(p_B - p_1 - p_2)_\mu + i\omega_+ (p_1 + p_2)_\mu \\
& + i\omega_- (p_2 - p_1)_\mu + h \epsilon_{\mu\nu\alpha\beta} p_B^\nu (p_1 + p_2)^\alpha (p_2 - p_1)^\beta \,,
\end{aligned} \tag{6.43}$$

where the relevant form factors are obtained by considering pole diagrams such as those shown in Figure 6.7. The key idea in these diagrams is that the mesons can fluctuate into other states, such as the vector meson $\bar{B}_s^{*0}$ by weak and/or strong interactions [37, 38].

The couplings in the pole diagrams are calculable using the Lagrangian [39]

$$\begin{aligned}
\mathcal{L}_{PP^*} = {} & D_\mu P D^\mu P^\dagger - m_P^2 P P^\dagger + f_Q \big(P A^\mu P_\mu^{*\dagger} + P_\mu^* A^\mu P^\dagger \big) \\
& - \frac{1}{2} P^{*\mu\nu} P_{\mu\nu}^{*\dagger} + m_{P^*}^2 P^{*\mu} P_\mu^{*\dagger} + \frac{1}{2} g_Q \epsilon_{\mu\nu\lambda\kappa} \big(P^{*\mu\nu} A^\lambda P^{*\kappa\dagger} + P^{*\kappa} A^\lambda P^{*\mu\nu\dagger} \big) \,,
\end{aligned} \tag{6.44}$$

where

$$P_{\mu\nu}^{*\dagger} = D_\mu P_\nu^{*\dagger} - D_\nu P_\mu^{*\dagger} \,, \tag{6.45}$$

$$P_{\mu\nu}^{*} = \big(\partial_\mu + V_\mu^* \big) P_\nu^* - (\partial_\nu + V_\nu^*) P_\mu^* \,, \tag{6.46}$$

and A^μ are the fields for the Goldstone bosons. The diagrams are thus calculated

using this Lagrangian, with the results for the form factors given in [36, 40] as

$$\omega_+ = -\frac{g}{f_\pi^2}\frac{f_{B_s^*} m_{B_s^*}\sqrt{m_B m_{B_s^*}}}{t - m_{B_s^*}^2}\left[1 - \frac{(p_B - p_1)\cdot p_1}{m_{B_s^*}^2}\right] + \frac{f_B}{2f_\pi^2}\,, \tag{6.47}$$

$$\omega_- = \frac{g}{f_\pi^2}\frac{f_{B_s^*} m_{B_s^*}\sqrt{m_B m_{B_s^*}}}{t - m_{B_s^*}^2}\left[1 + \frac{(p_B - p_1)\cdot p_1}{m_{B_s^*}^2}\right], \tag{6.48}$$

$$\begin{aligned} r = {} & \frac{f_B}{2f_\pi^2} - \frac{f_B}{f_\pi^2}\frac{p_B\cdot(p_2 - p_1)}{(p_B - p_1 - p_2)^2 - m_B^2} + \frac{2g f_{B_s^*}}{f_\pi^2}\sqrt{\frac{m_B}{m_{B_s^*}}}\frac{(p_B - p_1)\cdot p_1}{t - m_{B_s^*}^2} \\ & - \frac{4g^2 f_B}{f_\pi^2}\frac{m_B m_{B_s^*}}{(p_B - p_1 - p_2)^2 - m_B^2}\frac{p_1\cdot p_2 - p_1\cdot(p_B - p_1)p_2\cdot(p_B - p_1)/m_{B_s^*}^2}{t - m_{B_s^*}^2}\,, \end{aligned} \tag{6.49}$$

where

$$t \equiv (p_B - p_1)^2 = (p_2 + p_3) = (p_{K^+} + p_\pi)^2 \equiv m_{K\pi}^2\,. \tag{6.50}$$

The contribution from the form factor h vanishes when we contract equation (6.43) with the vacuum to pion matrix element in equation (6.42), so its form is not required.

In contracting the pair of matrix elements, we end up needing to compute the term $(p_B - p_1)\cdot p_1$. It turns out that we can rewrite this in terms of the invariant masses of the K^+K^- and $K^+\pi^-$ pairs and thus compute the CP asymmetry with the same integration method as used previously (integrating over the Dalitz plot for

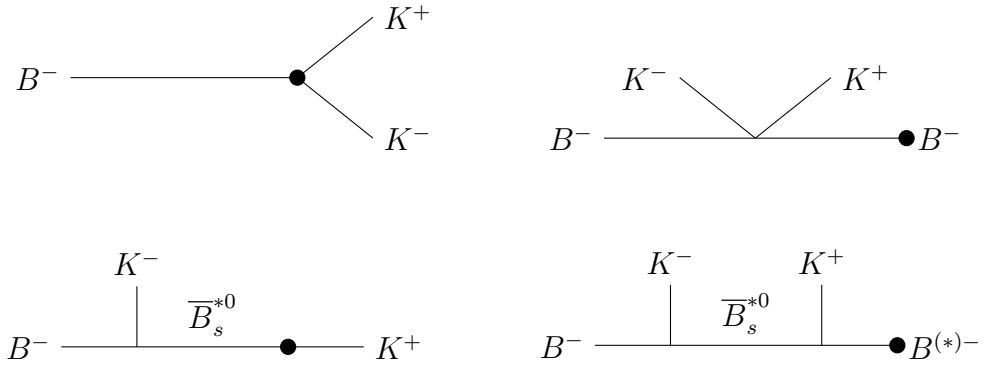

Figure 6.7: Point-like (top left) and pole diagrams for the decay $B^- \to K^+K^-$. The coloured circle denotes an insertion of the current $\bar{u}\gamma_\mu(1-\gamma_5)b$. These figures are based on those found in [36].

m_{KK} and $m_{K\pi}$). We find, using the fact that $p_B = p_1 + p_2 + p_3 = p_{K^-} + p_{K^+} + p_\pi$,

$$\begin{aligned}(p_B - p_1)\cdot p_1 &= p_B \cdot p_1 - p_1^2 \\ &= p_B \cdot p_1 - m_1^2 \\ &= (p_1 + p_2 + p_3)\cdot p_1 - m_1^2 \\ &= m_1^2 + p_2 \cdot p_1 + p_3 \cdot p_1 - m_1^2 \\ &= \frac{1}{2}(p_1+p_2)^2 - \frac{1}{2}m_1^2 - \frac{1}{2}m_2^2 + \frac{1}{2}(p_1+p_3)^2 - \frac{1}{2}m_1^2 - \frac{1}{2}m_3^2 \\ &= \frac{1}{2}\left[(p_1+p_2)^2 + (p_1+p_3)^2 - 2m_1^2 - m_2^2 - m_3^2\right].\end{aligned}$$

We recognise the bracketed terms as just the squares of the invariant masses for the K^+K^- and $K^+\pi^-$ pairs and write

$$(p_B - p_{K^-})\cdot p_{K^-} = \frac{1}{2}\left[m_{KK}^2 + m_{K\pi}^2 - 3m_K^2 - m_\pi^2\right]. \tag{6.51}$$

Hence, the form factors can be calculated explicitly in terms of the invariant masses. The next thing to do is contract the matrix elements written in terms of their form factors. This is the topic of the following section.

Matrix Element Contraction

Recall equation (6.43) which shows the form factor description of the non-resonant B^- to K^+K^- matrix element. We now contract this with the corresponding form factor representation of the pion matrix element

$$\begin{aligned}&\left\langle \pi^- \middle| (\bar{d}u)_{V-A} \middle| 0 \right\rangle \left\langle K^+K^- \middle| (\bar{u}b)_{V-A} \middle| B^- \right\rangle \\ &= if_\pi p_3^\mu \big[ir(p_B - p_1 - p_2)_\mu + i\omega_+(p_1+p_2)_\mu + i\omega_-(p_2-p_1)_\mu \\ &\qquad\qquad + h\varepsilon_{\mu\nu\alpha\beta}p_B^\nu (p_1+p_2)^\alpha (p_2-p_1)^\beta\big] \\ &= -f_\pi\big[p_3^\mu(p_B - p_1 - p_2)_\mu r + p_3^\mu(p_1+p_2)_\mu\omega_+ + p_3^\mu(p_2-p_1)_\mu\omega_- \\ &\qquad\qquad + i\varepsilon_{\mu\nu\alpha\beta}p_3^\mu p_B^\nu (p_1+p_2)^\alpha (p_1-p_2)^\beta h\big].\end{aligned} \tag{6.52}$$

We will investigate the above result term by term, starting with the h contribution (recall that we claimed it vanishes). This term is proportional to

$$\begin{aligned}&\varepsilon_{\mu\nu\alpha\beta}p_3^\mu p_B^\nu (p_1+p_2)^\alpha (p_1-p_2)^\beta \\ &= \varepsilon_{\mu\nu\alpha\beta}(p_B - (p_1+p_2))^\mu p_B^\nu (p_1+p_2)^\alpha (p_1-p_2)^\beta \\ &= \varepsilon_{\mu\nu\alpha\beta}(p_B^\mu p_B^\nu (p_1+p_2)^\alpha (p_1-p_2)^\beta - (p_1+p_2)^\mu p_B^\nu (p_1+p_2)^\alpha (p_1-p_2)^\beta).\end{aligned}$$

The Levi Civita symbol is totally antisymmetric under the exchange of any of its two indices while in the first term in the parentheses $p_B^\mu p_B^\nu$ is totally symmetric under the exchange $\mu \leftrightarrow \nu$. Hence the first term is zero. Likewise, the second term

involving $(p_1+p_2)^\mu(p_1+p_2)^\alpha$ which is totally symmetric under $\mu \leftrightarrow \alpha$ also vanishes. So the total contribution from the h term is zero, as originally stated.

For convenience, we define $X \equiv \langle \pi^-|(\bar{d}u)_{V-A}|0\rangle \ \langle K^+K^-|(\bar{u}b)_{V-A}|B^-\rangle$ and rewrite equation (6.52) as

$$X = -f_\pi[p_3^\mu(p_B - p_1 - p_2)_\mu r + p_3^\mu(p_1+p_2)_\mu\omega_+ + p_3^\mu(p_2-p_1)_\mu\omega_-]\,. \tag{6.53}$$

It turns out that it will prove more convenient to have a factor of 2 in the brackets and so we write

$$X = -\frac{f_\pi}{2}[2p_3^\mu(p_B - p_1 - p_2)_\mu r + 2p_3^\mu(p_1+p_2)_\mu\omega_+ + 2p_3^\mu(p_2-p_1)_\mu\omega_-]\,. \tag{6.54}$$

The contribution due to r is then

$$2p_3^\mu(p_B - p_1 - p_2)_\mu = 2p_3^\mu p_{3\mu} = 2m_3^2\,. \tag{6.55}$$

The ω_+ contribution is

$$\begin{aligned} 2p_3^\mu(p_1+p_2)_\mu &= 2(p_B-(p_1+p_2))^\mu(p_1+p_2)_\mu \\ &= 2p_B^\mu(p_1+p_2)_\mu - 2(p_1+p_2)^2 \\ &= 2p_B^\mu(p_B-p_3)_\mu - 2(p_1+p_2)^2 \\ &= 2m_B^2 - 2p_B^\mu p_{3\mu} - 2s\,, \end{aligned}$$

where

$$s \equiv (p_1+p_2)^2 = (p_B-p_3)^2\,. \tag{6.56}$$

From here, it isn't so obvious how we should proceed. Consider though the following:

$$\begin{aligned} m_B^2 - s - m_3^2 &= m_B^2 - (p_B-p_3)^2 - m_3^2 \\ &= 2p_B^\mu p_{3\mu} - 2m_3^2 \\ \Rightarrow\ 2p_B^\mu p_{3\mu} &= m_B^2 - s + m_3^2 \end{aligned}$$

Then the contribution due to ω_+ becomes

$$\begin{aligned} 2m_B^2 - 2p_B^\mu p_{3\mu} - 2s &= 2m_B^2 - (m_B^2 - s + m_3^2) - 2s \\ &= m_B^2 - s - m_3^2\,. \end{aligned} \tag{6.57}$$

Finally, consider the contribution due to ω_-, that is, $2p_3^\mu(p_2-p_1)_\mu$. We start with

$$2t + s - m_B^2 - 2m_2^2 - m_3^2 = 2(p_2+p_3)^2 + (p_B-p_3)^2 - m_B^2 - 2m_2^2 - m_3^2\,. \tag{6.58}$$

Expanding out and collecting terms, we are left with

$$\begin{aligned} 2t + s - m_B^2 - 2m_2^2 - m_3^2 &= 4p_2^\mu p_{3\mu} + 2m_3^2 - 2p_B^\mu p_{3\mu} \\ &= 2p_2^\mu p_{3\mu} - 2(p_B - p_2)^\mu p_{3\mu} + 2m_3^2 \\ &= 2p_2^\mu p_{3\mu} - 2(p_1 + p_3)^\mu p_{3\mu} + 2m_3^2 \\ &= 2p_2^\mu p_{3\mu} - 2p_1^\mu p_{3\mu} - 2m_3^2 + 2m_3^2 \\ &= 2(p_2 - p_1)^\mu p_{3\mu} \,. \end{aligned} \tag{6.59}$$

Finally, substituting equations (6.55), (6.57) and (6.59) into our expression for X given by equation (6.54), we obtain

$$X = -\frac{f_\pi}{2}[2m_3^2 r + (m_B^2 - s - m_3^2)\omega_+ + (2t + s - m_B^2 - 2m_2^2 - m_3^2)\omega_-] \,. \tag{6.60}$$

Now we can simply recall that $m_1 = m_2 = m_K$ and $m_3 = m_\pi$. Then, since the mass of the pion is negligible on the scale of the mass of the B meson, we can neglect the first term. Rewriting our final expression for X in a more suggestive way, we have

$$X = -\frac{f_\pi}{2}[(m_B^2 - m_{KK}^2 - m_\pi^2)\omega_+ + (2m_{K\pi}^2 + m_{KK}^2 - m_B^2 - 2m_K^2 - m_\pi^2)\omega_-] \,. \tag{6.61}$$

Recalling that both ω_+ and ω_- are functions of the invariant masses m_{KK} and $m_{K\pi}$ we see that the contraction of the factorised matrix elements from the non-resonant tree decay can be expressed in terms of just these invariant masses. With equation (6.41) and our definition of X, we can then write the tree vertex amplitude as

$$\begin{aligned} t_{NR} = &-\frac{G_F}{\sqrt{2}} V_{ud} V_{ub}^* a_1 \frac{f_\pi}{2} \times \\ &\left[(m_B^2 - m_{KK}^2 - m_\pi^2)\omega_+ + (2m_{K\pi}^2 + m_{KK}^2 - m_B^2 - 2m_K^2 - m_\pi^2)\omega_-\right] . \end{aligned} \tag{6.62}$$

Noting the forms of ω_+ and ω_-, this concludes the tree calculation. All that remains is to perform the analogous calculation of the penguin matrix elements. These are achieved in exactly the same manner as we had previously, albeit with the $f_0(980)$ replacing the $\phi(1020)$. From the Naive Factorisation we obtain

$$\begin{aligned} \left\langle f_0\pi^- \middle| \mathcal{O}_3 \middle| B^- \right\rangle &= -\left\langle \pi^- \middle| (\bar{d}b)_{V-A} \middle| B^- \right\rangle \langle f_0 | (\bar{u}u + \bar{d}d + \bar{s}s)_{V-A} | 0 \rangle = 0 \,, \\ \left\langle f_0\pi^- \middle| \mathcal{O}_4 \middle| B^- \right\rangle &= \left\langle f_0 \middle| (\bar{u}b)_{V-A} \middle| B^- \right\rangle \left\langle \pi^- \middle| (\bar{d}u)_{V-A} \middle| 0 \right\rangle \,, \\ \left\langle f_0\pi^- \middle| \mathcal{O}_5 \middle| B^- \right\rangle &= \langle f_0 | (\bar{u}u + \bar{d}d + \bar{s}s)_{V+A} | 0 \rangle \left\langle \pi^- \middle| (\bar{d}b)_{V-A} \middle| B^- \right\rangle = 0 \,, \\ \left\langle f_0\pi^- \middle| \mathcal{O}_6 \middle| B^- \right\rangle &= -2\big[\left\langle f_0 \middle| \bar{u}(1-\gamma_5)b \middle| B^- \right\rangle \left\langle \pi^- \middle| \bar{d}(1+\gamma_5)u \middle| 0 \right\rangle \\ &\qquad + \langle f_0 | \bar{d}(1+\gamma_5)d | 0 \rangle \left\langle \pi^- \middle| \bar{d}(1-\gamma_5)b \middle| B^- \right\rangle \big] = 0 \,. \end{aligned}$$

Note that all but one of the matrix elements above vanish; this is mostly due to the fact that a scalar meson requires either a scalar or vector transition current to couple to the vacuum. In the case of the f_0 though, C invariance implies that the contribution from a vector current is zero [31]. This eliminates the contributions due

to $\mathcal{O}_3$ and $\mathcal{O}_5$ as well as one of the contributions from $\mathcal{O}_6$. For the other contribution in $\mathcal{O}_6$, we note that the pion to B meson transition requires either a vector or axial vector current. Since none are available, this contribution also vanishes, meaning that only $\mathcal{O}_4$ gives a non-zero contribution. We thus have

$$p_f \equiv -\frac{G_F}{\sqrt{2}} V_{td}^* V_{tb} a_4 \left\langle f_0 \pi^- \middle| \mathcal{O}_4 \middle| B^- \right\rangle \tag{6.63}$$

$$= -\frac{G_F}{\sqrt{2}} V_{td}^* V_{tb} a_4 \left\langle f_0 \middle| (\bar{u}b)_{V-A} \middle| B^- \right\rangle \left\langle \pi^- \middle| (\bar{d}u)_{V-A} \middle| 0 \right\rangle . \tag{6.64}$$

This is easily calculable in the same manner as was used previously using the form factors in equations (5.22) to (5.28), taking the form

$$p_f = \frac{G_F}{\sqrt{2}} V_{td}^* V_{tb} a_4 f_\pi (m_B^2 - m_f^2) F_0(m_\pi^2) . \tag{6.65}$$

Then we use the same Dalitz plot phase space as before to perform the integration; our intermediate states have changed but the overall phase space allowed by the final states is the same. Recall that we write the full, phase space dependent CP asymmetry as

$$\mathcal{A}_{CP} = \frac{\int m_{KK} m_{K\pi} (-2r \sin\delta \sin\phi) |A_T|^2 dm_{KK} dm_{K\pi}}{\int m_{KK} m_{K\pi} (1 + 2r \cos\delta \cos\phi + r^2) |A_T|^2 dm_{KK} dm_{K\pi}} . \tag{6.66}$$

The terms $r \sin\delta$, $r \cos\delta$ and $|A_T|^2$are made up of t_{NR}, p_f and the associated propagators and couplings to the kaons; these are obtained from the factorisation approximation and are functions of the Dalitz plot parameters. The $\sin\phi$ and $\cos\phi$ terms are found directly from the CKM matrix and are constant with respect to the Dalitz plot parameters. We then integrate over the Dalitz plot phase space in the same manner used previously, thereby obtaining a final value for the CP asymmetry.

Chapter 7

Results and Discussion

We are now in a position to report results for the integrated CP asymmetry involving non-resonant tree processes. We report our results for various choices of N_c, q^2/m_b^2, ρ and η and later in this chapter we also use form factor descriptions other than the simple $n = 1$ monopole dominance assumption we made earlier.

7.1 Non-resonant Tree with $f_0(980)$ Penguin

We present here the results for the CP asymmetry produced via the interference of the non-resonant (NR) tree process with the resonant (R) $f_0(980)$ penguin process. Table 7.1 shows the total integrated CP asymmetry for a given value of the number of effective colours N_c. Recall that the number of effective colours differs for the two values of q^2/m_b^2; for a value of 0.3, the number of effective colours is taken to be 0.98, 2.01 or 3.00, while for a value of 0.5, N_c is 0.94, 1.95 or 3.00. For the moment we are interested in the columns labelled NR.

Figure 7.1 shows the theory curves for the asymmetry. We obtained these by integrating over 50 equally spaced bins in the range $2m_K \leq m_{KK} \leq 1.1$ GeV/c^2.

The model appears to perform better for higher values of N_c with the $N_c = 2.01$ and $N_c = 1.95$ results being particularly promising. However, we note that the non-resonant decay may not be the dominant mode for the tree decay in this region of phase space. There could be some resonant decay, such as decay through the $\phi(1020)$ or $f_0(980)$, which has a greater amplitude and thus a larger contribution to the overall tree amplitude. We'll ignore the $\phi(1020)$ for the same reasons we abandoned it in the penguin diagram in addition to the fact that there is no $\bar{s}s$ pair in the tree diagram for it to couple to. However, this still leaves us with the possibility of the $f_0(980)$ coupling to the tree decay. We thus need to check which process, NR or R tree decay, is dominant in the region of phase space of interest to us.

We do this by directly comparing the amplitudes for the decays where we recall the expressions for the amplitudes are

$$A(B^{\pm} \xrightarrow{\text{R tree}} K^+K^-\pi^{\pm}) = \frac{t_f g_f}{s_f}\,, \tag{7.1}$$

$$A(B^{\pm} \xrightarrow{\text{NR tree}} K^+K^-\pi^{\pm}) = t_{NR}\,. \tag{7.2}$$

We then take the ratio

$$\frac{A(B^{\pm} \xrightarrow{\text{NR tree}} K^+K^-\pi^{\pm})}{A(B^{\pm} \xrightarrow{\text{R tree}} K^+K^-\pi^{\pm})}\,, \tag{7.3}$$

and look for how far this number deviates from zero as a function of the K^+K^- invariant mass. This is shown in Figure 7.2. Clearly the ratio, labelled NR/R, remains between 0 and 1 across the entirety of the region of phase space of interest to us. Hence, we would not be justified in claiming that the non-resonant process contributes more to the CP asymmetry than the resonant process. Rather, we should include the $f_0(980)$ with the non-resonant diagram in the overall tree process. This leads us to our final model.

7.2 Non-resonant and $f_0(980)$ Tree with $f_0(980)$ Penguin

In view of these findings we now include the resonant tree process involving the $f_0(980)$. We do this by writing the amplitudes as

$$A_T = \frac{t_f g_f}{s_f} + t_{NR}\,, \qquad A_P = \frac{p_f g_f}{s_f}\,, \tag{7.4}$$

where we recall that the individual amplitudes $t_f\,,\ t_{NR}$ and p_f include the factors $G_F/\sqrt{2}\,,\ V^T$ and V^P. The total tree amplitude receives contributions from the two tree processes we've identified; the resonant $f_0(980)$ decay and the non-resonant process. It is worth clarifying that the *total* tree amplitude is written as A_T and this should not be confused with, for example, $A(B^- \xrightarrow{tree} f_0\pi^-) \equiv t_f$.

This leads to the integrated CP asymmetries shown in Table 7.1 in the NR+R column and the theoretical asymmetry plots shown in Figure 7.3. Unfortunately, the asymmetry is significantly reduced, especially for the $N_c = 2.01$ and $N_c = 1.95$ cases. The reasons for this reduction in the asymmetry will be explored shortly.

7.3 Discussion

To understand our results, it may prove useful to recall our overall approach. First, we started with a model involving the $f_0(980)$ participating in the tree diagram and the $\phi(1020)$ in the penguin diagram. Calculating the CP asymmetry due to the interference of these two diagrams led us to the promising result shown in Figure 5.1. However, in comparing this result to the desired number from Belle, we realised that we needed to consider the full, phase space dependent decay rates. This led to a much less impressive result and so we introduced some new models. The first of these had a non-resonant tree decay interfering with an $f_0(980)$ penguin process and gave some highly significant results. We showed however that the amplitude for

	$q^2/m_b^2 = 0.3$			$q^2/m_b^2 = 0.5$	
	NR	NR + R		NR	NR + R
$N_c = 0.98$			$N_c = 0.94$		
ρ_{max} , η_{max}	-0.130	-0.0324	ρ_{max} , η_{max}	-0.114	-0.0561
ρ_{min} , η_{min}	-0.144	-0.0363	ρ_{min} , η_{min}	-0.126	-0.0629
$N_c = 2.01$			$N_c = 1.95$		
ρ_{max} , η_{max}	-0.344	-0.0243	ρ_{max} , η_{max}	-0.293	-0.0613
ρ_{min} , η_{min}	-0.343	-0.0273	ρ_{min} , η_{min}	-0.296	-0.0689
$N_c = 3.00$			$N_c = 3.00$		
ρ_{max} , η_{max}	-0.180	-0.0196	ρ_{max} , η_{max}	-0.168	-0.0601
ρ_{min} , η_{min}	-0.163	-0.0220	ρ_{min} , η_{min}	-0.152	-0.0675

Table 7.1: Table of values for the integrated CP asymmetry for $n = 1$ monopole dominant form factors.

the non-resonant decay was typically smaller than that for a resonant tree process involving the $f_0(980)$. We thus computed the asymmetry for a third model with both non-resonant and resonant $f_0(980)$ contributions in the tree diagram and the $f_0(980)$ in the penguin diagram. Unfortunately, this gave much less promising results, and we'd like to understand why that is. Our first point of call is the ratio of penguin and tree amplitudes r (see equation (5.41)).

7.3.1 Penguin to Tree Ratio

Consider Figure 7.2 once more. In the region of interest, the resonant decay dominates. However, this resonant decay won't interfere with the penguin diagram which has the same $f_0(980)$ resonance. Hence, we can imagine that we have two opposing effects; on the one hand, the NR decay gives rise to values close to 1 for the ratio t_{NR}/p_f (improving the CP asymmetry). On the other hand the R decay gives rise to values much larger than 1 for the ratio t_f/p_f (producing no asymmetry)[1]. Taking the sum of these and inverting, we get a small value for r due to the resonant contribution and so a small value for the CP violating asymmetry. Showing this

[1]There cannot be any asymmetry produced if we just consider the $f_0(980)$ tree and penguin diagrams since there is no phase difference between them. However, we can still calculate the amplitudes t_f and p_f and see how they contribute to the ratio of total tree and penguin amplitudes.

explicitly, we have

$$r \equiv \frac{|A_P|}{|A_T|} = \left| \frac{p_f g_f / s_f}{t_{NR} + t_f g_f / s_f} \right|.$$

Inverting this equation we get

$$\frac{1}{r} = \left| \frac{t_{NR} + t_f g_f / s_f}{p_f g_f / s_f} \right| = \left| \frac{t_{NR}}{p_f g_f / s_f} + \frac{t_f g_f / s_f}{p_f g_f / s_f} \right| = \left| \frac{t_{NR}}{p_f g_f / s_f} + \frac{t_f}{p_f} \right|.$$

The term t_f/p_f is typically large in the physically relevant region between 0.98 and 2.01 (in the case where we have $q^2/m_b^2 = 0.3$) and up to the limiting value $N_c = 3$, with the ratio $|t_f/p_f|$ approximately constant at a value of ~ 20.

Then, since t_f/p_f is relatively large while the non-resonant term is typically much closer to 1, $1/r$ is much larger than 1. Inverting this, we see that r is much smaller than 1, leading to the small CP asymmetry observed. To show just how small r is, we present the plots shown in Figure 7.4. These required taking the magnitudes of the tree and penguin amplitudes across the region of phase space for $0.986 \leq m_{KK} \leq 1.1$ GeV/c^2 and plotting their ratio as a density/colour plot. Although there are slight variations throughout each individual plot, these amount to small fluctuations around a value of $r \sim 0.1$. These are non-conducive with a significant CP asymmetry and so we try some final calculations with alternative form factors.

7.3.2 Pole Dominance

Recall that there was a two fold ambiguity associated with the initial choice of form factors in the hadronic matrix elements. First, that we assumed that the form factor was dominated by a single pole (also known as monopole dominance), and second, that the order of the pole was a free parameter which we set to $n = 1$. As a final attempt at producing a significant asymmetry, we perform the same calculations but under an order 2 monopole dominance assumption [5, 26, 41] and finally with a dipole model [5, 26, 41].

By repeating the calculation for a higher order pole, we might expect that this should reduce the $f_0(980)$ contribution in both the tree and penguin diagrams. However, it is unclear exactly how this should affect the CP asymmetry. We report the results in Table 7.2 and, comparing to Table 7.1, find that the asymmetry is increased, particularly for the low values of N_c.

For the case of a dipole form factor, we take as our $B \to P$ and $B \to S$ transition form factors

$$f_\pm(k^2) = \frac{f_\pm(0)}{1 - a_1 \dfrac{k^2}{m_B^2} + b_1 \left(\dfrac{k^2}{m_B^2} \right)^2}, \tag{7.5}$$

	$q^2/m_b^2 = 0.3$			$q^2/m_b^2 = 0.5$	
	NR	NR + R		NR	NR + R
$N_c = 0.98$			$N_c = 0.94$		
$\rho_{max}\,,\ \eta_{max}$	-0.156	-0.0466	$\rho_{max}\,,\ \eta_{max}$	-0.114	-0.0902
$\rho_{min}\,,\ \eta_{min}$	-0.172	-0.0523	$\rho_{min}\,,\ \eta_{min}$	-0.126	-0.101
$N_c = 2.01$			$N_c = 1.95$		
$\rho_{max}\,,\ \eta_{max}$	-0.346	-0.0293	$\rho_{max}\,,\ \eta_{max}$	-0.293	-0.0801
$\rho_{min}\,,\ \eta_{min}$	-0.343	-0.0330	$\rho_{min}\,,\ \eta_{min}$	-0.296	-0.0899
$N_c = 3.00$			$N_c = 3.00$		
$\rho_{max}\,,\ \eta_{max}$	-0.174	-0.0219	$\rho_{max}\,,\ \eta_{max}$	-0.168	-0.0714
$\rho_{min}\,,\ \eta_{min}$	-0.157	-0.0247	$\rho_{min}\,,\ \eta_{min}$	-0.152	-0.0802

Table 7.2: Table of values for the integrated CP asymmetry for the NR+R tree and R penguin diagrams for $n = 2$ monopole dominant form factors.

and for the $B \to V$ transitions

$$A_0(k^2) = \frac{h_{A_0}}{1 - a_0 \dfrac{k^2}{m_B^2} + b_0 \left(\dfrac{k^2}{m_B^2} \right)^2}\,, \tag{7.6}$$

with $h_{A_0} = 0.28,\ a_1 = 0.266,\ b_1 = -0.752,\ a_0 = 1.4$ and $b_0 = 0.437$ [5, 26]. The results for the CP asymmetry are given in Table 7.3. For each of the form factor models tested, the NR tree model performs best, but in each case it is suppressed by the resonant tree amplitude. This leads to the typically smaller values for the NR+R columns. It thus appears that we simply haven't chosen our intermediate states well enough. Since there are several resonances in the region of interest, many of which are not well understood (such as the $f_0(980)$ and $a_0(980)$), it may be that we either haven't used the correct intermediate states in our calculations, or we simply do not have the correct description of these intermediate states. Further recommendations on future avenues of research are given in the concluding chapter.

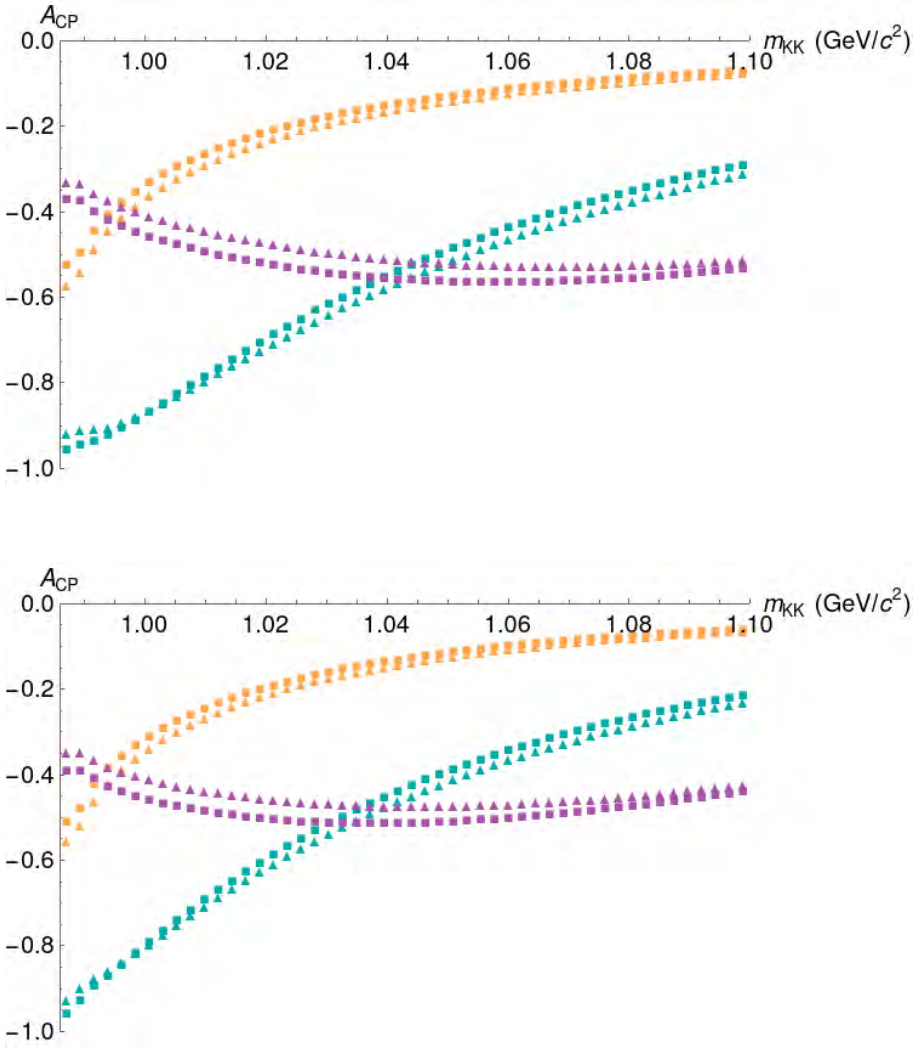

Figure 7.1: Plot of the CP asymmetry for a non-resonant tree decay interfering with an $f_0(980)$ penguin diagram, for $q^2/m_b^2 = 0.3$(top) and $q^2/m_b^2 = 0.5$(bottom). The squares represent points for which ρ and η take their maximum values, while the triangles are for the minimum values. The colours correspond to the number of effective colours N_c in the top(bottom) diagram: orange for $N_c = 0.98(0.94)$, blue for $N_c = 2.01(1.95)$ and purple for $N_c = 3.00(3.00)$.

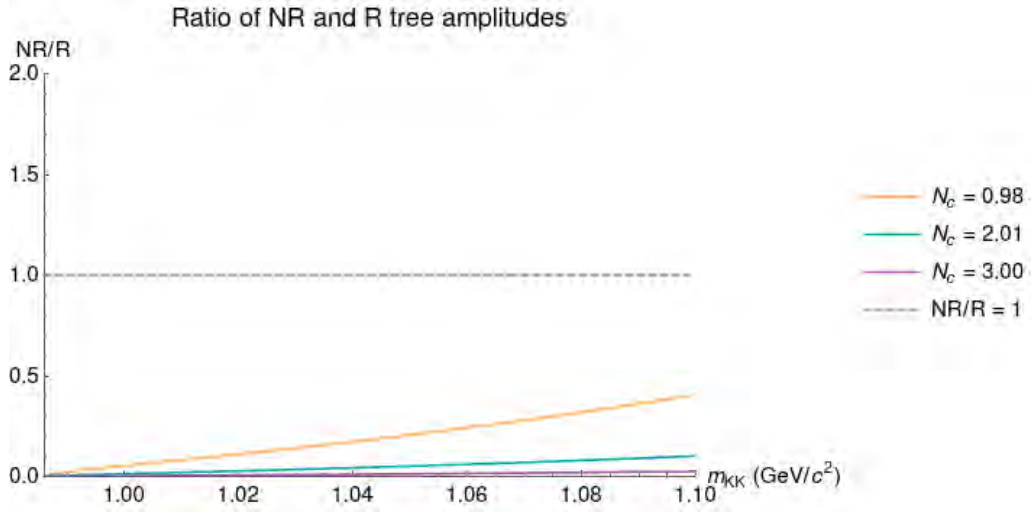

Figure 7.2: Plot of the ratio of non-resonant (NR) and resonant (R) amplitudes across the invariant mass range $2m_K \leq m_{KK} \leq 1.2$ GeV/c^2 for $q^2/m_b^2 = 0.3$.

	$q^2/m_b^2 = 0.3$			$q^2/m_b^2 = 0.5$	
	NR	NR + R		NR	NR + R
$N_c = 0.98$			$N_c = 0.94$		
ρ_{max} , η_{max}	-0.130	-0.0466	ρ_{max} , η_{max}	-0.0819	-0.0902
ρ_{min} , η_{min}	-0.144	-0.0523	ρ_{min} , η_{min}	-0.0907	-0.101
$N_c = 2.01$			$N_c = 1.95$		
ρ_{max} , η_{max}	-0.344	-0.0293	ρ_{max} , η_{max}	-0.273	-0.0801
ρ_{min} , η_{min}	-0.343	-0.0330	ρ_{min} , η_{min}	-0.278	-0.0900
$N_c = 3.00$			$N_c = 3.00$		
ρ_{max} , η_{max}	-0.181	-0.0219	ρ_{max} , η_{max}	-0.169	-0.0714
ρ_{min} , η_{min}	-0.163	-0.0247	ρ_{min} , η_{min}	-0.153	-0.0802

Table 7.3: Table of values for the integrated CP asymmetry for dipole dominated form factors.

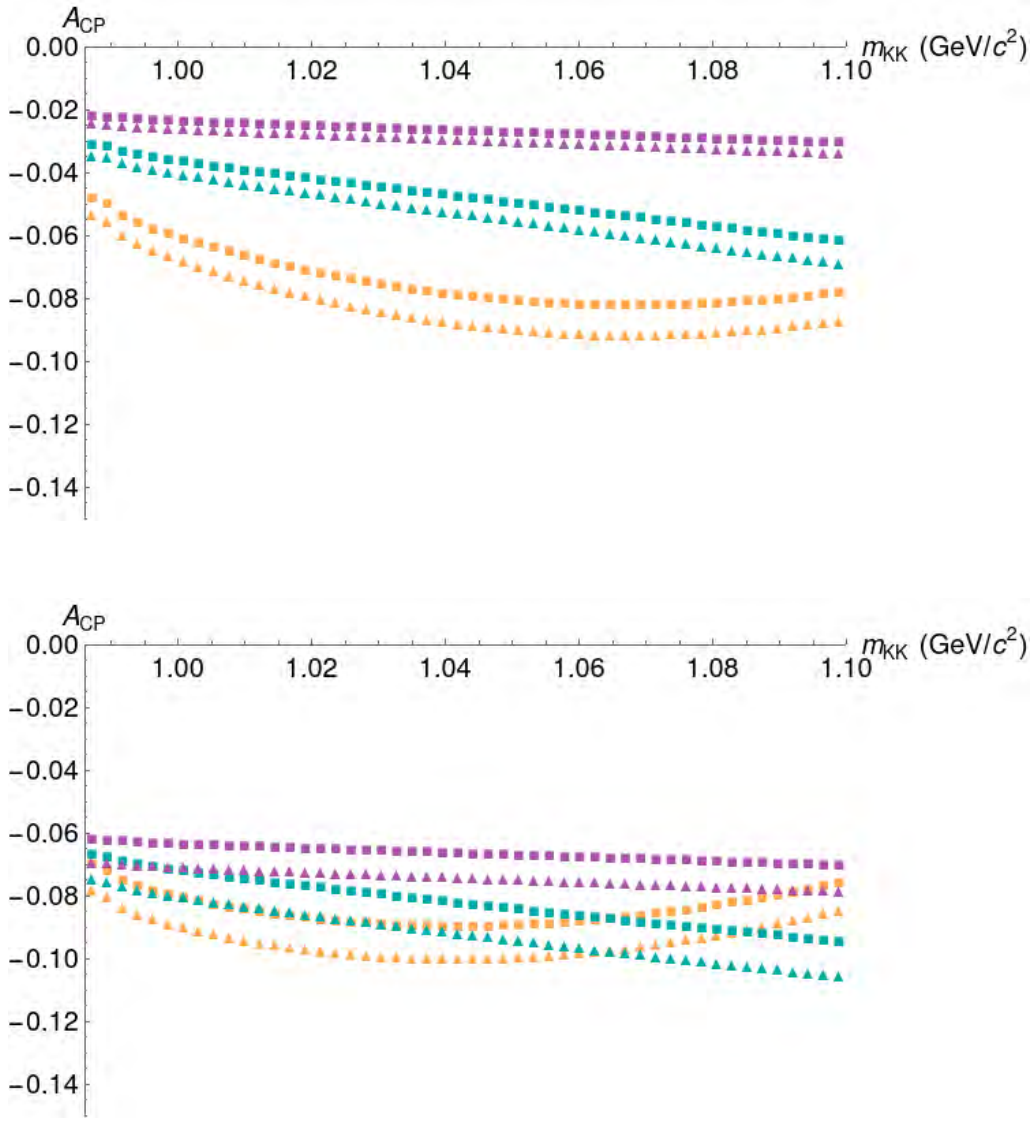

Figure 7.3: The top (bottom) plot shows the CP asymmetry for a non-resonant decay and $f_0(980)$ decay in the tree process, interfering with an $f_0(980)$ penguin diagram, for $q^2/m_b^2 = 0.3(0.5)$. The squares represent points for which ρ and η take their maximum values, while the triangles are for the minimum values. The colours correspond to the number of effective colours N_c in the top (bottom) plot: orange for $N_c = 0.98(0.94)$, blue for $N_c = 2.01(1.95)$ and purple for $N_c = 3.00(3.00)$.

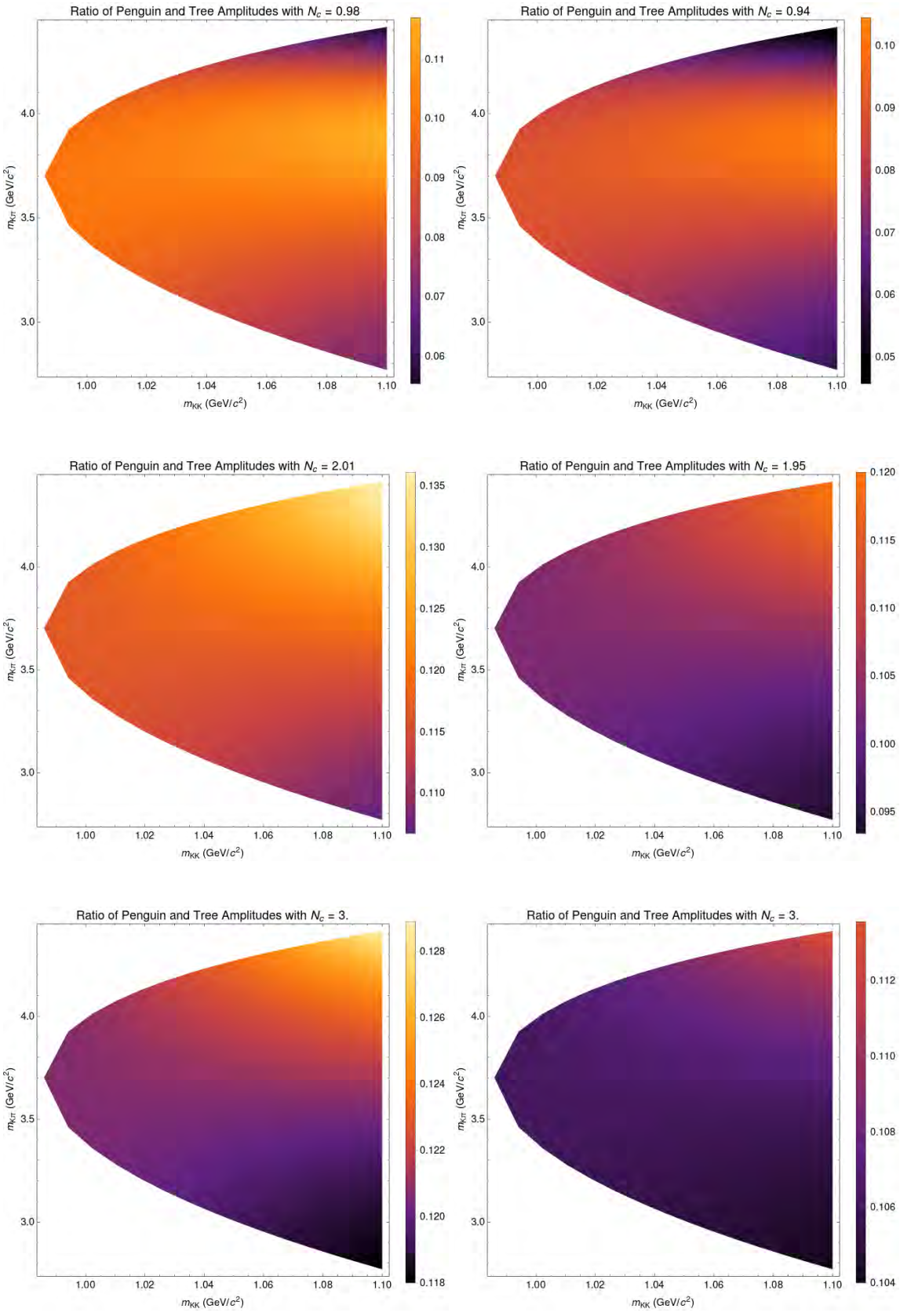

Figure 7.4: Colour plots of the ratio of R penguin and NR+R tree amplitudes r for various values of the number of colours and assuming $n = 1$ monopole dominance. The left column is for $q^2/m_b^2 = 0.3$ while the right is for $q^2/m_b^2 = 0.5$.

Chapter 8

Conclusion

8.1 Summary

In this work we've presented calculations of various CP asymmetries for the decays $B^{\pm} \to K^{+}K^{-}\pi^{\pm}$ with the aim to reproduce the asymmetry

$$\mathcal{A}_{CP} = -0.90 \pm 0.17 \pm 0.03$$

measured by Belle in the invariant mass region $0.986 < m_{KK} < 1.1$ GeV/c^2. Such asymmetries arise through the interference between tree and penguin diagrams with non-zero weak and strong phase differences and we've proposed several combinations of diagrams with which we compute our asymmetries. The first of these models had a tree diagram involving an intermediate $f_0(980)$ resonance and a penguin diagram with an intermediate $\phi(1020)$ resonance. We constructed an effective Hamiltonian based on four-fermion interactions and the Operator Product Expansion, then computed the asymmetry using the Naive Factorisation approximation. The initial result of this was promising, though it lacked any accounting for the finite resolution of real detectors.

We extended our method to include consideration of the phase space and realised that once we integrated over the angular degrees of freedom the $\phi(1020)$ would have its contribution diminished. This was supported by the results for the integrated asymmetry which took a minimum value of

$$\mathcal{A}_{CP} = -0.0554 \qquad \text{Tree: } f_0(980), \text{ Penguin: } \phi(1020)\,.$$

Thus we investigated a second model involving a non-resonant tree decay and a penguin diagram with the $f_0(980)$ replacing the $\phi(1020)$. This led to results significantly more comparable to the Belle data, with a minimum asymmetry of

$$\mathcal{A}_{CP} = -0.346 \qquad \text{Tree: NR, Penguin: } f_0(980)\,.$$

However, this non-resonant tree diagram is not the only contribution in this region of phase space; indeed we found the resonant diagram involving the tree decay of the $f_0(980)$ to be dominant here. Hence we proposed our third model where the tree process consists of a non-resonant contribution and a resonant contribution from

the $f_0(980)$. This overall process then interferes with an $f_0(980)$ penguin diagram. Since the $f_0(980)$ tree diagram gives rise to zero CP asymmetry when taken with the $f_0(980)$ penguin, the total CP asymmetry was found to be mostly negligible, with a minimum asymmetry

$$\mathcal{A}_{CP} = -0.101 \qquad \text{Tree: NR} + f_0(980), \text{ Penguin: } f_0(980)\,.$$

Hence, although our non-resonant model was initially promising, it is suppressed by the dominant resonant contribution and gives a less significant value for the asymmetry. We have thus been unable to reproduce the Belle result. Future work which may improve on our result for the asymmetry is outlined in the following section.

8.2 Future Work and Outlook

CP violation remains a promising avenue of physics research, especially with regards to flavour physics and physics beyond the Standard Model. As research in this area continues, we expect that uncertainties to do with the CKM matrix parameters and properties of the $f_0(980)$ should be improved. However, one of the key methods we've used is Naive Factorisation and this is likely to be the source of most of the uncertainty in our results. For one, Naive Factorisation fails to describe colour suppressed modes, although the parameter N_c goes towards rectifying this by absorbing non-factorizable effects which are unaccounted for by Naive Factorisation [42]. Even with this, the neglect of renormalisation scale dependence in the hadronic matrix elements means the amplitudes can be unphysical [42]. As such, future calculations could make use of alternative methods for calculating the hadronic matrix elements in these heavy quark decays. These include QCD Factorisation [5,42,43] and Lattice QCD [44].

In addition, we suggest that the calculation of the non-resonant tree amplitude should be made with minimal use of heavy meson chiral perturbation theory. Our calculation as it stands acts as an estimate for the asymmetry and future calculations should look to minimize the use of HMChPT, as per [36].

As a final remark, we have perhaps limited ourselves by mainly considering the $f_0(980)$ resonance in the intermediate states of tree and penguin processes. Although we noted that there can be no interference between the $f_0(980)$ and the closely related $a_0(980)$, there is no particular reason we could not have chosen to replace the $f_0(980)$ with the $a_0(980)$ in our models. These two resonances differ in their isospin but this is not necessarily conserved in weak interactions and so the $a_0(980)$ is a valid choice. Future work might investigate the role the $a_0(980)$ plays and possible mixing between it and the $f_0(980)$.

Appendix A

Additional Derivations

A.1 Propagators for Unstable Particles

Throughout this work we make repeated use of the propagator for unstable mesons M

$$s_M^{-1} = \frac{1}{s - m_M^2 + i m_M \Gamma_M} \,. \tag{A.1}$$

This is not the typical form of a propagator that one would usually be familiar with and so we shall need to prove it.

In quantum field theory (QFT) the first propagator one typically encounters is the Feynman propagator for a scalar field ϕ. This is typically written as D_F, but we will use the notation Π_ϕ to be clear that we are referring to the field ϕ. We write

$$\Pi_\phi \equiv \frac{i}{p^2 - m^2 + i\varepsilon} \tag{A.2}$$

to denote the bare propagator for the ϕ, where p and m are the 4-momentum and mass of the ϕ field and ε is an infinitesimal quantity.

Suppose now that the field ϕ is unstable and satisfies a Lagrangian with terms such as $\phi\psi\psi$ so can decay through the vertex

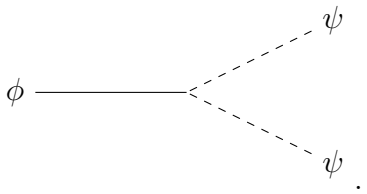

Then, the propagator can involve effective interactions called "dressings" such as

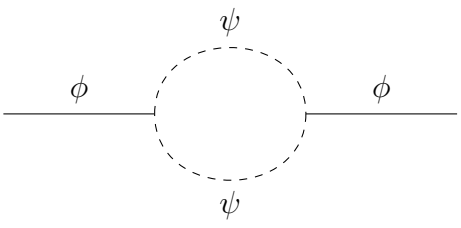

to first order. The matrix element for this ψ loop, denoted $i\mathcal{M}_{loop}$, will have an imaginary part if and only if $m < m_\psi/2$, that is, if the decay $\phi \to \psi\psi$ is allowed kinematically [8]. We can imagine having more ψ loops such that the dressed propagator $\tilde{\Pi}_\phi$ is written

$$\tilde{\Pi}_\phi = \Pi_\phi + \Pi_\phi(i\mathcal{M}_{loop})\Pi_\phi + \Pi_\phi(i\mathcal{M}_{loop})\Pi_\phi(i\mathcal{M}_{loop})\Pi_\phi + \dots \tag{A.3}$$

Clearly we can write the n-th order correction to the propagator as

$$\Pi_\phi^{(n)} = \Pi_\phi[(i\mathcal{M}_{loop})\Pi_\phi]^n\,, \tag{A.4}$$

and so

$$\begin{aligned}\tilde{\Pi}_\phi &= \Pi_\phi + \Pi_\phi[(i\mathcal{M}_{loop})\Pi_\phi] + \Pi_\phi[(i\mathcal{M}_{loop})\Pi_\phi]^2 + \dots \\ &= \Pi_\phi\big(1 + [(i\mathcal{M}_{loop})\Pi_\phi] + [(i\mathcal{M}_{loop})\Pi_\phi]^2 + \dots\big) \\ &= \Pi_\phi \sum_{k=0}^{\infty}(i\mathcal{M}_{loop}\Pi_\phi)^k\,.\end{aligned}$$

We recognise that this takes the form of a geometric series and so we'll make use of the general result

$$\sum_{k=0}^{\infty} ar^k = \frac{a}{1-r} \qquad \text{for } |r| < 1\,. \tag{A.5}$$

Writing the matrix element for each loop as $\mathcal{M}_{loop} = A + iB$ and dropping the $i\varepsilon$ in the bare propagator, we write

$$\begin{aligned}\tilde{\Pi}_\phi &= \Pi_\phi \sum_{k=0}^{\infty}(i\mathcal{M}_{loop}\Pi_\phi)^k \\ &= \frac{i}{p^2-m^2}\sum_{k=0}^{\infty}\left(i(A+iB)\frac{i}{p^2-m^2}\right)^k \\ &= \frac{i}{p^2-m^2}\sum_{k=0}^{\infty}\left(-\frac{(A+iB)}{p^2-m^2}\right)^k \\ &= \frac{i}{p^2-m^2}\frac{1}{1+\frac{(A+iB)}{p^2-m^2}} \\ &= \frac{i}{p^2-m^2+A+iB}\,.\end{aligned}$$

Rewriting this, we have

$$\tilde{\Pi}_\phi = \frac{i}{p^2-\tilde{m}^2+im\Gamma} \tag{A.6}$$

where we've absorbed the real part of the loop matrix element into the mass to obtain the dressed mass $\tilde{m}$ and we've defined the decay width $\Gamma \equiv B/m$. This form is supported by the fact that, calculating the cross section for s-channel scattering

using this propagator, one observes the characteristic "bump" associated with a particle with decay width Γ.

A.2 Momentum Transfer Region $0.3 < q^2/m_b^2 < 0.5$

At the quark level, one can draw the Feynman diagram shown in Figure A.1. Applying conservation of 4-momentum at each of the three vertices, we obtain the equations

$$\begin{aligned} p_b &= k + p_t \,, \\ p_t &= q + p_t' \,, \\ p_d &= k + p_t' \,, \end{aligned}$$

where p_b is the momentum of the bottom quark, q is the momentum of the gluon/photon participating in the penguin decay, p_d is the momentum of the down quark in the final state, k is the momentum of the W boson and p_t and p_t' are the momenta of the top quark in the intermediate state. These three equations combine to give the result

$$p_b = q + p_d \,.$$

Rearranging and squaring this, we can recognise that $m_d \ll m_b$ and get

$$q^2 = m_b^2 - 2p_b^\mu p_d^\mu \,. \tag{A.7}$$

The second term is written

$$p_b^\mu p_d^\mu = p_b^0 p_d^0 - \boldsymbol{p}_b \cdot \boldsymbol{p}_d = \sqrt{m_b^2 + |\boldsymbol{p}_b|^2} E_d \,, = m_b E_d$$

where we've used the fact that the momentum of the b quark is negligible. Then, by taking $E_d \simeq \frac{1}{3} m_b$ [5, 26] and substituting this back in to the equation for q^2, we

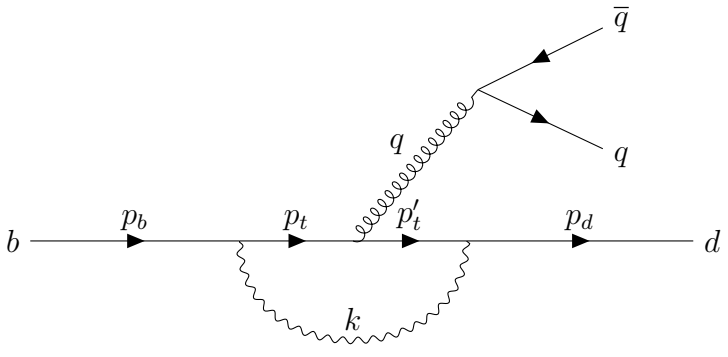

Figure A.1: Penguin decay $b \to q\bar{q}d$ through a gluon and W boson loop.

get

$$\frac{q^2}{m_b^2} \simeq \frac{1}{3}\,. \tag{A.8}$$

Hence, we take q^2 such that $0.3 < q^2/m_b^2 < 0.5$.

A.3 Momentum in Centre of Mass Frame

Here we prove a fairly straightforward kinematic result. Consider the 2-particle final state decay process

$$A \to B + C\,.$$

The magnitude of the 3-momenta of the outgoing particles in the rest frame of particle A is given by

$$|\boldsymbol{p}_B| = |\boldsymbol{p}_C| = \frac{c\sqrt{m_A^4 + m_B^4 + m_C^4 - 2m_A^2m_B^2 - 2m_A^2m_c^2 - 2m_B^2m_C^2}}{2m_A} \tag{A.9}$$

where m_i is the mass of the particle i and c is the speed of light [45].

Proof: First, we recall the forms of the 4-momenta involved. Using the relativistic energy equation $E^2 = |\boldsymbol{p}|^2c^2 + m^2c^4$ we can write the 4-momentum of particle A as

$$p_A = (E_A/c,\ \boldsymbol{p}_A) = (m_Ac,\ 0)\,. \tag{A.10}$$

Likewise, we can write the 4-momentum of particles B and C as

$$p_B = (E_B/c,\ \boldsymbol{p}_B)\,, \qquad\qquad p_C = (E_C/c,\ \boldsymbol{p}_C)\,. \tag{A.11}$$

Applying conservation of 4-momentum, we have

$$p_A^\mu = p_B^\mu + p_C^\mu\,. \tag{A.12}$$

Now, some forward thinking is essential here. We'll make use of the Lorentz invariant quantity $p^2 = p^\mu p_\mu = m^2c^2$. To get squared momenta, we'll need to square our conservation of momentum equation. However, this will necessarily lead to cross terms such as $p_B \cdot p_C$. It will be difficult to work with terms such as these when we have no information about $\boldsymbol{p}_B$ and $\boldsymbol{p}_C$. Rather, we'll rearrange equation (A.12) and square the result to obtain an equation where the cross term vanishes,

$$\begin{aligned} p_A^\mu &= p_B^\mu + p_C^\mu \\ \Rightarrow p_C^\mu &= p_B^\mu - p_A^\mu \\ \Rightarrow p_C^2 &= p_B^2 - 2p_A \cdot p_B + p_A^2\,. \end{aligned}$$

The cross term has

$$p_A \cdot p_B = \frac{E_AE_B}{c^2} - \boldsymbol{p}_A \cdot \boldsymbol{p}_B = \frac{E_AE_B}{c^2} = m_AE_B$$

where we've used the fact that particle A is at rest so has zero 3-momentum and that $E_A = \sqrt{|\boldsymbol{p}_A|^2 c^2 + m_A^2 c^4} = m_A c^2$. Substituting in the invariant quantities $p_i^2 = m_i^2 c^2$ we then have

$$\begin{aligned} m_C^2 c^2 &= m_B^2 c^2 + m_A^2 c^2 - 2 m_A E_B \\ \Rightarrow E_B &= \frac{(m_A^2 + m_B^2 - m_C^2)c^2}{2m_A} \,. \end{aligned} \tag{A.13}$$

Similarly, we could have rearranged equation (A.12) to be $p_B^\mu = p_A^\mu - p_C^\mu$ and followed the same process to obtain the energy for particle C as

$$E_C = \frac{(m_A^2 + m_C^2 - m_B^2)c^2}{2m_A} \,. \tag{A.14}$$

With the energies given by equations (A.13) and (A.14), we can make use of the following:

$$\begin{aligned} E^2 &= |\boldsymbol{p}|^2 c^2 + m^2 c^4 \\ \Rightarrow |\boldsymbol{p}| &= \frac{\sqrt{E^2 - m^2 c^4}}{c} \,. \end{aligned}$$

Then, applying conservation of 3-momentum

$$\begin{aligned} \boldsymbol{p}_A &= \boldsymbol{p}_B + \boldsymbol{p}_C \\ \Rightarrow \; 0 &= \boldsymbol{p}_B + \boldsymbol{p}_C \\ \Rightarrow \; |\boldsymbol{p}_B| = |\boldsymbol{p}_C| &= \frac{\sqrt{E_B^2 - m_B^2 c^4}}{c} \\ &= \frac{\sqrt{\left(\frac{(m_A^2+m_B^2-m_C^2)c^2}{2m_A}\right)^2 - m_B^2 c^4}}{c} \\ &= \frac{\sqrt{(m_A^2 + m_B^2 - m_C^2)^2 c^4 - 4 m_A^2 m_B^2 c^4}}{2 m_A c} \\ &= \frac{c^2 \sqrt{m_A^4 + m_B^4 + m_C^4 + 2m_A^2 m_B^2 - 2m_A^2 m_C^2 - 2m_B^2 m_C^2 - 4m_A^2 m_B^2}}{2 m_A c} \\ \therefore \; |\boldsymbol{p}_B| = |\boldsymbol{p}_C| &= \frac{c\sqrt{m_A^4 + m_B^4 + m_C^4 - 2m_A^2 m_B^2 - 2m_A^2 m_C^2 - 2m_B^2 m_C^2}}{2m_A} \,. \end{aligned}$$

A.4 Matrix Element Contractions

In chapter 5 we made use of the following results without proof (see equations (5.30) to (5.32)).

$$\langle P|J^\mu|0\rangle\ \langle S|J'_\mu|B\rangle = -f_P(m_B^2 - m_S^2)F_0(m_P^2)\,. \tag{A.15}$$
$$\langle V|J^\mu|0\rangle\ \langle P|J'_\mu|B\rangle = 2f_V m_B p_c F_1(m_V^2)\,. \tag{A.16}$$
$$\langle P|J^\mu|0\rangle\ \langle V|J'_\mu|B\rangle = 2f_P m_B p_c A_0(m_P^2) \tag{A.17}$$

where P is a pseudoscalar meson, V is a vector meson, B is a B meson; J^μ and J'^μ are $V-A$ currents; f_i is the decay constant for the $i = P, V$ meson; m_j is the mass of the $j = P, V$ or B meson; F_1 is a form factor for the pseudoscalar meson and A_0 is a form factor for the vector meson; p_c is the magnitude of the 3-momentum in the centre of momentum frame

$$p_c = |\boldsymbol{p}_P| = |\boldsymbol{p}_V| = \frac{\sqrt{(m_B^2 - (m_P + m_V)^2)(m_B^2 - (m_P - m_V)^2)}}{2m_B}\,. \tag{A.18}$$

We will now prove each of these results, recalling the form factor parametrisation of the various matrix elements given in chapter 5. We begin the proof of equation (A.15) with

$$\begin{aligned}
&\langle S|V_\mu - A_\mu|B\rangle\ \langle P|V_\mu - A_\mu|0\rangle \\
&= +i\left[\left(p_B + p_S - \frac{m_B^2 - m_S^2}{k^2}k\right)_\mu F_1(k^2) + \frac{m_B^2 - m_S^2}{k^2}k_\mu F_0(k^2)\right](+if_P p_P^\mu) \\
&= -f_P\left[(p_B + p_S)_\mu p_P^\mu F_1(k^2) - \frac{m_B^2 - m_S^2}{k^2}k_\mu p_P^\mu F_1(k^2) + \frac{m_B^2 - m_S^2}{k^2}k_\mu p_P^\mu F_0(k^2)\right].
\end{aligned}$$

Conservation of 4-momentum implies $p_P^\mu = p_B^\mu - p_S^\mu \equiv k^\mu$ so we can write

$$\begin{aligned}
&\langle S|V_\mu - A_\mu|B\rangle\ \langle P|V_\mu - A_\mu|0\rangle \\
&= -f_P\left[(p_B + p_S)_\mu (p_B - p_S)^\mu F_1(m_P^2) - \frac{m_B^2 - m_S^2}{k^2}k_\mu k^\mu F_1(m_P^2)\right. \\
&\qquad\qquad \left. + \frac{m_B^2 - m_S^2}{k^2}k_\mu k^\mu F_0(m_P^2)\right] \\
&= -f_P\big[\big(m_B^2 - m_S^2\big)F_1(m_P^2) - \big(m_B^2 - m_S^2\big)F_1(m_P^2) + (m_B^2 - m_S^2)F_0(m_P^2)\big] \\
&= -f_P\big(m_B^2 - m_S^2\big)F_0(m_P^2)\,.
\end{aligned}$$

Hence, we've proven equation (A.15). The proof of equation (A.16) is as follows.

$$\begin{aligned}
&\langle V|V_\mu - A_\mu|0\rangle\ \langle P|V^\mu - A^\mu|B\rangle \\
&= f_V m_V \varepsilon_\mu\left[(p_B + p_P)^\mu F_1(k^2) - \frac{m_B^2 - m_P^2}{k^2}k^\mu\big(F_1(k^2) - F_0(k^2)\big)\right].
\end{aligned}$$

Recalling equation (5.18) to (5.20), we note that $f_+(0) = f_-(0) \Rightarrow f_+(k^2) = f_-(k^2)$ and so we can write

$$\begin{aligned}
&\langle V|V_\mu - A_\mu|0\rangle \ \langle P|V^\mu - A^\mu|B\rangle \\
&= f_V m_V \varepsilon_\mu \Bigg[(p_B + p_P)^\mu F_1(k^2) - \frac{m_B^2 - m_P^2}{k^2} k^\mu F_1(k^2) + \frac{m_B^2 - m_P^2}{k^2} k^\mu F_1(k^2) \\
&\qquad\qquad + \frac{m_B^2 - m_P^2}{k^2} \frac{k^2}{m_B^2 - m_P^2} k^\mu F_1(k^2) \Bigg] \\
&= f_V m_V \varepsilon_\mu \big[(p_B + p_P)^\mu F_1(k^2) + k^\mu F_1(k^2) \big] \\
&= f_V m_V \varepsilon_\mu \big[(p_B + p_P)^\mu F_1(k^2) + (p_B - p_P)^\mu F_1(k^2) \big] \\
&= 2 f_V m_V \varepsilon_\mu p_B^\mu F_1(k^2) \,.
\end{aligned}$$

We can then substitute for the polarisation vector ε^μ since the vector meson is longitudinally polarised [8],

$$\varepsilon^\mu = \left(\frac{p_c}{m_V}, 0, 0, \frac{E_V}{m_V} \right). \tag{A.19}$$

which gives

$$\begin{aligned}
\langle V|V_\mu - A_\mu|0\rangle \ \langle P|V^\mu - A^\mu|B\rangle &= 2 f_V m_V \left(\frac{p_c}{m_V}, 0, 0, \frac{E}{m_V} \right) \cdot (m_B, 0, 0, 0) F_1(m_V^2) \\
&= 2 f_V m_B p_c F_1(m_V^2)
\end{aligned}$$

where again we've used conservation of 4-momentum to identify $p_V^\mu = p_B^\mu - p_P^\mu \equiv k^\mu$. We've thus proven equation (A.16).

The final proof is the longest but proceeds in the usual manner, by first writing out the form factor expressions for the matrix elements. This gives

$$\begin{aligned}
&\langle V|V_\mu - J_\mu|B\rangle \ \langle P|V^\mu A^\mu|0\rangle \\
&= -i f_P p_P^\mu \Bigg[\frac{2}{m_B + m_V} \varepsilon_{\mu\nu\rho\sigma} \varepsilon^\nu p_B^\rho p_V^\sigma \mathcal{V}(k^2) + i \Bigg(\varepsilon_\mu (m_B + m_V) A_1(k^2) \\
&\qquad\qquad - \frac{\varepsilon \cdot k}{m_B + m_V} (p_B + p_V)_\mu A_2(k^2) - \frac{\varepsilon \cdot k}{k^2} 2 m_V k_\mu (A_3(k^2) - A_0(k^2)) \Bigg) \Bigg] \\
&= f_P \Bigg[\frac{-2i}{m_B + m_V} \varepsilon_{\mu\nu\rho\sigma} p_P^\mu \varepsilon^\nu p_B^\rho p_V^\sigma \mathcal{V}(k^2) + \varepsilon_\mu p_P^\mu (m_B + m_V) A_1(k^2) \\
&- \frac{\varepsilon \cdot k}{m_B + m_V} (p_B + p_V)_\mu p_P^\mu A_2(k^2) - \frac{\varepsilon \cdot k}{k^2} 2 m_V k_\mu p_P^\mu \big(A_3(k^2) - A_0(k^2) \big) \Bigg] .
\end{aligned}$$

At this point, we digress to show

$$\begin{aligned}(\varepsilon\cdot k)(p_B+p_V)_\mu p_P^\mu &= \varepsilon^\nu k_\nu (p_B+p_V)_\mu p_P^\mu \\ &= \varepsilon^\nu g_{\mu\nu} k^\mu (p_B+p_V)_\mu p_P^\mu \\ &= \varepsilon^\nu g_{\mu\nu} p_P^\mu k^\mu (p_B+p_V)_\mu \\ &= (\varepsilon\cdot p_P)(p_B-p_V)^\mu (p_B+p_V)_\mu \\ &= (\varepsilon\cdot p_P)(m_B^2-m_V^2)\,.\end{aligned}$$

This allows us to write

$$\begin{aligned}&\langle V|V_\mu - J_\mu|B\rangle\ \langle P|V^\mu A^\mu|0\rangle \\ &= f_P\Bigg[\frac{-2i}{m_B+m_V}\varepsilon_{\mu\nu\rho\sigma}p_P^\mu\varepsilon^\nu p_B^\rho p_V^\sigma \mathcal{V}(k^2) + (\varepsilon\cdot p_P)(m_B+m_V)A_1(k^2) \\ &- (\varepsilon\cdot p_P)(m_B-m_V)A_2(k^2) - (\varepsilon\cdot p_P)2m_V\big(A_3(k^2)-A_0(k^2)\big)\Bigg]\,.\end{aligned}$$

Then, using the fact that according to [5, 26]

$$A_3(k^2) = \frac{m_B+m_V}{2m_V}A_1(k^2) - \frac{m_B-m_V}{2mV}A_2(k^2)\,, \tag{A.20}$$

we can write

$$\begin{aligned}&\langle V|V_\mu - J_\mu|B\rangle\ \langle P|V^\mu A^\mu|0\rangle \\ &= f_P\Bigg[\frac{-2i}{m_B+m_V}\varepsilon_{\mu\nu\rho\sigma}p_P^\mu\varepsilon^\nu p_B^\rho p_V^\sigma \mathcal{V}(k^2) \\ &+ (\varepsilon\cdot p_P)(m_B+m_V)A_1(k^2) - (\varepsilon\cdot p_P)(m_B-m_V)A_2(k^2) \\ &- (\varepsilon\cdot p_P)(m_B+m_V)A_1(k^2) + (\varepsilon\cdot p_P)(m_B-m_V)A_2(k^2) + (\varepsilon\cdot p_P)2m_V A_0(k^2)\Bigg] \\ &= f_P\Bigg[\frac{-2i}{m_B+m_V}\varepsilon_{\mu\nu\rho\sigma}p_P^\mu\varepsilon^\nu p_B^\rho p_V^\sigma \mathcal{V}(k^2) + 2m_V(\varepsilon\cdot p_P)A_0(k^2)\Bigg]\,.\end{aligned}$$

Before proceeding, we can argue that the first term vanishes. This occurs by noticing that

$$\begin{aligned}\varepsilon_{\mu\nu\rho\sigma}p_P^\mu\varepsilon^\nu p_B^\rho p_V^\sigma &= \varepsilon_{\mu\nu\rho\sigma}p_P^\mu\varepsilon^\nu (p_P+p_V)^\rho p_V^\sigma \\ &= \varepsilon_{\mu\nu\rho\sigma}p_P^\mu\varepsilon^\nu p_P^\rho p_V^\sigma + \varepsilon_{\mu\nu\rho\sigma}p_P^\mu\varepsilon^\nu p_V^\rho p_V^\sigma\,.\end{aligned}$$

The Levi Cevita tensor is antisymmetric under the exchange of any pair of its indices and in both terms there is a symmetric combination of momenta ($p_P^\mu p_P^\rho$ in the first term and $p_V^\rho p_V^\sigma$ in the second). Hence the total contribution is zero leaving us with

$$\langle V|V_\mu - J_\mu|B\rangle\ \langle P|V^\mu A^\mu|0\rangle = 2f_P m_V(\varepsilon\cdot p_P)A_0(m_P^2)\,, \tag{A.21}$$

where again we've recognised $p_P^\mu = k^\mu$. At this point, we need to write out the explicit forms of the 4-vectors. The vector and pseudoscalar come out with back-to-back momenta and have

$$p_V^\mu = (E_V, 0, 0, +p_c)\,, \qquad p_P^\mu = (E_P, 0, 0, -p_c)\,, \tag{A.22}$$

where p_c is the 3-momentum of the decay products in the rest frame of the B meson. The polarisation of the vector meson is longitudinal and so we write

$$\begin{aligned} m_V \varepsilon^\nu p_{P\nu} &= m_V(\varepsilon^0 p_{P0} - \boldsymbol{\varepsilon}\cdot\boldsymbol{p}_P) \\ &= m_V\left(\frac{p_c}{m_V}E_P + \frac{E_V}{m_V}p_c\right) \\ &= p_c(E_P + E_V) \\ &= p_c E_B \\ &= p_c m_B\,. \end{aligned}$$

We thus have the result

$$\langle V|V_\mu - J_\mu|B\rangle\ \langle P|V^\mu A^\mu|0\rangle = 2 f_P m_B p_c A_0(m_P^2)\,, \tag{A.23}$$

and so we've proven equation (A.17).

Appendix B

$\omega - \phi$ mixing

Here we briefly discuss the idea of $\omega - \phi$ mixing. This is useful for deciding which quark currents contribute to the ϕ.

Mesons are generally classified in J^{PC} multiplets. Isoscalar states (states with zero isospin) will mix if they belong to the same multiplet. For example, the ω and ϕ mesons both have isospin zero and $J^{PC} = 1^{--}$ so they are able to mix [21]. To see how this mixing occurs, consider the following.

Let the $I = 0$ members of the light quark nonet (ϕ and ω) be labelled by f and f'. These states will be composed of the SU(3) wave functions ψ_8 and ψ_1 corresponding to the octet and singlet respectively. The mixing occurs by

$$\begin{pmatrix} f \\ f' \end{pmatrix} = \begin{pmatrix} \cos\theta & -\sin\theta \\ \sin\theta & \cos\theta \end{pmatrix} \begin{pmatrix} \psi_8 \\ \psi_1 \end{pmatrix} .$$

Hence, we have

$$f' = \psi_8 \cos\theta - \psi_1 \sin\theta \,, \tag{B.1}$$
$$f = \psi_8 \sin\theta + \psi_1 \cos\theta \,, \tag{B.2}$$

where θ is the mixing angle and

$$\psi_8 = \frac{1}{\sqrt{6}}\left(u\bar{u} + d\bar{d} - 2s\bar{s}\right) ,$$
$$\psi_1 = \frac{1}{\sqrt{3}}\left(u\bar{u} + d\bar{d} + s\bar{s}\right) .$$

One can consider the case for "ideal" mixing, where the ideal mixing angle θ_I is such that $\tan\theta_I = 1/\sqrt{2}$ ($\theta_I = 35.3°$). Then, defining $\alpha = \theta + (90 - \theta_I)$, we note that ideal mixing occurs for $\alpha = 90°$. Using this expression for θ in equation (B.1)

we can write

$$\begin{aligned}\cos\theta &= \cos(\alpha - (90 - \theta_I)) = \cos\alpha\cos(90-\theta_I) + \sin\alpha\sin(90-\theta_I)\\ &= \sin\alpha\sin\theta_I + \cos\alpha\cos\theta_I\\ &= \frac{1}{\sqrt{3}}\sin\alpha + \sqrt{\frac{2}{3}}\cos\alpha\,,\end{aligned}$$

where we've made use of the fact that if $\tan\theta_I = 1/\sqrt{2}$, then $\cos\theta_I = \sqrt{2/3}$ and $\sin\theta_I = 1/\sqrt{3}$. Likewise

$$\begin{aligned}\sin\theta &= \sin(\alpha - (90 - \theta_I)) = \sin\alpha\cos(90-\theta_I) - \cos\alpha\sin(90-\theta_I)\\ &= \cos\alpha\sin\theta_I - \sin\alpha\cos\theta_I\\ &= \frac{1}{\sqrt{3}}\cos\alpha - \sqrt{\frac{2}{3}}\sin\alpha\,.\end{aligned}$$

This then allows us to write

$$\begin{aligned}f' &= \psi_8\left(\frac{1}{\sqrt{3}}\sin\alpha + \sqrt{\frac{2}{3}}\cos\alpha\right) - \psi_1\left(\frac{1}{\sqrt{3}}\cos\alpha - \sqrt{\frac{2}{3}}\sin\alpha\right)\\ &= \cos\alpha\left(\frac{1}{\sqrt{3}}\psi_8 + \sqrt{\frac{2}{3}}\psi_1\right) + \sin\alpha\left(\sqrt{\frac{2}{3}}\psi_8 - \frac{1}{\sqrt{3}}\psi_1\right)\\ &= \cos\alpha\left(\frac{1}{\sqrt{3}}\frac{1}{\sqrt{6}}\big(u\bar{u} + d\bar{d} - 2s\bar{s}\big) + \sqrt{\frac{2}{3}}\frac{1}{\sqrt{3}}\big(u\bar{u} + d\bar{d} + s\bar{s}\big)\right)\\ &\qquad + \sin\alpha\left(\sqrt{\frac{2}{3}}\frac{1}{\sqrt{6}}\big(u\bar{u} + d\bar{d} - 2s\bar{s}\big) - \frac{1}{\sqrt{3}}\frac{1}{\sqrt{3}}\big(u\bar{u} + d\bar{d} + s\bar{s}\big)\right)\\ &= \cos\alpha\left(\frac{1}{3}\frac{1}{\sqrt{2}}\big(u\bar{u} + d\bar{d}\big) - \frac{\sqrt{2}}{3}(s\bar{s}) + \frac{2}{3}\frac{1}{\sqrt{2}}\big(u\bar{u} + d\bar{d}\big) + \frac{\sqrt{2}}{3}(s\bar{s})\right)\\ &\qquad + \sin\alpha\left(\frac{1}{3}\big(u\bar{u} + d\bar{d}\big) - \frac{2}{3}(s\bar{s}) - \frac{1}{3}\big(u\bar{u} + d\bar{d}\big) - \frac{1}{3}(s\bar{s})\right)\\ &= \frac{1}{\sqrt{2}}\big(u\bar{u} + d\bar{d}\big)\cos\alpha - (s\bar{s})\sin\alpha\,.\end{aligned}$$

We can perform the same calculation for the f case and we thus end up with the two results

$$\begin{aligned}f' &= \frac{1}{\sqrt{2}}\big(u\bar{u} + d\bar{d}\big)\cos\alpha - (s\bar{s})\sin\alpha\,,\\ f &= \frac{1}{\sqrt{2}}\big(u\bar{u} + d\bar{d}\big)\sin\alpha + (s\bar{s})\cos\alpha\,.\end{aligned}$$

Hence, for ideal mixing where $\alpha = 90^o$, we see that the f' is a pure state of $s\bar{s}$ pairs and the f is a pure state of $u\bar{u}$ and $d\bar{d}$ pairs. We identify the physical $\phi(1020)$ meson with the f' and the $\omega(783)$ with the f. Further, the vector mixing angle can be determined theoretically using mass formulae and is found to be $\theta_V = 36.4^\circ$ [21]. Substituting this value into the expressions for f' and f above, we obtain the following expressions for ϕ and ω,

$$\phi = -0.01401(u\bar{u} + d\bar{d}) - 0.99980(s\bar{s})\,,$$
$$\omega = 0.70697(u\bar{u} + d\bar{d}) - 0.01982(s\bar{s})\,.$$

Hence we see that the ϕ is predominantly composed of $s\bar{s}$ pairs while the ω is mostly $u\bar{u}$ and $d\bar{d}$ pairs. In addition, the ϕ having a non-zero $u\bar{u} + d\bar{d}$ contribution indicates that there is some small amplitude for an ω to mix to a ϕ.

Appendix C

Tables

C.1 Meson Reference Table

Throughout this work we reference the mesons listed in Table C.1. The mesons are ordered by their mass which is given in MeV/c^2 (noting that the rest of this work uses units of GeV/c^2). The scalar mesons are not well known in terms of their quark structure and mass widths.

Meson Name	Quark Structure	Mass (MeV/c^2)	Width (MeV/c^2)	J^{PC}
$\pi^{\pm}$	$u\bar{d}$, $\bar{u}d$	139.57018 ± 0.00035	–	0^{-}
$K^{\pm}$	$u\bar{s}$, $\bar{u}s$	493.677 ± 0.016	–	0^{-}
K^0, $\bar{K}^0$	$d\bar{s}$, $\bar{d}s$	497.614 ± 0.024	–	0^{-}
$f_0(980)$	$*$	990 ± 20	10 to 100	0^{++}
$a_0(980)$	$*$	990 ± 20	10 to 100	0^{++}
$\phi(1020)$	$s\bar{s}$ $(**)$	1019.461 ± 0.019	4.266 ± 0.031	1^{--}
$B^{\pm}$	$u\bar{b}$, $\bar{u}b$	5279.26 ± 0.17	–	0^{-}
B^0, $\bar{B}^0$	$d\bar{b}$, $\bar{d}b$	5279.58 ± 0.17	–	0^{-}
B_s^0, $\bar{B}_s^0$	$s\bar{b}$, $\bar{s}b$	5366.77 ± 0.24	–	0^{-}

Table C.1: Table of relevant mesons, their J^{PC} classifications (J^P where C is not applicable), their quark content, masses and widths. $(*)$ The exact quark structure of the $f_0(980)$ and $a_0(980)$ is still an open question. Several models claim a mixture of $u\bar{u} + d\bar{d}$ with $s\bar{s}$ while others postulate more exotic states of quark matter [27]. $(**)$ The $\phi(1020)$ is predominantly composed of $s\bar{s}$ under a typical quark mixing scheme [21].

C.2 Wilson Coefficients

One of the key pieces in our calculations is the Wilson Coefficients. These are calculated at some scale where perturbation theory is applicable and then scaled to

a new scale μ under some regime. We take coefficients at the scale $m_b = 5$ GeV/c^2.

c_1	-0.3125
c_2	1.1502
c_3	0.0174
c_4	-0.0373
c_5	0.0104
c_6	-0.0459
c_7	-1.050×10^{-5}
c_8	3.839×10^{-4}
c_9	-0.0101
c_{10}	1.959×10^{-3}

Table C.2: Table of Wilson coefficients [5, 26].

c_i'	$q^2/m_b^2 = 0.3$	$q^2/m_b^2 = 0.5$
c_1'	-0.3125	-0.3125
c_2'	1.1502	1.1502
c_3'	$2.433 \times 10^{-2} + 1.543 \times 10^{-3} i$	$2.120 \times 10^{-2} + 2.174 \times 10^{-3} i$
c_4'	$-5.808 \times 10^{-2} - 4.628 \times 10^{-3} i$	$-4.869 \times 10^{-2} - 1.552 \times 10^{-2} i$
c_5'	$1.733 \times 10^{-2} + 1.543 \times 10^{-3} i$	$1.420 \times 10^{-2} + 5.174 \times 10^{-3} i$
c_6'	$-6.668 \times 10^{-2} - 4.628 \times 10^{-3} i$	$-5.729 \times 10^{-2} - 1.552 \times 10^{-2} i$
c_7'	$-1.435 \times 10^{-4} - 2.963 \times 10^{-5} i$	$-8.340 \times 10^{-5} - 9.938 \times 10^{-5} i$
c_8'	3.839×10^{-4}	3.839×10^{-4}
c_9'	$-1.023 \times 10^{-2} - 2.963 \times 10^{-5} i$	$-1.017 \times 10^{-2} - 9.938 \times 10^{-5} i$
c_{10}'	1.959×10^{-3}	1.959×10^{-3}

Table C.3: Table of effective Wilson coefficients [5, 26].

Appendix D

Mathematica Code

Over the following pages, we present the Wolfram Mathematica code used for the work in this thesis. The calculation is shown for the case of a non-resonant and $f_0(980)$ tree amplitude interfering with an $f_0(980)$ penguin. However, it is a simple matter of changing to include the $\phi(1020)$ and the propagator for the $\phi(1020)$ is included for reference. Mathematica was used for the majority of the calculations, namely for its simple to use `NIntegrate` function.

As a note, the plot of Figure 5.1 was produced in Python, but the code used follows the same general structure as that shown over the next pages. A key difference though is that Mathematica doesn't lend itself so well to vectorised code. Rather, it relies more heavily on function definitions. In our case, we define functions for most things, including the Wilson coefficients. In this case, the coefficients depend on the momentum transfer q^2. Then, when we combine the Wilson coefficients to form the a_i's, we introduce a dependence on the effective number of colours N_c. As we continue building up the code, we hold off on evaluating the functions until the last possible moment, in other words, when we compute the CP asymmetries. This allows us to obtain asymmetries for a given set of starting parameters $\{q^2/m_b^2\,, n\}$ where we recall that q^2 is the momentum transferred by the gluon in the penguin diagram and n is the order of the poles in a monopole dominated form factor parametrisation.

Since functions play such a large role in the following code, it is worth noting that the syntax in Mathematica for calling a function f depending on a set of variables x_i is `f[x1 , x2 , ...]`. When defining functions, one writes

$$\texttt{f[x1\_ , x2\_ , ...]:=}$$

followed by the function definition. The function definition is some combination of explicit terms and predefined functions involving the variables `xi` (with no underscores after variables).

Calculation of CP Asymmetry

```
In[1]:= Clear["Global`*"]
In[2]:= qmRatio = 0.3;(* 0.3 or 0.5*)
In[3]:= If[qmRatio == 0.3, Nc1 = 0.98, Nc1 = 0.94];
In[4]:= If[qmRatio == 0.3, Nc2 = 2.01, Nc2 = 1.95];
In[5]:= Nc3 = 3.00;
In[6]:= n = 1; (* Pole dominance, use either n=1 or n=2 *)
In[7]:= G_fermi = 1.1663787 * 10^-5;
```

List the Relevant constants

Note that all masses are given in units of GeV/c^2.

Masses

```
In[8]:= m_k = 0.493; (* Mass of the charged kaons *)
In[9]:= m_k0 = 0.4976; (* Mass of the neutral kaons *)
In[10]:= m_pi = 0.1396; (* Mass of the charged pions *)
In[11]:= m_pi0 = 0.1350; (* Mass of the neutral pion *)
In[12]:= m_eta = 0.547862; (* Mass of the eta meson *)
In[13]:= m_f = 0.990; (* Mass of the f0(980) resonance *)
In[14]:= m_a0 = 0.980; (* Mass of the a0(980) resonance *)
In[15]:= m_ϕ = 1.019461; (* Mass of the ϕ resonance *)
In[16]:= m_B = 5.27926; (* Mass of the B mesons *)
In[17]:= m_Bs = 5.4154; (* Pole mass *)
```

Decay Widths

```
In[18]:= Γ_f = 0.050; (* Total decay width of the f0(980) *)
In[19]:= Γ_ϕ = 4.266 * 10^-3; (* Total decay width of the ϕ(1020) *)
```

Coupling Constants

In[20]:= `g_f = 7.8; (* Coupling of the f_0 to two charged kaons *)`

In[21]:= `(*g_ϕ = 4.54 Coupling of the ϕ to two charged kaons *)`

In[22]:= `strongg = 0.59; (* Strong coupling constant *)`

Wilson Coefficients

In[23]:= `c_1 = -0.3125;`

In[24]:= `c_2 = 1.1502;`

In[25]:= `If[qmRatio == 0.5, c_3 = 2.12 * 10^-2 + 2.174 * 10^-3 * i, c_3 = 2.433 * 10^-2 + 1.543 * 10^-3 * i];`

In[26]:= `If[qmRatio == 0.5, c_4 = -4.869 * 10^-2 - 1.552 * 10^-2 * i, c_4 = -5.808 * 10^-2 - 4.628 * 10^-3 * i];`

In[27]:= `If[qmRatio == 0.5, c_5 = 1.420 * 10^-2 + 5.174 * 10^-3 * i, c_5 = 1.733 * 10^-2 + 1.543 * 10^-3 * i];`

In[28]:= `If[qmRatio == 0.5, c_6 = -5.729 * 10^-2 - 1.552 * 10^-2 * i, c_6 = -6.668 * 10^-2 - 4.628 * 10^-3 * i];`

In[29]:= `If[qmRatio == 0.5, c_7 = -8.340 * 10^-5 - 9.938 * 10^-5 * i, c_7 = -1.435 * 10^-4 - 2.963 * 10^-5 * i];`

In[30]:= `c_8 = 3.839 * 10^-4;`

In[31]:= `If[qmRatio == 0.5, c_9 = -1.017 * 10^-2 - 9.938 * 10^-5 * i, c_9 = -1.023 * 10^-2 - 2.963 * 10^-5 * i];`

In[32]:= `c_10 = 1.959 * 10^-3;`

Construct the a's; the combinations of Wilson coefficients we make use of.

In[33]:= `If[OddQ[i] == True, a[i_, Nc_] := c_i + 1 / Nc * c_i+1, a[i_, Nc_] := c_i + 1 / Nc * c_i-1]`

In[34]:= `a[1, Nc_] := c_1 + 1 / Nc * c_2`

Decay Constants and Form Factor Coefficients

In[35]:= `f_ϕ = 0.233; (* Decay constant for the ϕ meson *)`

In[36]:= `f_pi = 0.1307; (* Decay constant for the π meson *)`

In[37]:= `f_B_s = 0.217284; (* Decay constant for the pole mass *)`

In[38]:= `f_B = 0.191; (* Decay constant for the B meson *)`

In[39]:= `h_1 = 0.330;`

In[40]:= `h_0 = 0.28;`

In[41]:= `m_1 = 5.320; (* Pole mass for F_1 *)`

In[42]:= `m_0 = 5.270; (* Pole mass for A_0 *)`

CKM Parameters

```
In[43]:= λ = 0.22453; (* see PDG *)
In[44]:= rhomax = 0.122 + 0.018;
In[45]:= rhomin = 0.122 - 0.017;
In[46]:= etamax = 0.355 + 0.012;
In[47]:= etamin = 0.355 - 0.011;
In[48]:= V_ud = 0.97446;
In[49]:= V_ub = 0.00365;
In[50]:= V_td = 0.00896;
In[51]:= V_tb = 0.999105;
```

Form Factors and Vertex Amplitude Calculation

Center of Mass Momentum

$$\text{In[52]:=}\quad p_c = \frac{\text{Sqrt}\left[\left(m_B^2 - (m_\phi - m_{pi})^2\right) * \left(m_B^2 - (m_\phi + m_{pi})^2\right)\right]}{2 * m_B};$$

Form Factors

$$\text{In[53]:=}\quad F_1[x\_] := \frac{h_1}{\left(1 - \frac{x}{m_1^2}\right)^n}$$

$$\text{In[54]:=}\quad F_0[x\_] := \frac{h_1}{\left(1 - \frac{x}{m_1^2}\right)^n} + \frac{x}{m_B^2 - m_f^2} * \frac{h_1}{\left(1 - \frac{x}{m_1^2}\right)^n}$$

$$\text{In[55]:=}\quad A_0[x\_] := \frac{h_0}{\left(1 - \frac{x}{m_0^2}\right)^n}$$

$$\text{In[56]:=}\quad w_+[mkk\_, mkpi\_] := -\frac{strongg}{(f_{pi})^2} * \frac{f_{B_s} * m_{B_s}\, \text{Sqrt}[m_B * m_{B_s}]}{mkpi^2 - m_{B_s}^2} * \left(1 - \frac{(1/2) * \left(mkk^2 + mkpi^2 - 3\, m_k^2 - m_{pi}^2\right)}{(m_{B_s})^2}\right) + \frac{f_B}{2 * (f_{pi})^2}$$

In[57]:=
$$w_{-}[mkk\_, mkpi\_] := \frac{strongg}{(f_{pi})^2} * \frac{f_{B_s} * m_{B_s}\, Sqrt[m_B * m_{B_s}]}{mkpi^2 - m_{B_s}{}^2} * \left(1 + \frac{(1/2) * \left(mkk^2 + mkpi^2 - 3\, m_k{}^2 - m_{pi}{}^2\right)}{(m_{B_s})^2}\right)$$

Tree and Penguin Vertex Amplitudes

In[58]:=
$$t_{NR}[Nc\_, mkk\_, mkpi\_] := -a[1, Nc] * \frac{f_{pi}}{2} * \left((m_B{}^2 - mkk^2 - m_{pi}{}^2) * w_{+}[mkk, mkpi] + (2\, mkpi^2 + mkk^2 - 2\, m_k{}^2 - m_{pi}{}^2) * w_{-}[mkk, mkpi]\right)$$

In[59]:=
$$t_f[Nc\_] := -\left(a[2, Nc] * f_{pi} * (m_B{}^2 - m_f{}^2) * F_0[m_{pi}{}^2]\right)$$

In[60]:=
$$p_f[Nc\_] := -a[4, Nc]\, f_{pi} * (m_B{}^2 - m_f{}^2) * F_0[m_{pi}{}^2]$$

In[61]:=
$$t_R[Nc\_] := t_f[Nc] + t_{a0}[Nc]$$

In[62]:=
$$t_{total}[Nc\_, mkk\_, mkpi\_] = t_{NR}[Nc, mkk, mkpi];$$

CKM Ratio

In[63]:=
$$MagCKM[\rho\_, \eta\_] := \frac{Sqrt\left[(1-\rho)^2 + \eta^2\right]}{\left(1 - \frac{\lambda^2}{2}\right) * Sqrt\left[\rho^2 + \eta^2\right]};$$

Amplitude Ratio

In[64]:=
$$strongr[Nc\_, mkk\_, mkpi\_, \rho\_, \eta\_] := -\frac{p_f[Nc]}{(t_{total}[Nc, mkk, mkpi])} * MagCKM[\rho, \eta]$$

Propagators (with mass dependent widths)

$f_0(980)$:

In[65]:=
$$g_{pi} = 0.165;\ (*\ GeV/c^2\ *);$$

In[66]:=
$$g_K = 4.21 * g_{pi};$$

In[67]:=
$$\rho_{pi}[mkk\_] := 2/3 * Sqrt\left[1 - 4\, m_{pi}{}^2 / mkk\right] + 1/3 * Sqrt\left[1 - 4\, m_{pi0}{}^2 / mkk\right]$$

In[68]:=
$$\rho_K[mkk\_] := 1/2 * Sqrt\left[1 - 4\, m_k{}^2 / mkk\right] + 1/2 * Sqrt\left[1 - 4\, m_{k0}{}^2 / mkk\right]$$

In[69]:=
$$G_f[mkk\_] := g_{pi} * \rho_{pi}[mkk] + g_K * \rho_K[mkk]$$

In[70]:=
$$s_f[mkk\_] := \left(mkk^2 - m_f{}^2 + m_f * G_f[mkk] * i\right)$$

$\phi(1020)$:

In[71]:=
$$\Gamma_{\phi KK} = 0.6340 * \frac{0.004266}{1.251} \text{ (* See partial widths for the } \phi \text{ in the PDG *);}$$

In[72]:=
$$d = 0.5 / 0.1973 * 10^{-15}; \text{ (* Impact parameter/ meson radius for the } \phi, \text{ in metres *)}$$

In[73]:=
$$G_\phi[mkk\_] := \Gamma_{\phi KK} * \frac{(mkk^2 - 4\, m_k{}^2)^{3/2}}{mkk} * \left(\frac{1 + \frac{1}{4} * (m_\phi{}^2 - 4\, m_k{}^2) * d^2}{1 + \frac{1}{4} * (mkk^2 - 4\, m_k{}^2) * d^2} \right) * \frac{m_\phi}{(m_\phi{}^2 - 4\, m_k{}^2)^{3/2}}$$

In[74]:=
$$s_\phi[mkk\_] := (mkk^2 - m_\phi{}^2 + m_\phi * G_\phi[mkk] * i)$$

Calculate the term $re^{i\delta}$ and get the r, rcos(δ) and rsin(δ) terms

Calculate various amplitudes for different values of mkk

These are for plotting

In[75]:=
$$A_{tree}[Nc\_, mkk\_, mkpi\_] := \text{Sqrt}\left[\text{Conjugate}\left[t_{NR}[Nc, mkk, mkpi] * \frac{G_{fermi}}{\text{Sqrt}[2]} * V_{ud} * V_{ub}\right] * t_{NR}[Nc, mkk, mkpi] * \frac{G_{fermi}}{\text{Sqrt}[2]} * V_{ud} * V_{ub}\right]$$

In[76]:=
$$A_{penguin}[Nc\_, mkk\_, mkpi\_] := \text{Re}\left[\text{Sqrt}\left[\text{Conjugate}\left[p_f[Nc] * \frac{g_f}{s_f[mkk]} * \frac{G_{fermi}}{\text{Sqrt}[2]} * V_{td} * V_{tb}\right] * \left(p_f[Nc] * \frac{g_f}{s_f[mkk]} * \frac{G_{fermi}}{\text{Sqrt}[2]} * V_{td} * V_{tb}\right)\right]\right]$$

In[77]:=
$$A_{NRT}[Nc\_, mkk\_, mkpi\_] := t_{NR}[Nc, mkk, mkpi] * \frac{G_{fermi}}{\text{Sqrt}[2]} * V_{ud} * V_{ub}$$

In[78]:=
$$A_{RT}[Nc\_, mkk\_, mkpi\_] := \left(t_f[Nc] * \frac{g_f}{s_f[mkk]}\right) * \frac{G_{fermi}}{\text{Sqrt}[2]} * V_{ud} * V_{ub}$$

In[79]:=
$$A_T[Nc\_, mkk\_, mkpi\_] := A_{NRT}[Nc, mkk, mkpi] + A_{RT}[Nc, mkk, mkpi] \text{ (*INCLUDE this term if we are looking at NR+R*)}$$

In[80]:=
$$A_P[Nc\_, mkk\_] := p_f[Nc] * \frac{g_f}{s_f[mkk]} \frac{G_{fermi}}{\text{Sqrt}[2]} * V_{td} * V_{tb}$$

Calculate $re^{i\delta}$

In[81]:=
$$\text{res}[Nc\_, mkk\_, mkpi\_, \rho\_, \eta\_] := -\frac{p_f[Nc]}{t_{NR}[Nc, mkk, mkpi] + t_f[Nc] * \frac{g_f}{s_f[mkk]}} * \frac{g_f}{s_f[mkk]} * \text{MagCKM}[\rho, \eta]$$

```
(*INCLUDE the second term in the denominator if we're looking at NR+R*)
```

In[82]:=
```
r[Nc_, mkk_, mkpi_, ρ_, η_] := Abs[res[Nc, mkk, mkpi, ρ, η]]
```

In[83]:=
```
rcosdelta[Nc_, mkk_, mkpi_, ρ_, η_] := Re[res[Nc, mkk, mkpi, ρ, η]]
```

In[84]:=
```
rsindelta[Nc_, mkk_, mkpi_, ρ_, η_] := Im[res[Nc, mkk, mkpi, ρ, η]]
```

Calculate the $\sin\phi$ and $\cos\phi$ terms

In[85]:=
$$\sin\phi[\rho\_, \eta\_] := \frac{\eta}{\text{Sqrt}\left[\left(\rho\,(1-\rho) - \eta^2\right)^2 + \eta^2\right]}$$

In[86]:=
$$\cos\phi[\rho\_, \eta\_] := \frac{\rho\,(1-\rho) - \eta^2}{\text{Sqrt}\left[\left(\rho\,(1-\rho) - \eta^2\right)^2 + \eta^2\right]}$$

Put it all together to get the integrands

In[87]:=
```
diff[Nc_, mkk_, mkpi_, ρ_, η_] :=
 -2 * rsindelta[Nc, mkk, mkpi, ρ, η] * sinϕ[ρ, η] * Abs[A_T[Nc, mkk, mkpi]]^2
```

In[88]:=
```
sum[Nc_, mkk_, mkpi_, ρ_, η_] :=
 (1 + 2 * rcosdelta[Nc, mkk, mkpi, ρ, η] * cosϕ[ρ, η] + (r[Nc, mkk, mkpi, ρ, η])^2) *
  Abs[A_T[Nc, mkk, mkpi]]^2
```

Setup the Integral bins: Dalitz plots etc

In[89]:=
```
num[Nc_, mkk_, mkpi_, ρ_, η_] := mkk * mkpi * diff[Nc, mkk, mkpi, ρ, η]
```

In[90]:=
```
denom[Nc_, mkk_, mkpi_, ρ_, η_] := mkk * mkpi * sum[Nc, mkk, mkpi, ρ, η]
```

Do the binning in the mkk direction

In[91]:=
```
numBin = 50;
```

In[92]:=
```
mkkmin_1 = 2 * m_k;
```

In[93]:=
```
mkkmax_numBin = 1.1;
```

```
In[94]:= di = (mkkmax[numBin] - mkkmin[1])/numBin;

In[95]:= Do[mkkmin[i] = mkkmin[i-1] + di, {i, 2, numBin}]

In[96]:= Do[mkkmax[i] = mkkmin[i+1], {i, 1, numBin - 1}]

In[97]:= mkkminfixed = 2 * m_k;

In[98]:= mkkmaxfixed = m_B - m_pi;
```

Construct bounds in the mkpi direction

```
In[99]:= E_2[mkk_] := (m_B^2 - mkk^2 - m_pi^2)/(2 * mkk)

In[100]:= E_3[mkk_] := mkk/2

In[101]:= mkpimax[mkk_] := Sqrt[(E_2[mkk] + E_3[mkk])^2 - (Sqrt[E_2[mkk]^2 - m_pi^2] - Sqrt[E_3[mkk]^2 - m_k^2])^2]

In[102]:= mkpimin[mkk_] := Sqrt[(E_2[mkk] + E_3[mkk])^2 - (Sqrt[E_2[mkk]^2 - m_pi^2] + Sqrt[E_3[mkk]^2 - m_k^2])^2]
```

Draw the Dalitz Plot for the phase space

```
In[103]:= dalitzmin =
  Plot[mkpimin[mkk], {mkk, mkkminfixed, mkkmaxfixed}, PlotRange → {{0.4, 5.6}, {0, 5.2}}];

In[104]:= dalitzmax =
  Plot[mkpimax[mkk], {mkk, mkkminfixed, mkkmaxfixed}, PlotRange → {{0.4, 5.6}, {0, 5.2}}];

In[105]:= Show[dalitzmin, dalitzmax, PlotRange → {{0.4, 5.6}, {0, 5.2}}]
```

Out[105]=

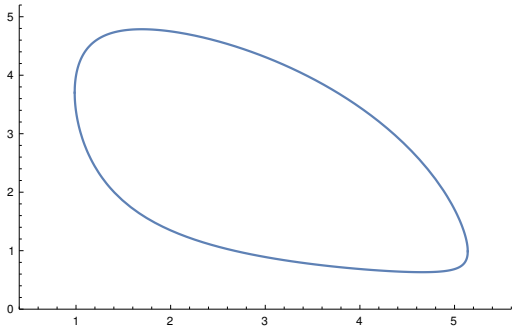

Setup the integrals for plotting the numerical curve

In[106]:=
```
Do[integratedNum_i[Nc_, ρ_, η_] := NIntegrate[num[Nc, mkk, mkpi, ρ, η],
    {mkk, mkkmin_i, mkkmax_i}, {mkpi, mkpimin[mkk], mkpimax[mkk]}], {i, 1, numBin}]
```

In[107]:=
```
Do[integratedDenom_i[Nc_, ρ_, η_] := NIntegrate[denom[Nc, mkk, mkpi, ρ, η],
    {mkk, mkkmin_i, mkkmax_i}, {mkpi, mkpimin[mkk], mkpimax[mkk]}], {i, 1, numBin}]
```

In[108]:=
$$\text{Do}\left[\text{Acp}_i[\text{Nc\_}, \rho\_, \eta\_] := \frac{\text{Re}[\text{integratedNum}_i[\text{Nc}, \rho, \eta]]}{\text{Re}[\text{integratedDenom}_i[\text{Nc}, \rho, \eta]]}, \{i, 1, \text{numBin}\}\right]$$

In[109]:=
$$\text{Do}\left[\text{xval}_i = \frac{\text{mkkmin}_i + \text{mkkmax}_i}{2}, \{i, 1, \text{numBin}\}\right]$$

In[110]:=
```
list[Nc_, ρ_, η_] := Reap[For[i = 1, i < numBin + 1, i++, Sow[{xval_i, Acp_i[Nc, ρ, η]}]];][[2, 1]];
```

In[111]:=
```
label = StringTemplate["Asymmetry with N_c="][N_c];
```

Calculate an integrated Acp for the first Belle bin

In[112]:=
```
Ncfixed = 0.94;
```

In[113]:=
```
theoryplot[Nc_, ρ_, η_] := ListPlot[list[Nc, ρ, η], PlotRange → {{0.8, 1.3}, {-1, 1}},
  AxesLabel → {"m_KK (GeV/c^2)", A_CP}, LabelStyle → {14, GrayLevel[0]},
  PlotLabel → ("Asymmetry with N_c = " <> ToString[Ncfixed]), ImageSize → Large]
```

In[114]:=
```
Acp_check [Nc_, ρ_, η_] := (Re[NIntegrate[num[Nc, mkk, mkpi, ρ, η],
    {mkk, 2 * m_k, 1.1}, {mkpi, mkpimin[mkk], mkpimax[mkk]}]]) /
  (Re[NIntegrate[denom[Nc, mkk, mkpi, ρ, η], {mkk, 2 * m_k, 1.1},
    {mkpi, mkpimin[mkk], mkpimax[mkk]}]])
```

In[115]:=
```
Acp_check[Nc1, rhomax, etamax]
```
Out[115]= −0.0465666

In[116]:=
```
Acp_check[Nc1, rhomin, etamin]
```
Out[116]= −0.0522811

In[117]:=
```
Acp_check[Nc2, rhomax, etamax]
```
Out[117]= −0.0293259

In[118]:=
```
Acp_check[Nc2, rhomin, etamin]
```
Out[118]= −0.0329731

In[119]:=
```
Acp_check[3, rhomax, etamax]
```
Out[119]= −0.0219389

In[120]:=
```
Acp_check[3, rhomin, etamin]
```
Out[120]=
```
-0.0246714
```

In[121]:=
```
(*theoryplot[Ncfixed]*)
```

In[122]:=
```
ListPlot[{list[Nc1, rhomax, etamax], list[Nc1, rhomin, etamin], list[Nc2, rhomax, etamax],
  list[Nc2, rhomin, etamin], list[3, rhomax, etamax], list[3, rhomin, etamin]},
 PlotRange → {{2 * m_k , 1.1}, {-0.1, 0}}, AxesLabel → {"m_KK  (GeV/c^2)", A_CP},
 LabelStyle → {14, GrayLevel[0]}, ImageSize → Large,
 PlotMarkers → {{■, 10}, {▲, 10}, {■, 10}, {▲, 10}, {■, 10}, {▲, 10}},
 PlotStyle → {Lighter[Orange], Lighter[Orange],
   Darker[Cyan], Darker[Cyan], Lighter[Purple], Lighter[Purple]}(*,
 PlotLegends→{"N_c = "<>ToString[Nc1] "","N_c = "<>ToString[Nc1] "","N_c = 3.00"}*)]
```
Out[122]=

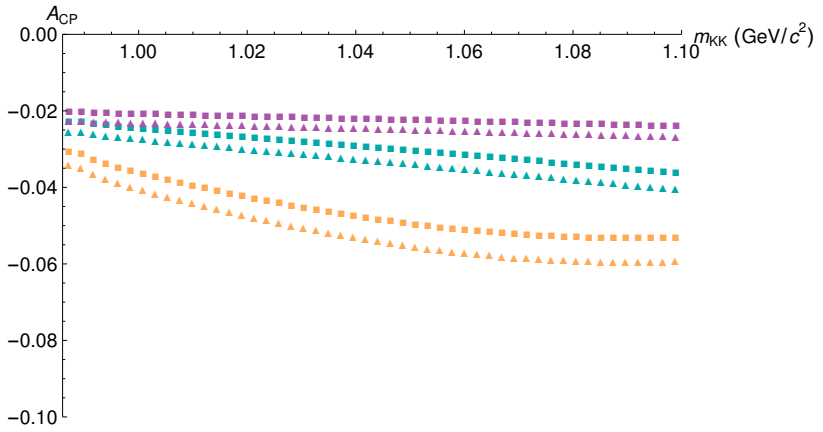

Check Amplitudes etc

Compare Tree in both Resonant and Non-resonant cases

In[138]:=
```
Plot3D[{Abs[A_NRT[Nc1, mkk, mkpi]], Abs[A_RT[Nc1, mkk, mkpi]]},
 {mkk, mkkminfixed, 1.1}, {mkpi, mkpimin[mkk], mkpimax[mkk]},
 AxesLabel → {"m_KK (GeV/c^2)", "m_Kπ (GeV/c^2)", "Amplitude"}, PlotLabel →
  ("Resonant and Non-resonant Tree Amplitudes with N_c = " <> ToString[Ncfixed]),
 LabelStyle → {14, GrayLevel[0]},
 PlotLegends → {"Non-resonant Tree Amplitude", "Resonant Tree Amplitude"},
 PlotRange → All, ImageSize → Large]
```

Out[138]=

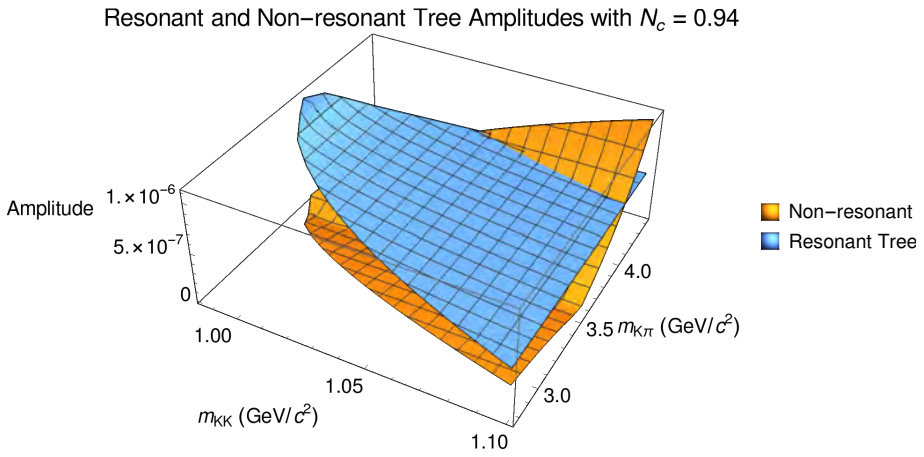

Plot the ratio of the resonant and non-resonant tree amplitudes

In[131]:=
```
NRoverR2[Nc_, mkk_] :=
 NIntegrate[A_NRT[Nc, mkk, mkpi] / Abs[A_RT[Nc, mkk, mkpi]], {mkpi, mkpimin[mkk], mkpimax[mkk]}]
```

In[132]:=
```
Plot[{NRoverR2[Nc1, mkk], NRoverR2[Nc2, mkk], NRoverR2[3.00, mkk], 1},
 {mkk, mkkminfixed, mkkmaxfixed}, PlotRange → {{2 * m_K, 1.1}, {0, 2}},
 PlotLabel → "Ratio of NR and R tree amplitudes",
 AxesLabel → {"m_KK (GeV/c^2)", "NR/R"}, LabelStyle → {14, GrayLevel[0]},
 PlotLegends → {"N_c = " <> ToString[Nc1], "N_c = " <> ToString[Nc2],
   "N_c = 3.00", "NR/R = 1"}, (*ImageSize→Large,*)PlotStyle →
  {{Line, Lighter[Orange]}, {Line, Darker[Cyan]}, {Line, Lighter[Purple]}, {Dashed, Gray}}]
```

Out[132]=

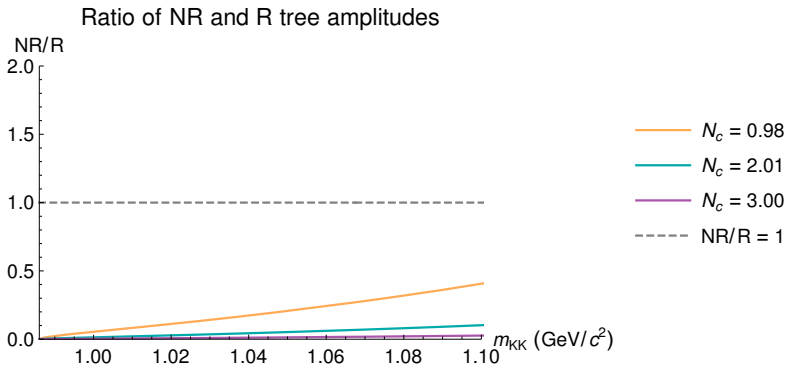

In[133]:=
```
Export["~/Desktop/NRoverR_Zoom_final.png", %];
```

Compare the amplitudes for the tree and penguin diagrams

In[134]:=
```
DensityPlot[Abs[AP[Nc3, mkk]] / Abs[AT[Nc3, mkk, mkpi]], {mkk, mkkminfixed, 1.1},
 {mkpi, mkpimin[mkk], mkpimax[mkk]}, LabelStyle → {14, GrayLevel[0]},
 PlotLegends → Automatic, FrameLabel → {"mKK (GeV/c^2)", "mKπ (GeV/c^2)"},
 PlotLabel → ("Ratio of Penguin and Tree Amplitudes with Nc = " <> ToString[Nc3]),
 ImageSize → Large,
 ColorFunction → (ColorData["SunsetColors"][Rescale[#, {0.118, 0.13}]] &),
 ColorFunctionScaling → False, PlotRange → {0, 0.15}]
```

Out[134]=

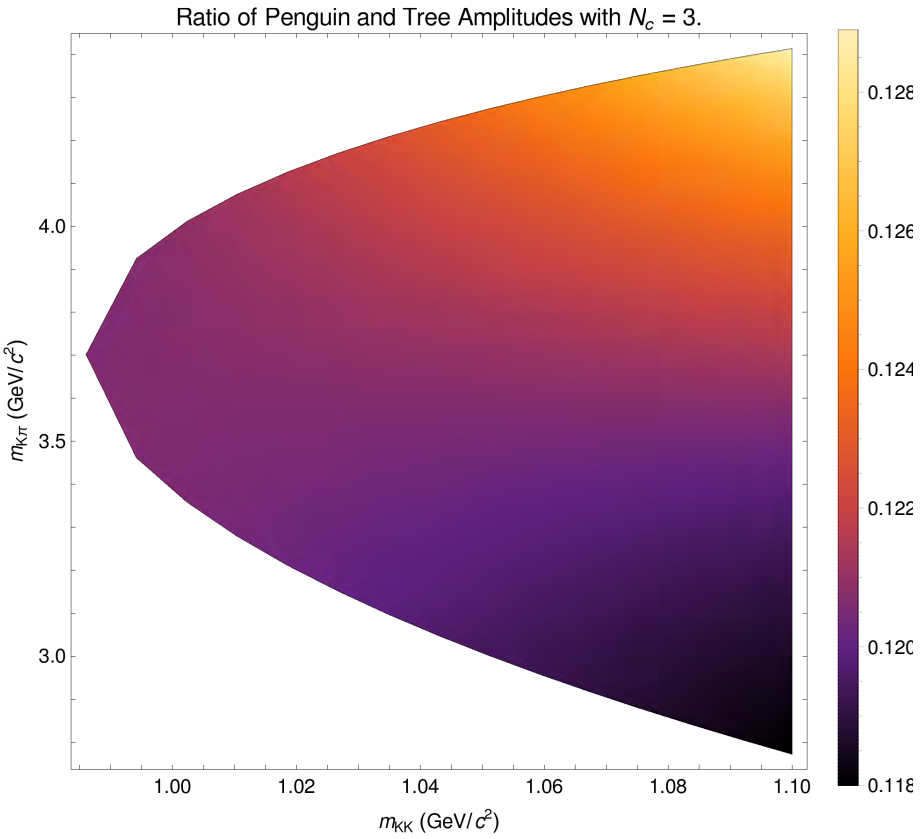

In[135]:=
```
Export["~/Desktop/PTcolor303.png", %];
```

Plot the values of t_f/p_f to check 1/r contribution from the resonant only decay

In[136]:=
```
Plot[Abs[tf[Nc]]/Abs[pf[Nc]], {Nc, 0, 3}, PlotRange → {{0, 3}, {0, 500}}, AxesLabel → {"Nc", "tf/pf"}]
```

Out[136]=

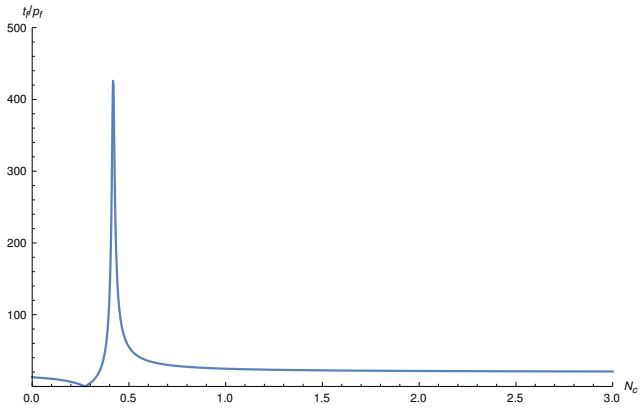

Bibliography

[1] Ian J R Aitchison and Anthony J G Hey. *Gauge theories in particle physics: a practical introduction; 4th ed.* CRC Press, Boca Raton, FL, 2013.

[2] Sheldon L. Glashow. Partial-symmetries of weak interactions. *Nuclear Physics*, 22(4):579 – 588, 1961.

[3] Abdus Salam. Gauge unification of fundamental forces. *Rev. Mod. Phys.*, 52:525–538, Jul 1980.

[4] Steven Weinberg. A Model of Leptons. *Phys. Rev. Lett.*, 19:1264–1266, Nov 1967.

[5] O. Leitner. *Direct CP violation in B decays including $\rho - \omega$ mixing and covariant light-front dynamics*. PhD thesis, Adelaide University, 2003.

[6] Siegfried Bethke. World Summary of α_s (2012). 2012. [Nucl. Phys. Proc. Suppl.234,229(2013)].

[7] Jun John Sakurai. *Modern quantum mechanics; rev. ed.* Addison-Wesley, Reading, MA, 1994.

[8] Matthew D. Schwartz. *Quantum Field Theory and the Standard Model*. Cambridge University Press, 2014.

[9] Brian R Martin and Graham Shaw. *Particle physics; 4th ed.* Manchester physics series. Wiley, New York, NY, 2017.

[10] T. D. Lee and Chen-Ning Yang. Question of Parity Conservation in Weak Interactions. *Phys. Rev.*, 104:254–258, 1956.

[11] C. S. Wu, E. Ambler, R. W. Hayward, D. D. Hoppes, and R. P. Hudson. Experimental Test of Parity Conservation in Beta Decay. *Phys. Rev.*, 105:1413–1414, 1957.

[12] R. L. Garwin, L. M. Lederman, and Marcel Weinrich. Observations of the Failure of Conservation of Parity and Charge Conjugation in Meson Decays: The Magnetic Moment of the Free Muon. *Phys. Rev.*, 105:1415–1417, 1957.

[13] T. D. Lee, R. Oehme, and Chen-Ning Yang. Remarks on Possible Noninvariance Under Time Reversal and Charge Conjugation. *Phys. Rev.*, 106:340–345, 1957.

[14] Michael E. Peskin and Daniel V. Schroeder. *An Introduction to quantum field theory.* Addison-Wesley, Reading, USA, 1995.

[15] J. H. Christenson, J. W. Cronin, V. L. Fitch, and R. Turlay. Evidence for the 2π Decay of the K_2^0 Meson. *Phys. Rev. Lett.*, 13:138–140, Jul 1964.

[16] A. J. Bevan et al. The Physics of the B Factories. *Eur. Phys. J.*, C74:3026, 2014.

[17] A. D. Sakharov. Violation of CP Invariance, C asymmetry, and baryon asymmetry of the universe. *Pisma Zh. Eksp. Teor. Fiz.*, 5:32–35, 1967. [Usp. Fiz. Nauk161,no.5,61(1991)].

[18] Edward W. Kolb and Stephen Wolfram. Baryon Number Generation in the Early Universe. *Nucl. Phys.*, B172:224, 1980. [Erratum: Nucl. Phys.B195,542(1982)].

[19] C. L. Hsu et al. Measurement of branching fraction and direct CP asymmetry in charmless $B^+ \to K^+K^-\pi^+$ decays at Belle. *Phys. Rev.*, D96(3):031101, 2017.

[20] Phillip. A. Macklin. Normal Matrices for Physicists. *American Journal of Physics*, 52(6):513–515, 1984.

[21] M. Tanabashi, K. Hagiwara, K. Hikasa, K. Nakamura, Y. Sumino, F. Takahashi, J. Tanaka, K. Agashe, G. Aielli, C. Amsler, M. Antonelli, D. M. Asner, H. Baer, Sw. Banerjee, R. M. Barnett, T. Basaglia, C. W. Bauer, J. J. Beatty, V. I. Belousov, J. Beringer, S. Bethke, A. Bettini, H. Bichsel, O. Biebel, K. M. Black, E. Blucher, O. Buchmuller, V. Burkert, M. A. Bychkov, R. N. Cahn, M. Carena, A. Ceccucci, A. Cerri, D. Chakraborty, M.-C. Chen, R. S. Chivukula, G. Cowan, O. Dahl, G. D'Ambrosio, T. Damour, D. de Florian, A. de Gouvêa, T. DeGrand, P. de Jong, G. Dissertori, B. A. Dobrescu, M. D'Onofrio, M. Doser, M. Drees, H. K. Dreiner, D. A. Dwyer, P. Eerola, S. Eidelman, J. Ellis, J. Erler, V. V. Ezhela, W. Fetscher, B. D. Fields, R. Firestone, B. Foster, A. Freitas, H. Gallagher, L. Garren, H.-J. Gerber, G. Gerbier, T. Gershon, Y. Gershtein, T. Gherghetta, A. A. Godizov, M. Goodman, C. Grab, A. V. Gritsan, C. Grojean, D. E. Groom, M. Grünewald, A. Gurtu, T. Gutsche, H. E. Haber, C. Hanhart, S. Hashimoto, Y. Hayato, K. G. Hayes, A. Hebecker, S. Heinemeyer, B. Heltsley, J. J. Hernández-Rey, J. Hisano, A. Höcker, J. Holder, A. Holtkamp, T. Hyodo, K. D. Irwin, K. F. Johnson, M. Kado, M. Karliner, U. F. Katz, S. R. Klein, E. Klempt, R. V. Kowalewski, F. Krauss, M. Kreps, B. Krusche, Yu. V. Kuyanov, Y. Kwon, O. Lahav, J. Laiho, J. Lesgourgues, A. Liddle, Z. Ligeti, C.-J. Lin, C. Lippmann, T. M. Liss, L. Littenberg, K. S. Lugovsky, S. B. Lugovsky, A. Lusiani, Y. Makida, F. Maltoni, T. Mannel, A. V. Manohar, W. J. Marciano, A. D. Martin, A. Masoni, J. Matthews,

U.-G. Meißner, D. Milstead, R. E. Mitchell, K. Mönig, P. Molaro, F. Moortgat, M. Moskovic, H. Murayama, M. Narain, P. Nason, S. Navas, M. Neubert, P. Nevski, Y. Nir, K. A. Olive, S. Pagan Griso, J. Parsons, C. Patrignani, J. A. Peacock, M. Pennington, S. T. Petcov, V. A. Petrov, E. Pianori, A. Piepke, A. Pomarol, A. Quadt, J. Rademacker, G. Raffelt, B. N. Ratcliff, P. Richardson, A. Ringwald, S. Roesler, S. Rolli, A. Romaniouk, L. J. Rosenberg, J. L. Rosner, G. Rybka, R. A. Ryutin, C. T. Sachrajda, Y. Sakai, G. P. Salam, S. Sarkar, F. Sauli, O. Schneider, K. Scholberg, A. J. Schwartz, D. Scott, V. Sharma, S. R. Sharpe, T. Shutt, M. Silari, T. Sjöstrand, P. Skands, T. Skwarnicki, J. G. Smith, G. F. Smoot, S. Spanier, H. Spieler, C. Spiering, A. Stahl, S. L. Stone, T. Sumiyoshi, M. J. Syphers, K. Terashi, J. Terning, U. Thoma, R. S. Thorne, L. Tiator, M. Titov, N. P. Tkachenko, N. A. Törnqvist, D. R. Tovey, G. Valencia, R. Van de Water, N. Varelas, G. Venanzoni, L. Verde, M. G. Vincter, P. Vogel, A. Vogt, S. P. Wakely, W. Walkowiak, C. W. Walter, D. Wands, D. R. Ward, M. O. Wascko, G. Weiglein, D. H. Weinberg, E. J. Weinberg, M. White, L. R. Wiencke, S. Willocq, C. G. Wohl, J. Womersley, C. L. Woody, R. L. Workman, W.-M. Yao, G. P. Zeller, O. V. Zenin, R.-Y. Zhu, S.-L. Zhu, F. Zimmermann, P. A. Zyla, J. Anderson, L. Fuller, V. S. Lugovsky, and P. Schaffner. Review of particle physics. *Phys. Rev. D*, 98:030001, Aug 2018.

[22] E. Fermi. An attempt of a theory of beta radiation. 1. *Z. Phys.*, 88:161–177, 1934.

[23] R.E. Marshak, Riazuddin, and C.P. Ryan. *Theory of Weak Interactions in Particle Physics*. John Wiley & Sons, Inc., 1969.

[24] N. G. Deshpande and Xiao-Gang He. Isospin Structure of Penguin Diagrams and Their Consequences in B Meson Physics. *Physical Review Letters*, 74(1):2629, Jan 1995.

[25] Andrzej J. Buras. Weak hamiltonian, cp violation and rare decays, 1998.

[26] Xin-Heng Guo, Olivier M. A. Leitner, and Anthony William Thomas. Enhanced direct CP violation in $B^{\pm} \to \rho^0 \pi^{\pm}$. *Phys. Rev.*, D63:056012, 2001.

[27] Ignacio Bediaga, Fernando S. Navarra, and Marina Nielsen. The Structure of $f_0(980)$ from charmed mesons decays. *Phys. Lett.*, B579:59–66, 2004.

[28] C. Itzykson and J. B. Zuber. *Quantum Field Theory*. International Series In Pure and Applied Physics. McGraw-Hill, New York, 1980.

[29] M. Wirbel, B. Stech, and Manfred Bauer. Exclusive Semileptonic Decays of Heavy Mesons. *Z. Phys.*, C29:637, 1985.

[30] Jing-Juan Qi, Zhen-Yang Wang, Xin-Heng Guo, Zhen-Hua Zhang, and Chao Wang. Study of CP Violation in $B^- \to K^-\pi^+\pi^-$ and $B^- \to K^-\sigma(600)$ decays in the QCD factorization approach. *Phys. Rev.*, D99(7):076010, 2019.

[31] Zhi-Qing Zhang. Study of scalar meson $f_0(980)$ and $K_0^*(1430)$ from $B \to f_0(980)\rho(\omega,\phi)$ and $B \to K_0^*(1430)\rho(\omega)decays$. *Physical Review D*, 82(3), Aug 2010.

[32] J. J. Cobos-Martnez, K. Tsushima, G. Krein, and A. W. Thomas. ϕ meson mass and decay width in nuclear matter and nuclei. *Phys. Lett.*, B771:113–118, 2017.

[33] P Colangelo and F De Fazio. Coupling $g_{f_0K^+K^-}$ and the structure of $f_0(980)$. *Physics Letters B*, 559(1):49 – 59, 2003.

[34] K. Nakamura et al.(Particle Data Group). Dalitz Plot Analysis Formalism.

[35] B. Aubert, R. Barate, M. Bona, D. Boutigny, F. Couderc, Y. Karyotakis, J. P. Lees, V. Poireau, V. Tisserand, A. Zghiche, and et al. Dalitz plot analysis of the decay $B^\pm \to K^\pm K^\mp \pi^\pm$. *Physical Review D*, 74(3), Aug 2006.

[36] Hai-Yang Cheng and Kwei-Chou Yang. Nonresonant three-body decays of D and B mesons. *Phys. Rev.*, D66:054015, 2002.

[37] Gustav Kramer and Cai-Dian Lü. Nonleptonic Decays of B Mesons and Strong Coupling Constants. *International Journal of Modern Physics A*, 13(19):33613384, Jul 1998.

[38] M. Jarfi, O. Lazrak, A. Le Yaouanc, L. Oliver, O. Pene, and J. C. Raynal. Decays of b mesons into baryon - anti-baryon. *Phys. Rev.*, D43:1599–1632, 1991.

[39] Tung-Mow Yan, Hai-Yang Cheng, Chi-Yee Cheung, Guey-Lin Lin, Y. C. Lin, and Hoi-Lai Yu. Heavy-quark symmetry and chiral dynamics. *Phys. Rev. D*, 46:1148–1164, Aug 1992.

[40] Clarence L. Y. Lee, Ming Lu, and Mark B. Wise. B_{l4} and D_{l4} decay. *Phys. Rev. D*, 46:5040–5048, Dec 1992.

[41] Yaw-Hwang Chen, Hai-Yang Cheng, B. Tseng, and Kwei-Chou Yang. Charmless hadronic two-body decays of B_u and B_d mesons. *Physical Review D*, 60(9), Oct 1999.

[42] Hai-Yang Cheng and Sechul Oh. Flavor SU(3) symmetry and QCD factorization in $B \to PP$ and PV decays. *Journal of High Energy Physics*, 2011(9), Sep 2011.

[43] Martin Beneke and Matthias Neubert. QCD factorization for $B \to PP$ and $B \to PV$ decays. *Nuclear Physics B*, 675(1-2):333415, Dec 2003.

[44] T. Blum, P. Chen, N. Christ, C. Cristian, C. Dawson, G. Fleming, R. Mawhinney, S. Ohta, G. Siegert, A. Soni, and et al. Kaon matrix elements and CP violation from quenched lattice QCD: The 3-flavor case. *Physical Review D*, 68(11), Dec 2003.

[45] David J Griffiths. *Introduction to elementary particles; 2nd rev. version.* Physics textbook. Wiley, New York, NY, 2008.